NEW STRATEGIES TO IMPROVE SELECTIVITY AND SENSITIVITY WITH ULTRAMICROELECTRODES

By

CHEN-CHAN HSUEH

A DISSERTATION PRESENTED TO THE GRADUATE SCHOOL
OF THE UNIVERSITY OF FLORIDA IN PARTIAL FULFILLMENT
OF THE REQUIREMENTS FOR THE DEGREE OF
DOCTOR OF PHILOSOPHY

UNIVERSITY OF FLORIDA

1995

ACKNOWLEDGMENTS

I would like to express my appreciation to my research advisor, Dr. Anna Brajter-Toth, for her guidance and assistance, especially for her encouragement and her great help in writing scientific papers. I wish to thank a former graduate student, Dr. Michael S. Freund, for his help in designing an on-line iR compensation circuit and writing a semi-integral analysis program.

My appreciation to my brothers, Chen-Nan and Chen-Sen, and my mother; without their support and love, I would never have been able to finish this work. Thanks to all the members of the Toth group (Maurice Thompson, Quan Cheng, Lisa Spurlock, and Merle Regino) for their assistance and friendship. The assistance of electronics shop's staff (especially Steven Miles) in designing the fast-scan instrument is also acknowledged.

I would like to thank Jau Yoh in the Pesticide Research Laboratory for her financial help, and the coworkers in PRL for their friendship. The financial support of this work through an Electrochemical Society Summer Fellowship is also gratefully acknowledged.

Last but certainly not least, I would like to thank my dear wife, YarJing Yang, for her support and love.

TABLE OF CONTENTS

ACKNOWLEDGMENTS ii

LIST OF FIGURES vi

ABSTRACT xi

CHAPTERS

1. INTRODUCTION 1

- Types of Ultramicroelectrodes 1
- Properties of UMEs and Their Analytical Applications 4
  - Small Physical Dimensions 5
    - In-vivo detection and single cell measurements 5
    - Microsensors and microdetectors 6
    - Scanning electrochemical microscopy 6
  - Low iR Drop and Small Cell Time Constant 7
    - Electrochemistry in highly resistive media 18
    - Fast scan voltammetry 19
    - Importance of iR compensation for accurate fast kinetic measurements 26
  - High Efficiency of Mass Transport 31
- Circuit Design for UMEs Experiments 38
  - Potentiostat for UMEs experiments at low scan rates 38
  - Potentiostat for UMEs experiments at high scan rates 39
  - Potentiostat for high-scan-rate measurements at UMEs with on-line iR compensation 40
- Surface Modification of UMEs 41
  - Polymer-film-modified electrodes 41
  - Surface-oxide-modified electrodes 43
- Purpose of Work 46

2. EXPERIMENTAL SECTION 48

Reagents and Solutions 48
Electrodes 48
- Reference and Auxiliary Electrodes 48
- Working Electrodes 49
- Fabrication of UMEs 49
    - Carbon fiber electrodes sealed in heat shrinkable Teflon tubes 49
    - Carbon fiber electrodes sealed in epoxy 50
    - Platinum wires sealed in soft glass 53
- Electrode Pretreatment 54

Instrumentation 54
- IR Compensation Circuit and Its Operational Principle 54
- The Current Transducer and the Potentiostat for the UME Experiments 62
- Instrumental Setup for Low and High Scan Rate Experiments 66
    - Voltammetry at low scan rates 67
    - Voltammetry at high scan rates 72

Fundamentals of Electrochemical Methods 78
- Cyclic Voltammetry 78
- Kinetic Measurements with Cyclic Voltammetry 83
- Semi-Integration Analysis 85
- Measurement of Diffusion Coefficients with Rotating Disk Electrodes 91
- Chronocoulometry 92

3. FAST KINETIC MEASUREMENTS IN AQUEOUS SOLUTIONS WITH ON-LINE IR COMPENSATION 93

Background 93
Signal Averaging and its Effect on Surface Properties 95
Surface Properties of Carbon Fiber and Their Effect on Response of Ru(NH$_3$)$_6^{(3+/2+)}$, Fe(CN)$_6^{(3-/4-)}$, and Uric Acid 96
Kinetics of Ru(NH$_3$)$_6^{(3+/2+)}$ on Freshly Cut Carbon Fiber 104
Kinetics of Fe(CN)$_6^{(3-/4-)}$ on Freshly Cut Carbon Fiber 108
Redox Reaction of Uric Acid 109
Conclusions 113

4. ELECTROCHEMICAL PREPARATION OF ULTRATHIN OVEROXIDIZED POLYPYRROLE FILMS AND THEIR ANALYTICAL APPLICATIONS 115

Background 115

Procedure of Ultrathin OPPy Film Formation by Polymerization and Overoxidation 121
Procedure for Coating Ultrathin OPPy Films on Pt 122
Preparation of Ultrathin OPPy Films 122
Cation Permselectivity of Ultrathin OPPy at GC Electrodes 126
Permselectivity of Ultrathin OPPy Films at Carbon Fiber Electrodes 130
Applications of OPPy-Coated Ultramicroelectrodes 133
Permselectivity of Ultrathin OPPy Films at Pt Ultramicroelectrodes 134
Stability of the OPPy Films 140
Coating Polymer Films of PPy-2-COOH on Pt Electrodes 140
Conclusions 146

5. NEW STRATEGIES FOR IMPROVING SENSITIVITY AND SELECTIVITY WITH FAST SCAN VOLTAMMETRY 148

Background 148
Effects of Surface Oxides on Sensitivity and Selectivity 151
Detection of DA Without the Interference of AA 159
Fast Scan Voltammetry with Signal Averaging 167
Limitations of Fast Scan Voltammetry 168
Conclusions. 171

6. CONCLUSIONS AND FUTURE WORK 173

APPENDICES

A. DATA ACQUISITION, DISPLAY AND PROCESSING PROGRAM SOURCE CODE 176

B. SEMI-INTEGRAL ANALYSIS PROGRAM SOURCE CODE 185

REFERENCE LIST 187

BIOGRAPHICAL SKETCH 195

LIST OF FIGURES

Figure page
1.1. Different types of ultramicroelectrodes. 3

1.2. Illustration of the basic operation principle of scanning electrochemical microscopy (SECM). As the diffusion of electroactive species is blocked by the protruding part of the substrate, the tip current decreases. By plotting the fluctuations of the tip current vs. the position of the tip, the topography of the substrate is revealed. 9

1.3. Illustration of an electrochemical cell and its equivalent circuit. The electrochemical cell contains a working electrode and a reference electrode. Under common experimental conditions, the capacitance of the reference electrode is much higher than the double layer capacitance of the working electrode, thus the capacitance of the reference electrode can be neglected. The electrochemical cell can be simplified into a combination of cell resistance and the working electrode double layer capacitance. 11

1.4. A graphic illustration of the double layer capacitance. As the electrode surface becomes more positive, the negative ions in the solution begin to accumulate on the electrode. These negative ions then attract positive ions. Therefore, a double layer forms. 13

1.5. The origin of the faradaic current. An electroactive molecule (in this case, the oxidant) diffuses to the electrode surface and exchanges electrons with the electrode. The oxidant is reduced to the reductant and diffuses away. The electron exchange between the electroactive molecule and the electrode produces the faradic current. The current is a function of redox kinetics (rate of electron transfer between the electroactive species and the electrode) and the diffusion process (rate of diffusion of the electroactive species). 15

1.6. Illustrations of fast cyclic voltammetry and background subtraction: (a) applied potential waveform as a function of time; (b) current as a function of time; the solid line is the background current and the dashed line is the current in the presence of electroactive species; (c) A background subtracted voltammogram of (b); dashed line in (b) subtracted from solid line in (b) and the result plotted as a function of potential. 25

1.7. Simulation of the effects of the cell resistance and double layer capacitance on the effective scan rates (the shape of the applied potential); measured (effective) potential (solid line), applied potential (dashed line). Top: the effects of cell resistance only. Bottom: the effects of resistance and capacitance. 30

1.8. Growth of a diffusion layer as a function of time ($t_1 < t_2 < t_3 < t_4 < t_5$) where the lines represent a cross section of the interface between the diffusion layer and the solution bulk. At time t_1, diffusion is linear. As time scale increases, diffusion becomes a mix of linear and radial diffusion. Eventually, diffusion behavior transforms to a radial diffusion. 34

1.9. The effects of electrode size on diffusion behavior at common experimental time scales (several seconds or less). 37

1.10. A possible structure of surface oxide groups on a carbon electrode (reference 78). 45

2.1. Schematics of UMEs used in this work. (A). Carbon fiber (7μm) sealed with Teflon. (B). Carbon fiber sealed with epoxy (C). Pt wire sealed (5μm) in glass. 52

2.2. Schematic of a potentiostat built for fast measurements with iR compensation. 56

2.3. Schematic of the current transducer. 64

2.4. Instrumental setup for UME experiments at low scan rates. 69

2.5. Instrumental setup for UME experiments at high scan rates. 71

2.6. Cyclic voltammogram of 0.1 mM $Fe(CN)_6{}^{3-}$ in 70 mM pH 7.0 phosphate buffer obtained from the current transducer connected to BAS. The scan rate is 10 mV/s. The gain of the current transducer is 10000 and the time constant of the first order filter is 100 μs. The working electrode is a carbon electrode (7 μm). 74

2.7. Voltammogram of 0.18 mM dopamine at 2,000 V/s in 70 mM pH 7.0 phosphate buffer with a carbon electrode (7 μm). The voltammogram is background subtracted and signal averaged 1000 times. 77

2.8. A typical cyclic voltammogram. 81

2.9. A plot of ΔE_p vs kinetic parameter ψ (reference 88 and 89). 87

2.10. Division of experimental i(t) vs. t [or vs. E(t)] curve for semi-integration. 90

3.1. Semiintegrated cyclic voltammetric current of 10 mM $Ru(NH_3)_6^{(+2/+3)}$ in 1 M KCl solution at a freshly cut carbon fiber electrode (7 μm). Scan rate is 5000 V/s. 98

3.2. Cyclic voltammograms of 1 mM uric acid in 1 M pH 7.0 phosphate buffer at a carbon fiber electrode (7 μm). Scan rate 400 V/s. Solid line - freshly cut; dashed line - electrochemically pretreated. (For pretreatment procedure see the Experimental Section). 101

3.3. Semiintegrated cyclic voltammetric currents of uric acid in Figure 3.2. Solid line - freshly cut; dashed line - electrochemically pretreated. .. 103

3.4. Cyclic voltammograms of 10 mM $Ru(NH_3)_6^{(+2/+3)}$ in 1 M KCl solution at a freshly cut carbon fiber electrode (7 μm). Scan rate is 11,000 V/s. The solid line is the current response with iR compensation (Compensated resistance R_c=6.9 KΩ). The dashed line is the current response without iR compensation. 107

3.5. Redox and follow-up reactions of uric acid in aqueous solutions. 111

4.1. Chemical structures of Py , PPy, and OPPy. 117

4.2. A cartoon representation of the proposed carbonyl group in OPPy films hindering anion diffusion. 119

4.3. A cartoon representation of pin holes gradually filled with OPPy by a repeated coating procedure. 125

4.4. Cyclic voltammograms: (a) 10 mM $Fe(CN)_6^{3-}$ in 0.5 M phosphate buffer (pH 7.0) at OPPy modified glassy carbon electrode. Curve 1 is the response of the bare electrode. Curves 2-7 are the responses after first time (curve 2) to sixth time (curve 7) of repeated coating; (b)10 mM

$Ru(NH_3)_6^{3+}$ at the same electrode and buffer as in (a). Solid line is the response before coating. Dashed line is the response after coating six times. Scan rate is 20 mV/s. Electrode area is 0.067 cm^2. 129

4.5. Cyclic voltammograms: (a) 10 mM $Fe(CN)_6^{3-}$ in 0.5 M phosphate buffer (pH 7.0) at OPPy modified carbon fiber ultramicroelectrode. Curve 1 is the response of the bare electrode. Curves 2-5 are the responses after first (curve 2) to four times (curve 5) of repeated coating; (b) 10 mM $Ru(NH_3)_6^{3+}$ at the same electrode and buffer as in (a). Solid line is the response before coating. Dashed line is the response after coating four times. Scan rate is 20 mV/s. Electrode diameter is 7 μm. 132

4.6. Cyclic voltammograms of 10 mM dopamine (solid line) and ascorbic acid (dashed line) in 0.5 M phosphate buffer (pH 7.0) at carbon fiber electrode modified four times with the same film as in Figure 4.5. Scan rate is 20 mV/s. Electrode diameter is 7 μm. 136

4.7. Cyclic voltammograms: (a) 10 mM $Fe(CN)_6^{3-}$ obtained at Pt ultramicroelectrode in 0.5 M phosphate buffer (pH 7.0). Solid line is the response at the bare electrode. Dashed line is the response at an electrode modified with adsorbed/polymerized monolayer of OPPy film; (b) 10 mM $Ru(NH_3)_6^{3+}$ at the same electrode and buffer as in (a). Solid line is the response at the bare electrode. Dashed line corresponds to the conditions for dashed line in (a). Scan rate is 20 mV/s. Electrode diameter is 5 μm. 139

4.8. (a) Cyclic voltammograms of three consecutive scans at Pt ultramicroelectrode in 50 mM Py-2-COOH and 0.1 M TBAP in MeCN. Scan rate is 50 mV/s. The reference electrode is a Ag wire. Electrode diameter is 5 μm. The peak potential is ca. +1.5 V vs. Ag wire; (b) Cyclic voltammograms of three consecutive scans at a glassy carbon electrode in 50 mM Py-2-COOH and 0.1 M TBAP in MeCN. Scan rate is 100 mV/s. Electrode area is 0.067 cm^2. The peak potential is ca. +1.65 V vs. Ag wire. 143

4.9. Cyclic voltammograms: (a) 10 mM $Ru(NH_3)_6^{3+}$ and (b) 10 mM $Fe(CN)_6^{3-}$ in 0.5 M phosphate buffer (pH 7.0) at a Pt ultramicroelectrode before and after coating with PPy-2-COOH in one CV scan. Solid lines are the voltammograms at the bare electrodes. Dashed lines are the voltammograms at the modified electrodes. Scan rate is 20 mV/s. Ultramicroelectrode diameter is 5 μm. 145

5.1. Background currents after repetition of fast cycle scans. Cyclic voltammogram obtained: (line 1) with a freshly polished carbon fiber electrode (7 μm diameter); (line 2) after 30 minutes of repeated cycling, at a scan rate of 100 V/s, in the potential window of -0.8 to +1.2 V vs SCE; (line 3) after one hour of cycling; (line 4) after one and a half hour of cycling. 154

5.2. Plots of log of 0.1 mM DA peak current, log i_p vs log scan rate. Scan range is from 50 to 10,000 V/s. Working electrode is a carbon fiber electrode (7 μm diameter) and buffer solution is 70 mM pH 7.4 phosphate buffer. 158

5.3a. Cyclic voltammograms of 10^{-4} M DA (solid line) and 10^{-2} M AA (dashed line) at a scan rate of 100 V/s at a 7 μm carbon fiber electrode. The buffer used in the experiment is a 70 mM phosphate buffer. Electrode cycled for ca. 30 minutes in the buffer solution before use (see Experimental). Time constant of the potentiostat filter is 1μs. Gain of the current transducer of the potentiostat is 1V/μA. 161

5.3b. Cyclic voltammograms of 10^{-4} M DA (solid line) and 10^{-2} M AA (dashed line) at a scan rate of 10,000 V/s. Same electrode and solution conditions as in Figure 5.3A. 163

5.4. Cyclic voltammogram of 5 μM DA in the presence of 1.2mM AA in 70 mM pH 7.4 phosphate buffer. Scan rate is 2,000 V/s, electrode diameter 7 μm . The voltammogram was averaged 1000 times. 166

5.5. Signal averaged cyclic voltammograms of 50 μM DA in 70 mM phosphate buffer, scan rate 2,000 V/s. Only the oxidation peaks are shown. Lines 1, 2, 3, and 4 averaged 1, 10, 100, and 1000 times, respectively. 170

Abstract of Dissertation Presented to the Graduate School
of the University of Florida in Partial Fulfillment of the
Requirements for the Degree of Doctor of Philosophy

NEW STRATEGIES TO IMPROVE SELECTIVITY AND SENSITIVITY WITH ULTRAMICROELECTRODES

By

Chen-Chan Hsueh

May 1995

Chairperson: Anna Brajter-Toth
Major Department: Department of Chemistry

The objective of this work is to develop new analytical strategies for analytical measurements with ultramicroelectrodes (UMEs), especially in biosensing. We focus most of our efforts on the development of fast scan technique using UMEs in characterizing fast redox reactions of biological species, and improving signal-to-noise ratio (S/N), selectivity, and detection limit. Instrumention which has been built to perform these experiments with UMEs is described.

There are three major parts in the dissertation. The first part describes fast scan voltammetry in the investigation of rapid redox reactions in aqueous solutions with UMEs. Fast scan voltammetry has been used in organic solvents and most of the electrodes used were metal electrodes. This part of the work tries to establish the use of fast scan voltammetry in the investigation of fast redox reactions in aqueous solutions with carbon electrodes. An on-line iR-drop-compensation circuit was designed for this work. This circuit can perform fast scan voltammetry up to 200,000 V/s without iR-drop distortion. The surface characteristics of carbon fiber ultramicroelectrodes have been investigated under fast scan voltammetry conditions. The standard reaction rate constants of a biological compound (uric acid) and two well-know inorganic probes ($Ru(NH_3)_6^{(3+/2+)}$ and $Fe(CN)_6^{(3-/4-)}$) were measured. The influence of surface oxides on the measured rate constants is discussed.

The second part focuses on the improvement of selectivity of UMEs with polymer film coatings. The complexity of a biological matrix makes selectivity an important consideration in biosensing and bioanalysis. The work aimed to improve the selectivity and stability in electrochemical measurements by modifying electrode surface properties with polymer films. A method of making ultrathin overoxidized polypyrrole films was designed to modify electrode surfaces without sacrificing sensitivity.

The third part of this research focuses on the potential analytical advantages of fast scan voltammetry. A specific consideration was the method design for improving selectivity and sensitivity of analytical measurements in complex environments. To reach this goal, a circuit with low instrumental noise was designed to perform fast scan voltammetry. The new method was tested in dopamine detection at low concentrations in the presence of a large excess of ascorbic acid. By pushing the scan rate up to 10,000 V/s, it is demonstrated that a substantial improvement in selectivity can be achieved even though the reaction potentials of dopamine and ascorbic acid are similar. At high scan rates, it is possible to detect dopamine in the presence of 1000-fold excess of ascorbic acid because of the kinetic differences in the electrochemical responses of the two probes. Other advantages of ultrafast

scan rate measurements in aqueous solutions are also investigated in this work. These include improved temporal resolution and higher signal-to-noise ratios resulting from the fact that more voltammetric scans can be acquired and averaged in a short period of time.

CHAPTER 1
INTRODUCTION

Types of Ultramicroelectrodes

In the 1970s a number of research groups exploited the advantages of ultramicroelectrodes (UMEs), normally defined as electrodes with characteristic dimensions smaller than 20 μm.[1,2,3] A variety of materials, shapes, and sizes of UMEs have been reported since. Carbon, gold, and platinum are the most commonly used materials, with a few publications describing copper and mercury. Carbon fiber is the most popular material used in bioanalysis due to its rich chemical properties and compatibility with bio-tissue. The geometries of several different types of UMEs are illustrated in Figure 1.1. The cylindrical UMEs are usually prepared by allowing a portion of the wire or fiber to protrude from the insulator. The cylindrical geometry has the advantage of larger currents, but these electrodes tend to be mechanically fragile and cannot be easily polished.

At present, the most widely used UMEs are probably ultramicrodisk electrodes with a radius of less than 10 μm. They are constructed relatively easily by encasing a metal wire or a carbon fiber in glass or epoxy; the flat surface of the end of the insulated wire serves as the active electrode surface. Because disk-like UMEs have smaller electrode areas and good spatial resolution, they are commonly used in fast measurements and in in-vivo detection. Recently, the use of band and ring electrodes is being reported more often.[4,5,6] Electrodes

Figure 1.1. Different types of ultramicroelectrodes.

Typical types of ultramicroelectrodes

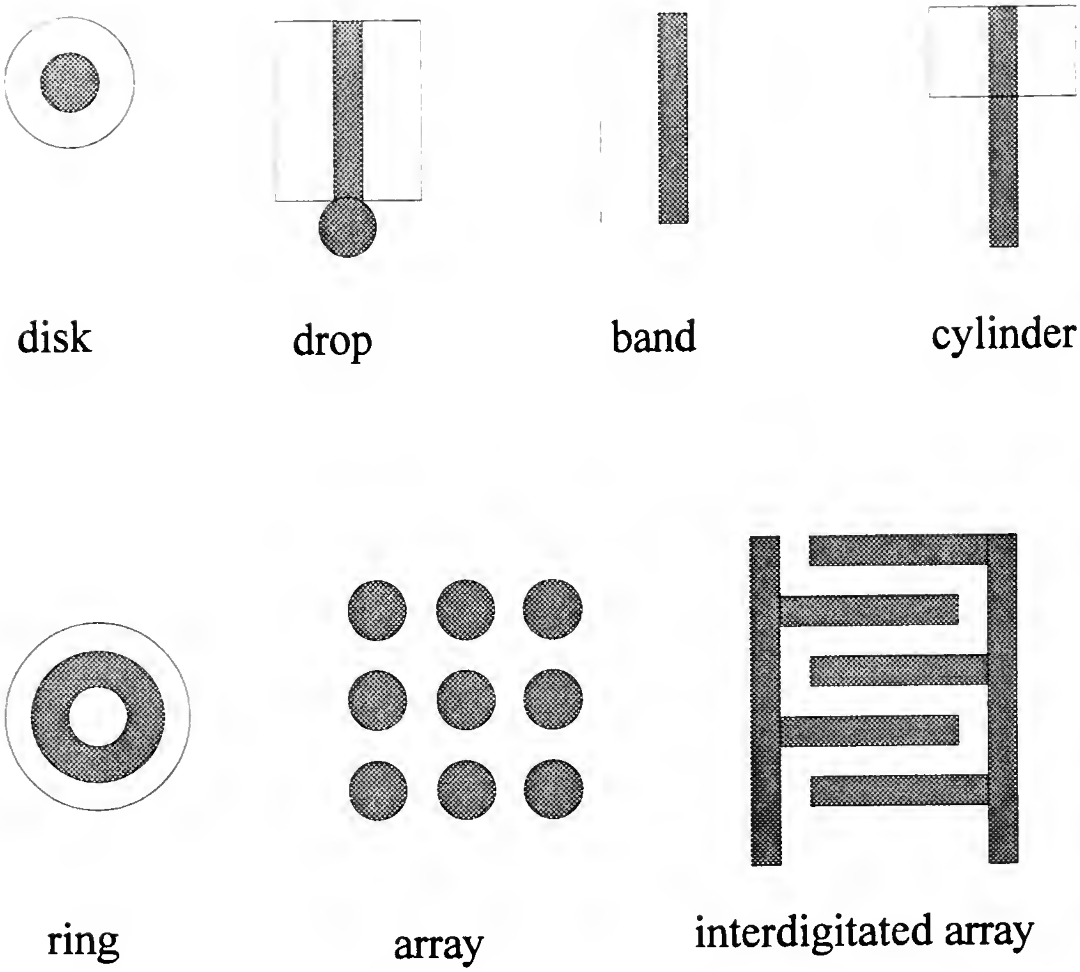
disk
drop
band
cylinder
ring
array
interdigitated array

with a band or ring geometry are attractive because they can be fabricated on a nanometer scale in one dimension. One approach to their fabrication is to sandwich thin metal film between glass or epoxy insulators. Bands with a smallest dimension of 20 Å have been prepared in this way.[7] The surface areas of band and ring UMEs can be enlarged by changing the length of the band or the circumference of the ring without losing the desired properties of UMEs.

It should be noticed that the area of a UME can be as large as that of a conventional electrode. As long as one of the dimensions of the electrode is less than 20 μm, it can be called an ultramicroelectrode. An enlarged surface area ensures large faradaic currents which can be detected without difficulty by conventional potentiostats. The same objective can be achieved with ultramicroelectrode arrays. One of the most interesting designs of UME arrays is the interdigitated UME.[8] The individual band UMEs are arranged close to each other, yet different potentials can be applied to these individual UMEs. This can make redox species diffuse back and forth between two adjacent electrodes, thus amplifying the signal. A common approach to the construction of an ultramicroelectrode array is to use lithographic techniques to prepare arrays of band electrodes on insulating substrates.[9,10]

Properties of UMEs and Their Analytical Applications

Because many obstacles in electrochemistry can be reduced or eliminated with UMEs, their use has grown rapidly in the past ten years.[11,12,13,14] Compared to the conventional macroelectrodes, UMEs have many unique properties including small physical dimensions, low iR drop, and high mass transport. These unique properties of UMEs have opened totally new possibilities for electrochemists. In the following discussion, these unique properties and their analytical applications will be introduced.

Small Physical Dimensions

One of the most obvious advantages of UMEs is related to their small physical dimensions. Since the electrode is typically very small, a microliter volume of solution can be used in the experiments with UMEs. Because the electrochemical measurements are concentration sensitive rather than mass sensitive, the mass detection limit can be extremely low if a small volume of a sample is used. A 10^{-21} mole detection limit of insulin has been reported in the literature.[15]

In-vivo detection and single cell measurements

The most common applications based on the small dimensions of UMEs are in-vivo detection and single cell measurements.[16,17,18,19,20,21] The small dimensions of the electrode allow in-vivo detection with minimal tissue damage and with a high spatial resolution. The most intensively investigated area of in-vivo measurements is in neuroscience where UMEs allow pinpointing the area of interest in the brain without damaging the brain tissue. Recent development of even smaller electrodes allows electrochemical detection inside a single cell.[22]

Microsensors and microdetectors

In the separation science, the miniaturization of instrumentation is the current trend. Miniaturization reduces the amount of required sample, the waste produced, and in many cases the time required to complete the analysis. One of the biggest challenges in miniaturization is to maintain the performance of the detector as the size of the detector decreases. Most detectors require a large detection volume in order to perform well, which makes miniaturization difficult. However, the small dimensions of UMEs and the inherent concentration sensitive properties of the electrochemical detection make UMEs very compatible with detector miniaturization. Moreover, the small diffusion layer at UMEs makes them less dependent upon the flow rate. Many reports have shown the power of UMEs combined with capillary zone electrophoresis (CZE) and micro-column high performance liquid chromatography (HPLC).[23,24,25]

Scanning electrochemical microscopy

Another interesting application based on the small dimensions of UMEs is scanning electrochemical microscopy (SECM). This technique resembles scanning tunneling microscopy (STM) as far as the movement of the electrode across the substrate surface is concerned, but the principles of the measurement are different. In SECM, an UME with a tip radius on the order of 10 μm or less is moved in close proximity to a substrate of interest, in contact with a solution containing an electroactive species. The electrochemical reactions at the tip give rise to a tip current that is affected by substrate topography. Generally, the tip current is controlled by diffusion of electroactive species at the electrode tip. As the tip moves across the substrate, the mountain part of the substrate blocks the diffusion of electroactive species (lower faradaic current), and the valley part of the substrate allows efficient diffusion (higher faradaic current). Consequently, the fluctuation of the tip current reflects the topography of the substrate as the tip moves across the substrate (Figure 1.2).

Low iR Drop and Small Cell Time Constant

Two main obstacles of conventional large electrodes are large iR drop and large time constant. An electrochemical cell can be considered as a circuit consisting of a resistor (cell resistance) and a capacitor (double-layer capacitance). Figure 1.3 illustrates an electrochemical cell and its equivalent circuit. The double-layer capacitance originates at a charged electrode surface in contact with an electrolyte solution which attracts ions of opposite charge and repels ions of like charge. A graphic illustration of the double-layer capacitance is shown on Figure 1.4. When a change of voltage occurs at a working electrode, the charge of the electrode surface changes accordingly, thus the charged ions need to move into or move out from the double-layer. The movement of the charged ions produces a current which is called the double-layer charging current. Another source of current is from the redox reaction of electroactive species in the cell. When the applied voltage is sufficient to provide energy for the redox reaction, faradaic current flows (see Figure 1.5).

As the current is passing through the cell, the applied voltage is consumed by the cell resistance, contributing to the iR loss or the iR drop, as the following equation shows,

Figure 1.2. Illustration of the basic operation principle of scanning electrochemical microscopy (SECM). As the diffusion of electroactive species is blocked by the protruding part of the substrate, the tip current decreases. By plotting the fluctuations of the tip current vs. the position of the tip, the topography of the substrate is revealed.

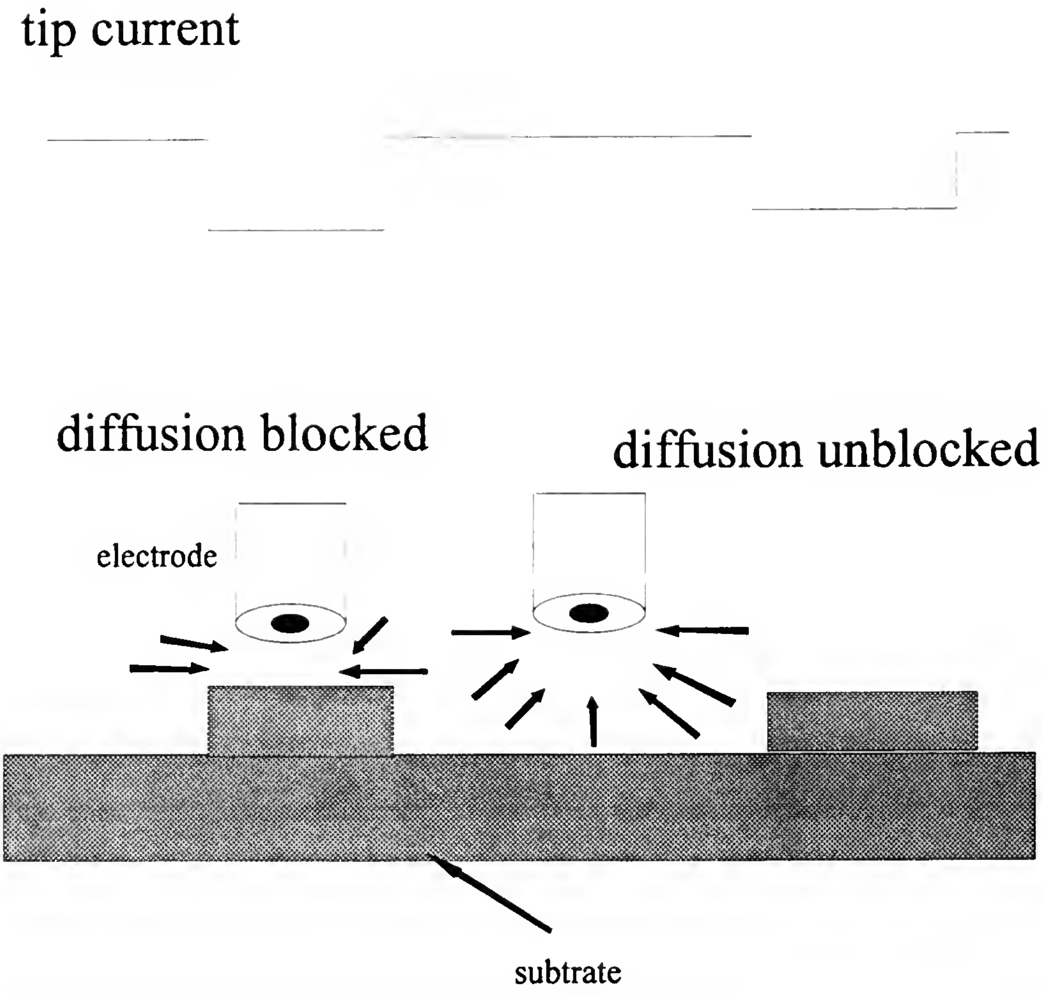
tip current
diffusion blocked
diffusion unblocked
electrode
subtrate

Figure 1.3. Illustration of an electrochemical cell and its equivalent circuit. The electrochemical cell contains a working electrode and a reference electrode. Under common experimental conditions, the capacitance of the reference electrode is much higher than the double layer capacitance of the working electrode, thus the capacitance of the reference electrode can be neglected. The electrochemical cell can be simplified into a combination of cell resistance and the working electrode double layer capacitance.

(A)

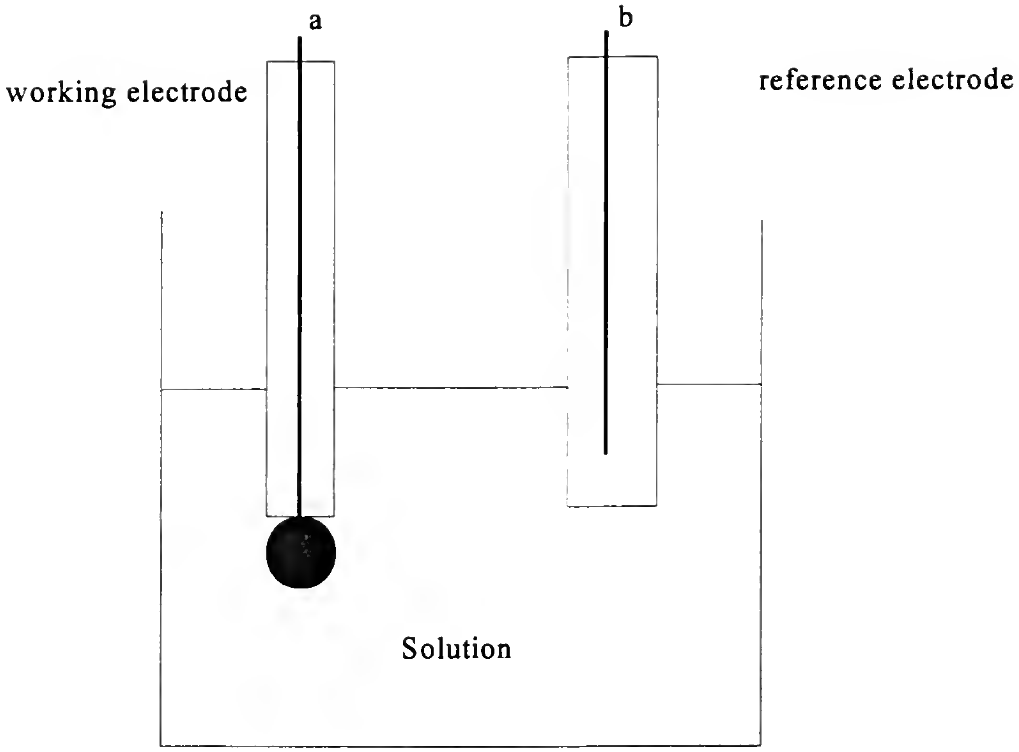
a
b
working electrode
reference electrode
Solution

(B)

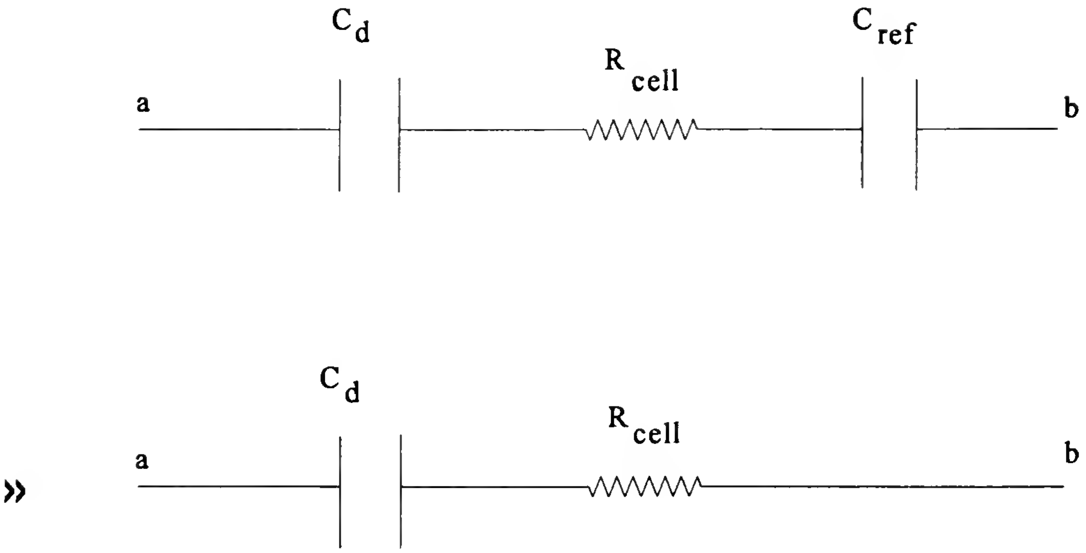
C_d
R_{cell}
C_{ref}
a
b
C_d
R_{cell}
»
a
b

Figure 1.4. A graphic illustration of the double layer. As the electrode surface becomes more positive, the negative ions in the solution begin to accumulate on the electrode. These negative ions then attract positive ions. Therefore, a double layer capacitance forms. For the sake of simplicity, the solvent molecules are omitted in the figure.

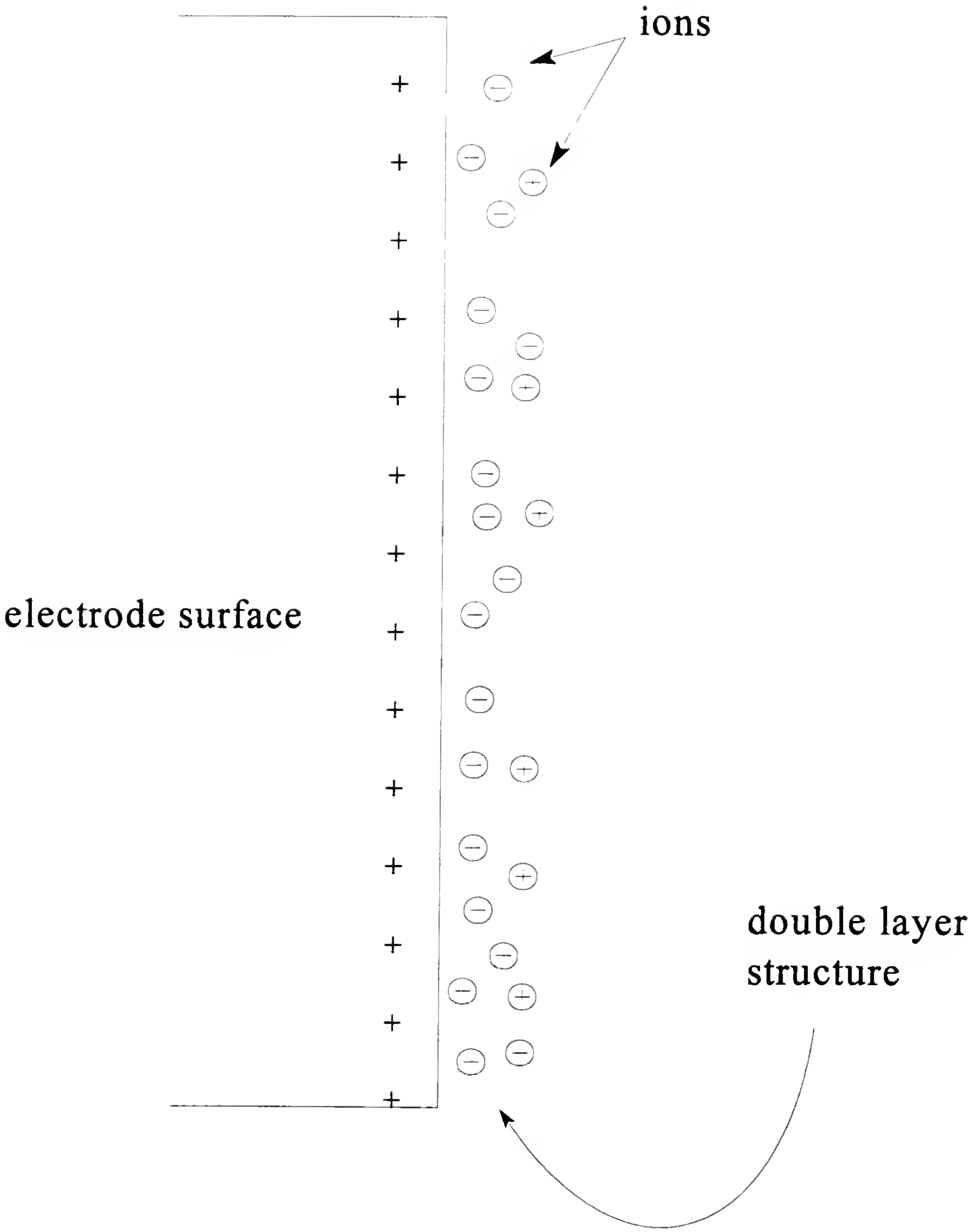
ions
electrode surface
double layer
structure

Figure 1.5. The origin of the faradaic current. An electroactive molecule (in this case, the oxidant) diffuses to the electrode surface and exchanges electrons with the electrode. The oxidant is reduced to the reductant and diffuses away. The electron exchange between the electroactive molecule and the electrode produces the faradic current. The current is a function of redox kinetics (rate of electron transfer between the electroactive species and the electrode) and the diffusion process (rate of diffusion of the electroactive species).

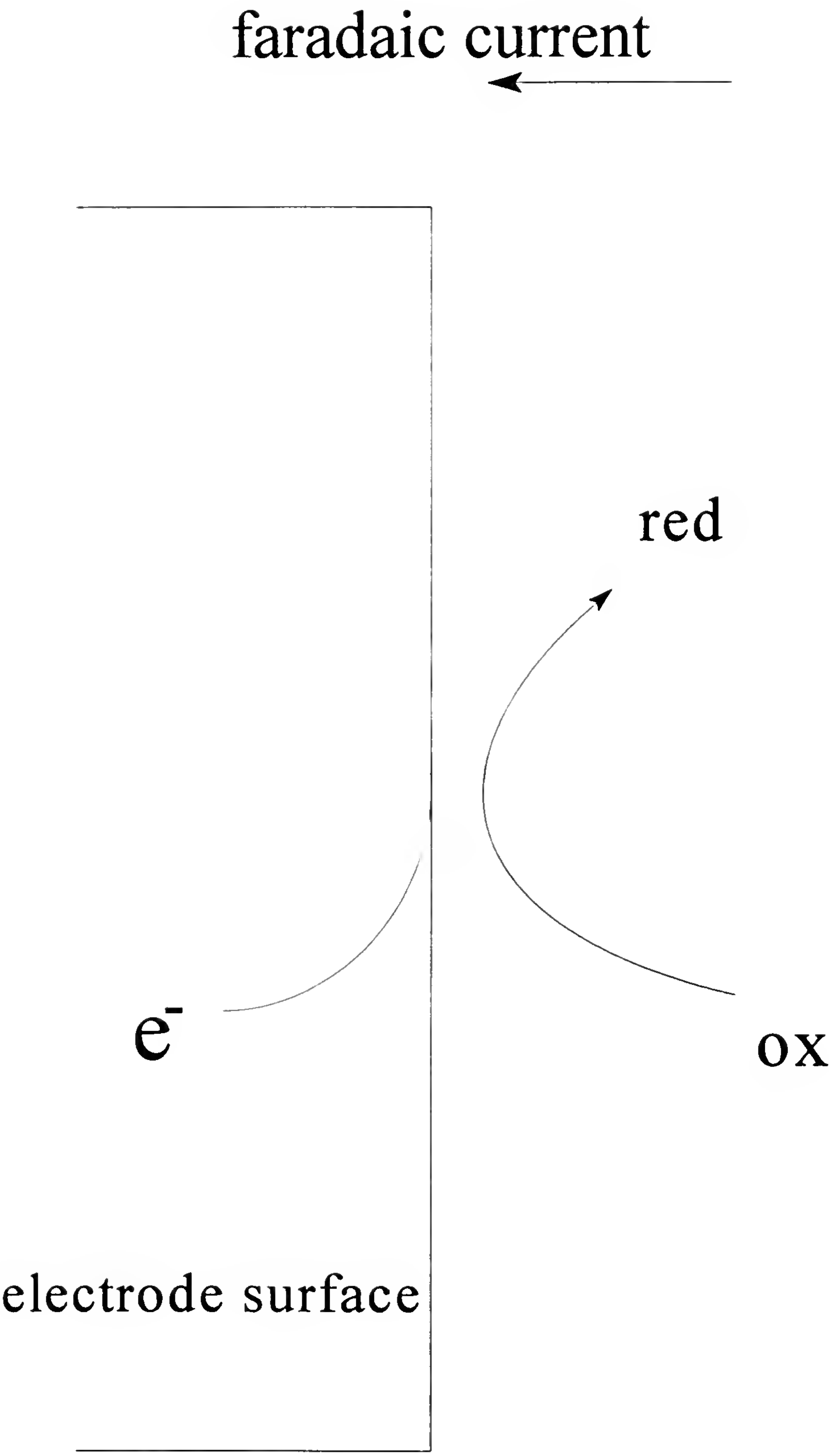
faradaic current
red
e^-
ox
electrode surface

$$E_w = E_{app} + iR \tag{1.1}$$

where E_{app} (V) is the potential applied to the cell, E_w (V) is the true potential of the working electrode, i (μA) is the current flowing through the working electrode, and R (Ω) is the cell resistance.

The cell resistance R can be expressed as follows,

$$R = \frac{\rho}{4r} \propto \frac{1}{r} \tag{1.2}$$

where r is the radius of the disk electrode (cm) and ρ is the specific resistivity of the solution (Ωcm). According to equation 1.2, the cell resistance increases as the size of the electrode decreases. However, the charging current from the double-layer capacitance, and the faradaic current from the redox reactions of the electroactive species in the electrochemical cell, are proportional to the electrode area because both of them originate at the electrode surface. The total cell current can be described as follows,

$$i = (i_c + i_f) \propto A \propto r^2 \tag{1.3}$$

where i (μA) is the cell current, i_c (μA) is the charging current, i_f (μA) is the faradaic current, A (cm^2) is the electrode area, and r (cm) is the radius of the disk electrode. According to equation 1.3, the magnitude of the current decreases with the square of the electrode radius, which is a significant decrease. Combining equations 1.2 and 1.3, a relationship between the iR drop and the electrode size is follows.

$$iR \propto r \tag{1.4}$$

Equation 1.4 clearly shows that the iR drop will be reduced as the size of the electrode decreases. This ensures the superiority of UMEs over conventional macroelectrodes in terms of reducing the iR drop.

Another problem associated with the conventional macroelectrodes is the large cell-time constant. When a sudden change of voltage is applied to the working electrode, time is required to charge the capacitor (double-layer capacitance) to reflect the change in the voltage. This time is called the cell-time constant and can be expressed as follows,

$$\tau = C_d R \tag{1.5}$$

where τ (sec) is the cell-time constant, C_d is the double-layer capacitance (F), and R is the cell resistance (Ω). The doubl- layer capacitance is a function of the electrode area,

$$C_d = CA = C\pi r^2 \propto r^2 \tag{1.6}$$

where C is the double-layer capacitance per unit area (F/cm^2). Substitution of equations 1.2 and 1.6 into equation 1.5 gives the following,

$$\tau = C_d R \propto r \tag{1.7}$$

According to equation 1.7, the cell-time constant will be very small when a UME is used because the time constant is proportional to the electrode radius. Experimentally, with UMEs of 5 μm radius cell-time constants are less than a microsecond.[26]

Electrochemistry in highly resistive media

One important application exploiting the low iR drop at UMEs is in the electrochemical measurements in highly resistive media which are typically inaccessible with conventional size electrodes due to the enormous iR drop. The reduced iR drop allows measurements to be made in novel systems such as nonpolar solvents with low concentrations of supporting electrolytes,[27] polar solvents in the absence of supporting electrolytes,[28] and gas phase.[29,30,31] The ability to perform electrochemistry in these novel media makes UMEs a very valuable tool.

Nonpolar solvents were incompatible with electrochemical measurements due to their extremely high resistance. Lines and Parker were the first to show that voltammetry at UMEs is possible in benzene (a nonpolar solvent).[32] Other groups, such as Bond's,[33,34,35] Fleischmann's,[36] and Wightman's[37,38,39] had reported voltammetric measurements with UMEs in benzene, toluene, and even hexane.

In conventional electrochemistry, a supporting electrolyte is required to ensure that the medium conducts properly. Supporting electrolytes often limit the maximum useful potential range because the electrolyte itself may become electroactive. The ability to perform the measurements in polar solvents in the absence of supporting electrolyte enables the expansion of the useful potential range. Pons and Fleischmann have reported that alkanes can be oxidized in electrolyte-free acetonitrile at potentials above + 3.5 V.[40] Bard's group has reported that alkali metal ions can be successfully oxidized in liquid SO_2 at potential of +5.0 V.[41]

Applications of UMEs to electrochemistry in the gas phase are another interesting field. Pons and Fleischmann have published several reports of such experiments.[29,30,31] The UMEs coated with an ionic conducting membrane were used to determine the quantity of organic gases. The cell conductivity was maintained by proton transfer in the membrane while the gases could diffuse into the membrane to react at the electrodes or affect the conductivity of the cell.[30]

Fast scan voltammetry

At the conventional macroelectrodes, it is impossible to perform fast scan voltammetry (voltammetry at scan rates higher than 100 V/s) because the cell time constant and the iR drop are too large. In voltammetric experiments, the dependence of the charging current (i_c) on the cell time constant (τ) and the scan rate (v) can be expressed by the following equation,

$$i_c = [-\exp(-\frac{t}{\tau})+1]vC_d \tag{1.8}$$

where t is time (s) and v is scan rate (V/s). The first term indicates the time (t) needed to charge the double-layer as the electrode potential changes. After the double-layer is fully charged, the charging current will remain as indicated by the second term ($C_d v$). This charging current is independent of time. According to equation 1.8, the first term approaches zero and the second term dominates if t/τ is much larger than one. In other words, if the experimental time scale is much larger than the cell-time constant, the effect of time constant on the charging current can be neglected. In fast scan voltammetry, the time scale (t) is extremely small. For fast scan voltammetry to be feasible, a small cell-time constant (τ) is needed to ensure that t/τ is large enough.

The second requirement for fast scan voltammetry is that the iR drop must be small. According to equation 1.8, the first term will be close to zero when the cell time constant (defined by equation 1.7) is small. Equation 1.8 can be simplified to the following.

$$i_c = \nu C_d \tag{1.9}$$

therefore, we have the following equation.

$$i_c R = \nu C_d R \propto \nu \tag{1.10}$$

Equation 1.10 shows that the iR drop is proportional to scan rate. To minimize the iR drop at high scan rates, C_dR needs to be as small as possible. In summary, a small cell-time constant and a small iR drop are the two essential requirements for fast scan voltammetry.

As equations 1.4 and 1.5 demonstrate, the cell-time constant and the iR drop are greatly reduced at a UME. Thus, the scan rate can be increased greatly. Experimentally, scan rates of 1,000,000 V/s have been achieved with a 5μm gold electrode in acetonitrile as a solvent (cell resistance = 16 kΩ and the double-layer capacitance = 5.5 pF).[42,43,44] This is an improvement of five orders of magnitude compared to scan rate of 10 V/s at macroelectrodes.

Fast scan voltammetry has been applied to measurements of fast redox reactions and fast follow-up chemical reactions (coupled chemical reactions). Since the introduction of UMEs fast heterogeneous electron-transfer kinetics have been studied with fast scan voltammetry. For example, redox reactions of anthracene, anthraquinone, naphthoquinone, and benzoquinone in organic solvents have been characterized.[45,46,47] The scan rates used in the experiments ranged from 1000 V/s to 1,000,000 V/s and the standard rate constants obtained were as large as 3.8 cm/s.[44,47]

Since 1980, many voltammetric investigations have been carried out on electron transfer reactions coupled with follow-up chemical reactions such as addition, isomerization, dimerization, and homolytic cleavage.[48,49,50] All of these reactions involved fast-decaying redox intermediates. Fast scan voltammetry can be used to measure the life time of redox intermediates. Fast scan voltammetry also prevents the intermediate from decaying and producing by-products which may react with the original reactants and complicate the reaction mechanism. In some applications, the follow-up products of the intermediates are electroactive and have close redox potentials to the parent molecules. By using fast scan voltammetry, the redox potentials and the redox kinetics of such follow-up products can be revealed.[51,52]

In addition to the application to the study of fast redox kinetics, fast scan voltammetry can be a powerful analytical tool. Recently, research has shown that fast scan voltammetry can be advantageous in trace analysis and in bioanalysis.[53,54] For example, fast scan voltammetry has been applied in quantitative measurements of biological species, such as NADH and dopamine.[54,55]

Inherently, fast scan voltammetry is not suitable for quantitative analysis due to the interference of large background currents. At solid electrodes, such as graphite, the background current consists of two components, namely pure capacitive charging current, and the current due to the surface redox processes. Charging current is proportional to scan rate (equation 1.9), and the current due to the surface redox processes is also proportional to scan rate. For surface bound species, peak current for an irreversible redox reaction is

$$i_p = \frac{n_a \alpha n F^2 A \nu \Gamma_o^*}{2.718RT} \qquad (1.11)$$

where C^* is the reactant concentration in solution bulk in mole/cm^3, n is the number of electrons involved in the reaction, α is the electron transfer coefficient, n_a is number of electrons involved in the rate determining step, and Γ_o^* is the surface excess (mole/cm^2).

Equation 1.11 shows that the faradaic background current is proportional to the scan rate. However, faradic peak current for a diffusion-controlled irreversible process is proportional to a square root of the scan rate.

$$i_p = (2.99\times10^5) n (\alpha n_a)^{1/2} A C{\cdot} D^{1/2} \nu^{1/2} \qquad (1.12)$$

where D is the diffusion coefficient of the reactant in cm^2/s. Thus the ratio of the faradic diffusional current to background current can be expressed as follows,

$$\frac{i_f}{i_b} \propto \frac{\sqrt{\nu}}{\nu} \propto \frac{1}{\sqrt{\nu}} \qquad (1.13)$$

where i_f and i_b are the faradic diffusional current and the background current, respectively.

Equation 1.13 indicates that as the scan rate increases, the current i_f(signal) decreases relative to the background current, i_b. Consequently, at high scan rates, this current is buried in the enormous background current. Thus, faradaic currents can not be measured directly from such voltammograms. Furthermore, the instrumental noise becomes noticeable as the background current increases. However, with the aid of background subtraction and noise-filtering techniques, fast scan voltammetry has been demonstrated to be useful for quantitative analysis.[52,56] In fact, submicromolar detection limits have been reported.[52,56] Figure 1.6 shows the effect of background subtraction on extraction of the faradaic current out of the background current.

One of the great advantages of fast scan voltammetry is its high temporal resolution, which allows observation of rapid concentration changes in the micromolar range. This advantage is particularly useful in monitoring rapid changes of concentration of biological species in vivo which may require subsecond or better temporal resolution.[15] Another significant advantage of fast scan voltammetry is its ability to differentiate different species by their kinetic differences as well as their redox potentials.[52,56] Species with fast electron transfer rates show reversible voltammetry at high scan rates, while species with slow electron transfer rates react at larger overpotentials at high scan rates and , consequently, can be easily distinguished from the more reversible species. This strategy of improving selectivity has been very effective in reducing interferences in the measurement of dopamine in vivo.[56]

The fact that the electrode stability can be improved with fast scan methods is of particular importance in bioanalysis. Many redox reactions of biological species (such as dopamine, uric acid, and NADH) have follow-up chemical reactions which produce side products. These products can adsorb and foul the electrode surface. In most experiments

Figure 1.6. Illustrations of fast cyclic voltammetry and background subtraction: (a) applied potential waveform as a function of time; (b) current as a function of time; the solid line is the background current and the dashed line is the current in the presence of electroactive species; (c) A background subtracted voltammogram of (b); dashed line in (b) subtracted from solid line in (b) and the result plotted as a function of potential.[13]

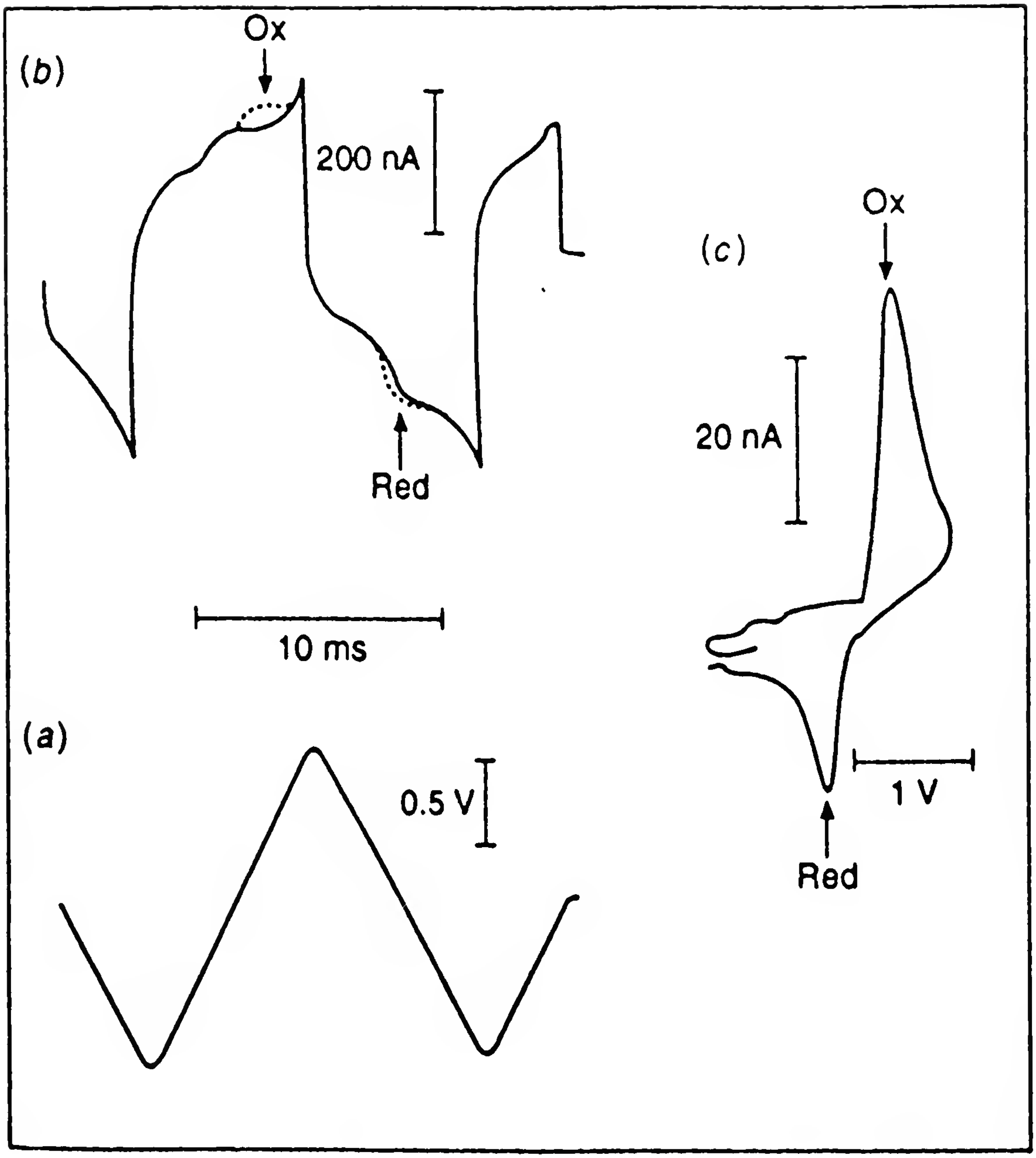
(b)
Ox
200 nA
Red
10 ms
(a)
0.5 V
(c)
Ox
20 nA
1 V
Red

electrode activity decreases after several scans. In fast scan voltammetry, because voltages are swept back and forth in a short time, the reductive or oxidative products are converted back to the original analyte before they have an opportunity to undergo follow-up reactions. Thus, surface fouling due to adsorption of products can be prevented. Consequently, the stability of electrodes can be improved.

Compared with chronoamperometry, fast scan voltammetry can provide more information about the analyte, which can help identify analytes of interest. Because different redox reactions have unique redox potentials, the information can add more confidence that the analyte of interest is being detected in a complicated environment. This advantage may be undermined during in vivo measurements if the diffusion layer of the analyte is blocked by tissue or clogged by blood. However, fast scan rates can alleviate this problem because the diffusion layer is smaller at higher scan rates.

Importance of iR compensation for accurate fast kinetic measurements

Even though iR loss and cell time constant are small at a UME, they are not negligible at scan rates above 1000 V/s if an accurate kinetic measurement is desired, especially at electrodes such as carbon. Carbon electrodes have a large and irregular background current in aqueous solutions which comes from large double-layer capacitance and from redox reactions of surface groups. Since a variety of surface-bound functional groups with different formal potential ($E^{0'}$) values may be present, the faradaic background current may be potential-dependent. This background current may affect the accuracy of kinetic measurements because background current is proportional to scan rate.

The large and irregular background current on carbon electrodes limits the upper limit of useful scan rates to around several hundred V/s.[52,56] Due to the large iR loss and the irregular shape of the background current at high scan rates (above 1000 V/s), the elimination of the iR drop and background subtraction become necessary if significant kinetic information is to be extracted from the voltammogram.

The relationship between the ohmic drop (iR) and the effective scan rate (v_{eff}) on a working electrode can be expressed by the following equations,

$$v_{eff} = \frac{dE_w}{dt} = \frac{d(E_{app}+iR)}{dt} = \frac{dE_{app}}{dt}+R(\frac{di}{dt})=v+R(\frac{di}{dt}) \qquad (1.14)$$

where E_{app} (V) is the potential applied to the cell, E_w (V) is the true potential of the working electrode, i (μA) is the current flowing through the working electrode, R (Ω) is the cell resistance, v_{eff} (V/s) is the effective scan rate at the working electrode, and v (V/s) is the scan rate applied to the cell which is constant during the experiment. The effective scan rate at the working electrode is not a constant when R is not zero and a faradaic current (background faradaic current due to the surface reactions or faradaic current of analytical species in solution) is present (equation 1.12), and the voltammograms cannot be treated according to theories developed for cyclic voltammetry which assume constant scan rate at the working electrode during the experiment.

Figure 1.7 demonstrates the effects of cell resistance and the double-layer capacitance on the applied potential. Figure 1.7 (top) is a simulation of the effect of the cell resistance on the potential at the working electrode. The deviations of the effective potential (potential on the working electrode) from the applied potential (triangular waveform) are caused by the faradic current (from the electroactive species in solution) and the cell resistance (i.e., iR drop). Furthermore, when the double-layer capacitance is considered (Figure 1.7 bottom), the combined effects of the double-layer charging and the cell resistance severely disfigure the shape of potential sweep.[57]

Two approaches are commonly used to compensate the iR drop. The first approach is to simulate and fit the distorted experimental voltammograms by incorporating the ohmic and the capacitive factors.[58,59,60] However, it is difficult and complicated to compensate the iR drop with the simulation method because the effective scan rate (ν_{eff}) and the total current (i) are mutually dependent on each other. To make the situation worse, the charging current is affected by the presence of the faradaic current, since,

$$i_c = C_d \nu_{eff} = C_d[(\nu + R(\frac{di}{dt})] = C_d \nu + C_d R(\frac{di}{dt}) \tag{1.15}$$

where i_c is the charging current, C_d is the capacitance of the electrode, i is the total current (faradaic and charging) passed at the working electrode. According to equation 1.14 , ν_{eff} is a function of the faradaic current and the charging current.

On the other hand, because the charging current affects the effective scan rate (equation 1.14), which affects the faradaic current, the faradaic current in the presence of the charging current is not the same as the pure faradaic current. These factors coupled together complicate the simulation approach.

Another approach to solve the problem of the iR drop is to use a potentiostat with an on-line iR compensation circuit.[61,62,63] This approach is simple and straightforward. A potentiostat with an on-line iR compensation circuit can be used to compensate cell

Figure 1.7. Simulation of the effects of cell resistance and double layer capacitance on the effective scan rates (the shape of the applied potential); measured (effective) potential (solid line), applied potential (dashed line).[57] Top: the effect of the cell resistance only. Bottom: the effects of the resistance and the capacitance.

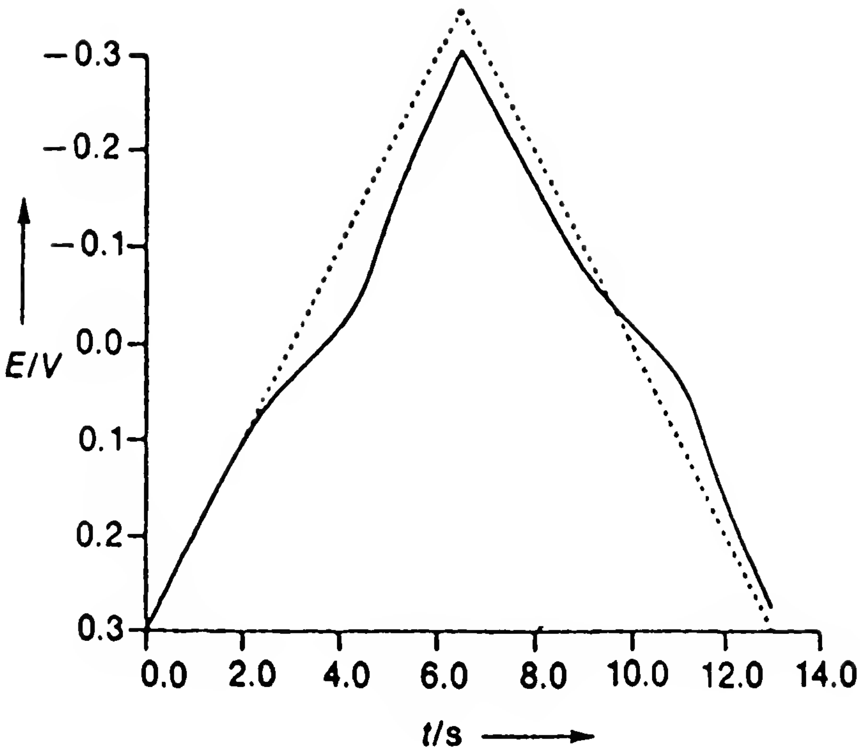
−0.3
−0.2
−0.1
0.0
0.1
0.2
0.3
E/V
0.0
2.0
4.0
6.0
8.0
10.0
12.0
14.0
t/s

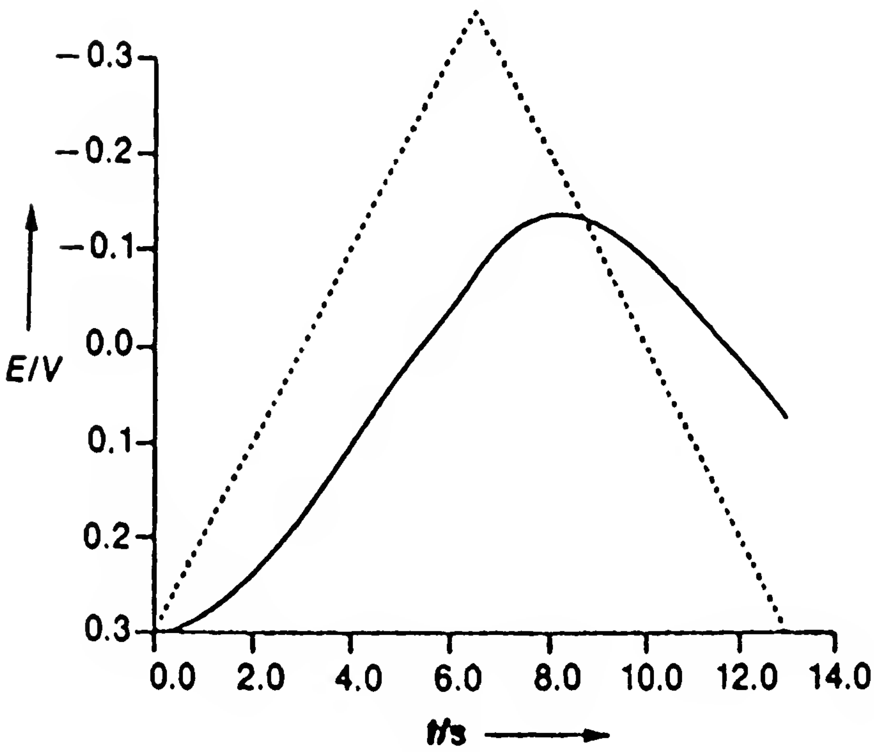
−0.3
−0.2
−0.1
0.0
0.1
0.2
0.3
E/V
0.0
2.0
4.0
6.0
8.0
10.0
12.0
14.0
t/s

resistance (R) to negligible values. This makes the second term (R(di/dt)) in equation 1.14 close to zero, thus ensuring that the scan rate at the working electrode is constant and the iR loss is eliminated. An iR corrected voltammogram can be acquired on-line and the kinetic information can be obtained directly, which is a simple and easy approach compared to the off-line mathematical simulation.

High Efficiency of Mass Transport

As the redox reaction occurs, the reactant is being depleted at the electrode surface. The depletion of the reactant at the surface causes the reactants in solution bulk to diffuse to the electrode due to the concentration gradient between the solution and the surface. If the rate of the redox reaction at the electrode surface is faster than the rate of mass transport (diffusion), a diffusion layer will begin to grow with time. The thickness of the diffusion layer, δ (cm), can be described by the following equation,

$$\delta = \sqrt{\pi D t} \qquad (1.16)$$

where D is the diffusion coefficient of the diffusing species (cm^2/s) and t is the experimental time (s). Figure 1.8 illustrates the growth of the diffusion layer as a function of time at a disk electrode. As the Figure 1.8 shows, the diffusion layer thickness at a short time (t_1) is very small compared to the electrode radius. When the reaction time becomes longer (t_3-t_5), the diffusion layer becomes thicker. At the UMEs, the diffusion profile is transformed from linear diffusion to radial diffusion, and the mass transport is greatly enhanced due to the diffusion from the edges. This enhancement of mass transport is called an edge effect or an effect of radial diffusion. Under radial diffusion conditions, the mass transport rate is given by the mass transport coefficient m (cm/s). The dependence of m on the electrode radius is described as follows,[13]

$$m = \frac{D}{r} \tag{1.17}$$

where m is the mass transport coefficient (cm/s), D is the diffusion coefficient of the diffusing species (cm^2/s), and r is the radius of the electrode. Consequently, for a very small electrode the mass transport coefficient can be very high.

As Figure 1.8 illustrates, the diffusion type (linear or radial) is determined by the ratio of the diffusion layer thickness (δ) to the radius of the electrode (r). If δ/r is much less than one, diffusion is linear. If δ/r is significantly greater than one, diffusion becomes radial. Because δ is a function of time (as equation 1.12 describes), radial diffusion can be achieved at an electrode of any size (r) as long as the experimental time is sufficiently long. However, as the radius of the electrode decreases, the value of δ/r increases, which ensures radial diffusion at shorter time scales. A more quantitative illustration of the relationship of the diffusion layer thickness, electrode size, and the experimental time scale can be obtained from the following equation,[13]

$$\eta = \sqrt{\frac{Dt}{r^2}} \tag{1.18}$$

Figure 1.8. Growth of a diffusion layer as a function of time ($t_1 < t_2 < t_3 < t_4 < t_5$) where the lines represent a cross section of the interface between the diffusion layer and the solution bulk. At time t_1, diffusion is linear. As time scale increases, diffusion becomes a mix of linear and radial diffusion. Eventually, diffusion behavior transforms to a radial diffusion.

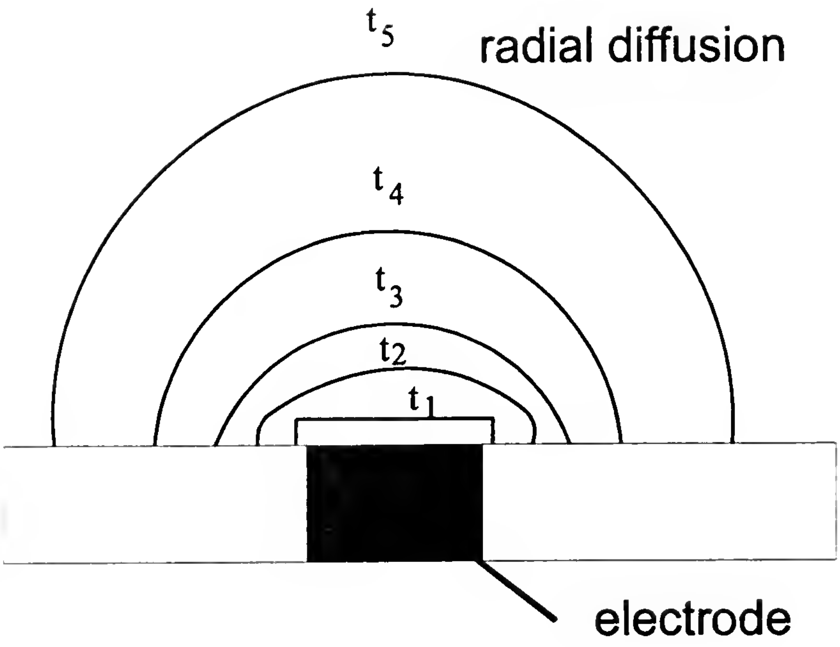
t_5
radial diffusion
t_4
t_3
t_2
t_1
electrode

where η is a unitless quantity, D is the diffusion coefficient (cm^2/s), t is time (s), and r is the radius of the electrode (cm). For values of η greater than 6, diffusion is considered as radial. For values of η less than 1, diffusion is linear.

The radius of an UME is small enough to establish radial diffusion at time scales of 1 s or less. For a 1 and a 10 μm UME, the time needed to reach radial diffusion is about 0.01 and 1.3 s, respectively. Thus, at common experimental time scales the enhancement in mass transport can be taken advantage of at UMEs. Figure 1.9 illustrates the effect of electrode size on diffusion behavior of time scales of seconds.

For a chronoamperometric experiment, the effect of enhanced mass transport on current density can be calculated,[13]

$$\frac{i_{radial}}{i_{linear}} = 1 + \sqrt{\pi \frac{Dt}{r^2}} \qquad (1.19)$$

where i_{radial} ($\mu A/cm^2$) is the current density under radial diffusion conditions, i_{linear} ($\mu A/cm^2$) is the current density under linear diffusion conditions, D (cm^2/s) is the diffusion coefficient (cm^2/s), t is time (s), and r is the electrode radius (cm). Based on equation 1.19, after 1 s the current density at an UME with a diameter of 1 μm is about 100 times greater than at a conventional size electrode (1 cm). This higher current density is particularly useful in analytical measurements. Since the noise or background in the electrochemical measurements is proportional to the electrode area, the high current density (faradic current per electrode area) can allow higher sensitivity and lower detection limits.

Figure 1.9. The effects of electrode size on diffusion behavior at common experimental time scales (several seconds or less).

Edge effect of UME

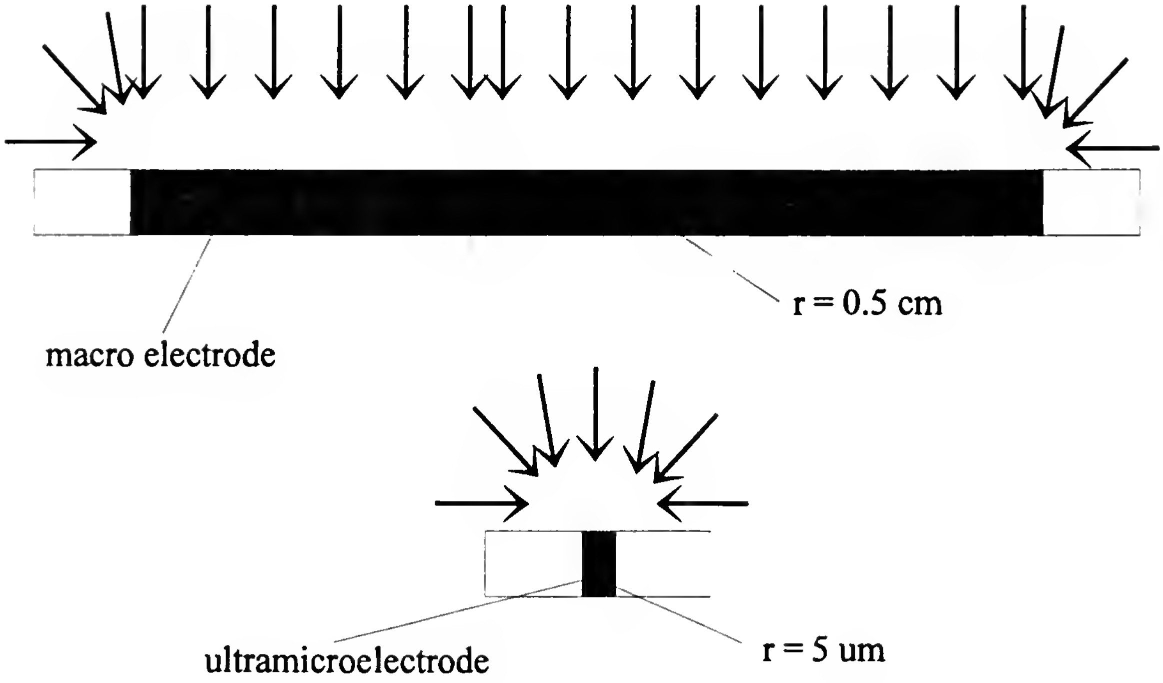
r = 0.5 cm
macro electrode
ultramicroelectrode
r = 5 um

Circuit Design for UMEs Experiments

Although current densities of UMEs are much higher than for conventional size electrodes, the absolute current magnitudes at UMEs are extremely small (nA to pA) due to the small electrode radius which determines the electrode current. Thus, current measurements at UMEs are difficults and can not be done with conventional potentiostats. A part of this project was to design and build a potentiostat for measurements at UMEs. The design and construction of such instrumentation played an important role in this work because it allowed us to investigate and exploit unique properties of UMEs under different experimental conditions. The instrumentation design took advantage of very small current magnitudes at UMEs. In a conventional three-electrode configuration potentiostat, an auxiliary electrode is needed to bypass the large current from the reference electrode, otherwise the reference electrode will be polarized by the large current which will cause the shift of the reference electrode potential. Unlike conventional potentiostats with a three-electrode configuration, the potentiostat for UME measurements can have a simple two-electrode configuration which is possible due to the small magnitude of the currents passed at UMEs.[64,65] The following sections introduce the basic design of such instrumentation. Details of the instrumental design will be discussed in Chapter 2.

Potentiostat for UMEs experiments at low scan rates (less than 10 V/s)

Because conventional potentiostats can not measure currents lower than µA, a current amplifier is necessary to amplify currents for a conventional potentiostat. The current amplifier built in our laboratory has different gains (10^2 to 10^4) and time constants (1 , 10, and 100 μs) to fit different experimental requirements. By using this current amplifier with a conventional potentiostat, pico ampere currents can be measured.

Potentiostat for UMEs experiments at high scan rates (higher than 10 V/s)

The conventional potentiostats were designed to perform cyclic voltammetry at scan rates below 10 V/s, thus, the time constant of the noise filter in these potentiostats is set above 100 μs to eliminate high frequency noise. In addition to the time constant of the noise filter, the instrumental time constant is also limited by the speed of the analog-to-digital converter (ADC) for digital potentiostats or by the speed of the plotter for analog potentiostats. Because the large cell time constant of macroelectrodes sets the limit on a maximum scan rate in cyclic voltammetry, before the instrumental time constant can affect the voltammograms, there has been no need for a short instrumental time constants or fast ADC in conventional potentiostats. However, at UMEs, the cell time constant is small (ca. 1μs) and the highest scan rate reported is as high as 200,000 V/s.[26] Because of the large instrumental time constants of the conventional potentiostats, voltammograms begin being distorted at scan rates above 10 V/s even though the cell time constant at UMEs permits scan rates up to 200,000 V/s. Thus, a new design of a potentiostat is needed to perform fast scan voltammetry. Since the small current at UMEs allows a two-electrode configuration potentiostat to be used, we modified the current amplifier described above to make a two-electrode configuration potentiostat for fast scan measurements. The potentiostat which was constructed is able to perform fast scan voltammetry up to 4,000 V/s without distortion from the time constant of the potentiostat. For the purpose of detecting low concentrations of analytes at high scan rates, the noise level of this homemade potentiostat was reduced by a first order filter and low noise operational amplifiers.

Potentiostat for high-scan-rate measurements at UMEs with on-line iR compensation

This potentiostat has a two-electrode configuration with an on-line positive current feedback iR compensation circuit. The operational amplifiers used in the circuit are current feedback operational amplifiers, having very wide bandwidths (above 100 MHz) and high gains. The main consideration in the circuit design was the speed (or bandwidth) of the operational amplifiers. In order to compensate on-line for the iR drop, the current passing through the working electrode needs to be fedback to the reference electrode as fast as possible to makeup the iR loss in the applied voltage. The circuit is very noisy due the wide bandwidth of the operational amplifiers. To extract the signal out of the noise, concentrations of analytes above 1mM are needed in order to produce sufficiently large signals. Therefore, this circuit is well suited for fast kinetic measurements but not for trace analysis.

Surface Modification of UMEs

Polymer-film-modified electrodes

Modified electrodes have received tremendous attention in the past 10 years.[66,67] The main goal is to improve the selectivity and the sensitivity of the electrodes with the modifiers. One of the best known modifiers is Nafion (a perfluorosulfonated ionomer) which is anion selective and repels anions with its negatively charged sites SO_3^-. As mentioned above, UMEs have many advantages due to their small size. However, selectivity of UMEs is not improved as the size of the electrode decreases. An useful strategy to improve selectivity is to modify the electrode surface with permselective films. For example, a common application of UMEs is in in-vivo measurements of neurotransmitters such as dopamine (DA) in the central nervous system. However, voltammetric responses of the neurotransmitters usually suffer from the interference of ascorbic acid (AA) which coexists in-vivo at concentrations 10^3 to 10^4 times higher than the concentration of the neurotransmitter. UMEs coated with Nafion films are usually used to resolve this problem, since Nafion can repel anions such as AA. Nevertheless, the use of Nafion has some disadvantages. Electrodes modified with Nafion films usually suffer from slow response times due to low diffusion coefficients of analytes in the film, memory effects due to the strong binding between the cation analytes and Nafion and saturation of negative sites when cations are present at high concentration.[68,69,70]. Besides these problems with the performance of Nafion, thickness and quality of Nafion films is difficult to control and reproduce.

Recently, a new class of cation permselective films has been investigated by our group.[71,72,73] It was shown that overoxidized polypyrrole (OPPy) films can be made quite permeable, and have ionic conductivity, although the electrical conductivity of polypyrrole (PPy) is lost after overoxidation. During overoxidation, carbonyl groups are introduced into the polymer backbone forming overoxidized polypyrrole (OPPy).[74] The high electron density of the carbonyl groups acts as a barrier to anion diffusion in the film. In our previous investigation, the OPPy films (thickness of 0.1 μm) were shown to have excellent cation permselectivity. Since OPPy repels anions with neutral carbonyl groups instead of the negative charge sites, electrostatic binding does not occur and the OPPy has a fast response time, fewer memory effects, and is free from the problem of binding site saturation.

A thinner ion-selective film is always desirable due to faster response time and higher sensitivity. The permeability of films is expressed by the following equation,

$$P_m = \frac{\alpha D_m}{\delta_m} = \frac{D_{app}}{\delta_m} \tag{1.20}$$

where P_m (cm/s) is ilm permeability, α is membrane partition coefficient, D_m (cm^2/s) is the diffusion coefficient within the film, D_{app} (cm^2/s) is the apparent diffusion coefficient in the film, and δ_m (cm) is the film thickness. According to equation 1.20, the permeability of the film increases as δ_m decreases. High permeability will allow analyte to reach the surface easily, hence a fast response time and a higher sensitivity can be achieved.

Besides the higher sensitivity gained from an ultrathin film, ultrathin organic films may be used as a precoated material to assist growth of compact conducting polymers. This subject has been addressed by several authors recently. Gottesfeld and coworkers have reported that preassembling an organic monolayer on electrodes can assist in the formation of a more compact conducting polymer with better adhesion characteristics.[75] Matsue and Uchida's group have reported that hydrophobic pretreatment of a substrate promotes lateral growth of PPy.[76] In general, growth of the conducting polymers can be manipulated at precoated organic films because of the hydrophobic interactions between the precoated organic film and the monomers. The OPPy ultrathin film may serve as a precoating material to control the growth of the conducting polymers. Since the film is compact but yet permeable to monomers, it may help grow more compact and adhesive conducting polymers. Similar work has been reported by Bélanger's group who used an ionically conducting polymer (Nafion) to promote lateral growth of PPy.[77]

Surface-oxide-modified electrodes

Electrochemical pretreatment (ECP) has been found to be quite effective in improving electrode selectivity and sensitivity.[78] It is particularly useful to pretreat carbon electrodes due to the ability to produce rich oxide surfaces.[78] The properties of the oxidized surface are different because of the high charge density and the ability of the surface functional groups to catalyze redox reactions.[78] Figure 1.10 illustrates various surface functional groups on carbon electrodes, such as phenol, quinone, carbonyl, and carboxylic acid, which can form as a result of surface treatment.[78] The negative charge of the carboxylic group at neutral pH and the abundance of electron density on oxygen on treated electrode surfaces can prevent anions from approaching the electrode surface. Consequently, redox

Figure 1.10. A possible structure of surface oxide groups on a carbon electrode (reference 78).

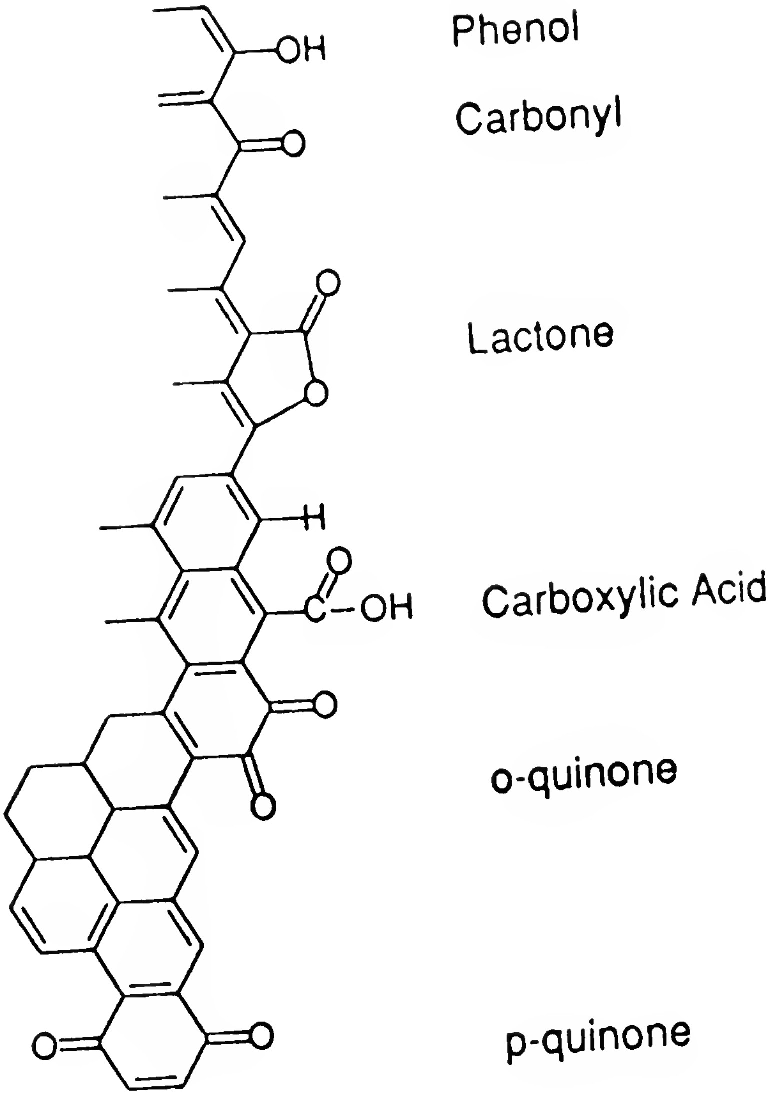
Phenol
Carbonyl
Lactone
Carboxylic Acid
o-quinone
p-quinone
OH
H
C–OH
O

reactions of anions can be deterred.[79] On the other hand, cations have been known to be concentrated on the pretreated electrode surfaces presumably due to the electrostatic attraction by the opposite charge of the surface.[78] The ability of the surface functional groups to preconcentrate and catalyze reactions of cations improves the sensitivity and the electrochemical kinetics increase at treated electrodes. ECP may also improve sensitivity by cleaning debris and impurities on electrode surfaces. ECP usually increases background currents as the surface becomes rougher and the amount of the surface functional groups is increased. Resistance of the electrode also increases after the electrochemical pretreatment which may be attributed to the insulating nature of the surface groups, especially oxides, which can form on the treated electrodes. We observed that the resistance of a freshly cut fiber carbon electrode is about 6 kΩ and it can go up to 50 kΩ after pretreatment.

Purpose of Work

The purpose of this work was to develop new strategies and fast scan techniques for analytical measurements with UMEs in aqueous solutions. We focus most of our efforts on the exploitation of fast scan technique with UMEs in the characterization of fast redox reactions of biological species, improvement of S/N, selectivity and detection limits. Fast redox reactions investigated with fast scan voltammetry in aqueous solutions at carbon fiber UMEs helped us understand the properties of the electrode surface and its effect on the redox reactions at fast scan rates. To improve selectivity of UMEs in biosensing, UMEs were modified with ultrathin polymer films. The ultrathin films provide selectivity by deterring anion diffusion but allowing cations to reach the electrode surface efficiently which results in higher sensitivity for cationic analytes. The properties of the ultrathin films were characterized and their applications in bioanalysis were demonstrated in this work.

New strategies for using fast scan voltammetry in detection of trace biological species in complex environments have been proposed and developed. These strategies involve signal averaging, improved temporal resolution, improved instrumental design, and selectivity enhancement through enhancement of the kinetic differences between the analyte and the interferant.

CHAPTER 2
EXPERIMENTAL SECTION

Reagents and Solutions

Acetonitrile (MeCN) was obtained from Fisher. Pyrrole and tetrabutylammonium perchlorate (TBAP) were from Kodak. Potassium ferricyanide ($Fe(CN)_6^{3-}$) and ascorbic acid (AA) were obtained from Mallinckrodt. Hexaamineruthenium (III) chloride ($Ru(NH_3)_6^{3+}$) was purchased from Alfa Products. Pyrrole-2-carboxylic acid (Py-2-COOH) was purchased from Aldrich. Dopamine (DA) was purchased from Sigma. All chemicals were used as received. Uric acid (Sigma) was prepared in 1 M phosphate buffer of pH 7.0. Hexaamineruthenium (III) chloride and potassium ferricyanide were prepared in 1 M aqueous KCl solution or in 0.5 M phosphate buffer at pH 7.4. DA and AA were prepared in 70 mM phosphate buffer of pH 7.4.

Electrodes

Reference and Auxiliary Electrodes

A saturated calomel electrode (SCE) was used as the reference electrode. When

MeCN was used as the solvent, a quasi-reference electrode (a 5 cm long Ag wire) was used as a reference to avoid water contamination of the organic solvent and to prevent establishment of liquid-liquid junction potentials.[80] If a three-electrode potentiostat was used, a 1 cm^2 platinum foil was used as an auxiliary electrode.

Working Electrodes

Glassy carbon electrodes (ca. 0.67 cm^2 , Electrosynthesis Co.), carbon fiber ultramicroelectrodes (7 μm diameter, Textron Specialty Materials, Inc.) , and platinum ultramicroelectrode (5 μm Pt wire sealed in glass, Goodfellow Co.) were used as working electrodes. The experiments using rotating disk electrode (RDE) were conducted with an IBM RDE Controller and Rotator. The screw-on electrode tip was made from Teflon, with a 3 mm diameter glassy carbon rod sealed into the end by heat pressing. Prior to each measurement the working electrodes were polished on an Alpha A polishing cloth (Mark V laboratory) with gamma alumina suspensions of 0.1 μm particle size (Gamal, Fisher Scientific Co.) and were ultra-sonicated afterwards in doubly distilled water for 5 minutes.

Fabrication of UMEs

Carbon fiber electrodes sealed in heat shrinkable Teflon tubes

Carbon fiber ultramicroelectrodes were prepared from 7 μm diameter carbon fibers (Textron specialty materials 7440-44-0) and were sealed in a heat shrinkable Teflon tube

(Zeus ZDS-S-036). This Teflon tube had two layers and when it was heated, the outer layer of the tube shrunk and the inner layer melted. The inner diameter of the tube could shrink to virtually zero. The details of making the UMEs are given below.

A piece of carbon fiber (ca. 3 cm long) was glued to a copper wire (ca. 6 cm long) with silver epoxy (EPO-TEK 410 E, Epoxy Technology Inc.). The epoxy was allowed to dry. The silver epoxy serves as a conductive connector which connects the carbon fiber and the copper wire. The carbon fiber connected to the copper wire was then placed into a Teflon tube and the tube was wrapped with an aluminum foil. A lighter or gas torch was used to heat the foil for about half a minute until the carbon fiber was well sealed in the tube. The heating process needs to be carefully controlled to avoid overheating. The tip of the carbon fiber sealed with Teflon was then cut with a scalpel to expose the disk-like UME. By following this procedure a well sealed ultramicroelectrode can be made easily and quickly. To avoid introducing contaminants, the electrodes were used directly without polishing. An illustration of this UME is shown in Figure 2.1-A.

Carbon fiber electrodes sealed in epoxy

Carbon fiber was first connected to a copper wire with silver epoxy. After the epoxy dried, the copper wire with attached carbon fiber was inserted into a capillary glass tube or a plastic micropipet tip (ca. 1mM radius). The copper wire was then glued with epoxy to the capillary glass tube for easy handling. Another epoxy mixture was made from the epoxy resin and the hardener. The mixture was heated on a hot plate until the epoxy became transparent and liquid-like. The epoxy liquid was carefully stirred to get rid of air bubbles

Figure 2.1 Schematics of UMEs used in this work. (a). Carbon fiber (7µm) sealed with Teflon. (b). Carbon fiber sealed with epoxy (c). Pt wire sealed (5µm) in glass.

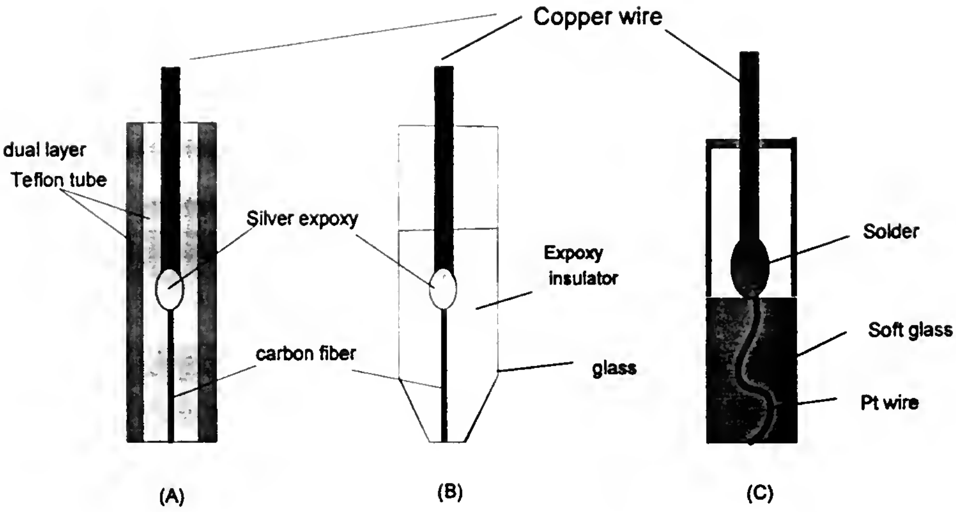
Copper wire
dual layer
Teflon tube
Silver expoxy
carbon fiber
Expoxy
insulator
glass
Solder
Soft glass
Pt wire
(A)
(B)
(C)

trapped in the liquid. The epoxy liquid was then pipetted into the capillary glass tube. The whole tube was then placed in an oven and heated for one hour at ca. 150 °C. After the epoxy hardened, the extra epoxy at the tip was removed with sandpaper to expose a disk-like UME. This working electrode was polished prior to each measurement on an Alpha A polishing cloth (Mark V laboratory) with gamma alumina suspension of particle size of 0.1 μm (Gamal, Fisher Scientific Co.). An illustration of this UME is shown in Figure 2.1-B.

Platinum wires sealed in soft glass

Metallic electrodes can be to be sealed with glass. A piece of Pt wire (r=2.5 μm) was inserted into a soft glass tube (melting point = 500 °C, Kimble Inc). A gas torch was used to melt the tip of the glass, which caused the melting glass to seal the Pt wire. The melting process has to be carefully controlled to minimize the formation of air bubbles in the melting glass which will cause imperfections in the seal. After the glass tube cooled to room temperature, the glass tip was removed with sandpaper until the end of the Pt wire was exposed. A disk-like Pt UME was formed. The electrical contact was made by inserting a Cu wire into the other end of the glass tube. Pieces of solder were put into the glass tube and the glass tube was gently heated until the solder melted and embedded the Pt and the Cu wire. The connection between the Pt wire and the Cu wire was formed after the glass tube cooled down to room temperature and the melted solder became solid. Figure 2.1-C shows a cartoon illustration of this type of electrodes.

Electrode Pretreatment

The electrochemical pretreatment of carbon fiber electrodes was carried out in 1 M phosphate buffer in the experiments with uric acid as analyte, and in 1 M KCl solutions in kinetic measurements with $Ru(NH_3)_6^{(3+/2+)}$ and $Fe(CN)_6^{(3-/4-)}$. The parameters for the treatment were as follows: square-wave potential, lower potential limit -1.0 V, upper potential limit +2.0 V, frequency 70 Hz; duration 5 min. The conditions for the pretreatment were chosen because a previous report had shown that such pretreatment can improve the reaction kinetics of uric acid.[81]

When analysis with fast scan voltammetry at carbon fiber electrodes, the electrodes were pretreated to stabilize the background. The electrodes were treated by a cycling for 30 minutes in the potential window from -0.8 to +1.2 V in 70mM phosphate buffer.

Instrumentation

IR Compensation Circuit and Its Operational Principle

All iR compensation experiments were carried out with a homemade instrument (see Figure 2.2) of a design which was adapted from that described by Saveant's group.[82] The design was modified to suit our experimental purposes. An operational amplifier (OP27) was added to the circuit to further amplify signal and eliminate noise at low scan rates (less than 1000 V/s). The potentiostat had a two-electrode configuration and an on-line positive

Figure 2.2 Schematic of a potentiostat built for fast measurements with iR compensation.

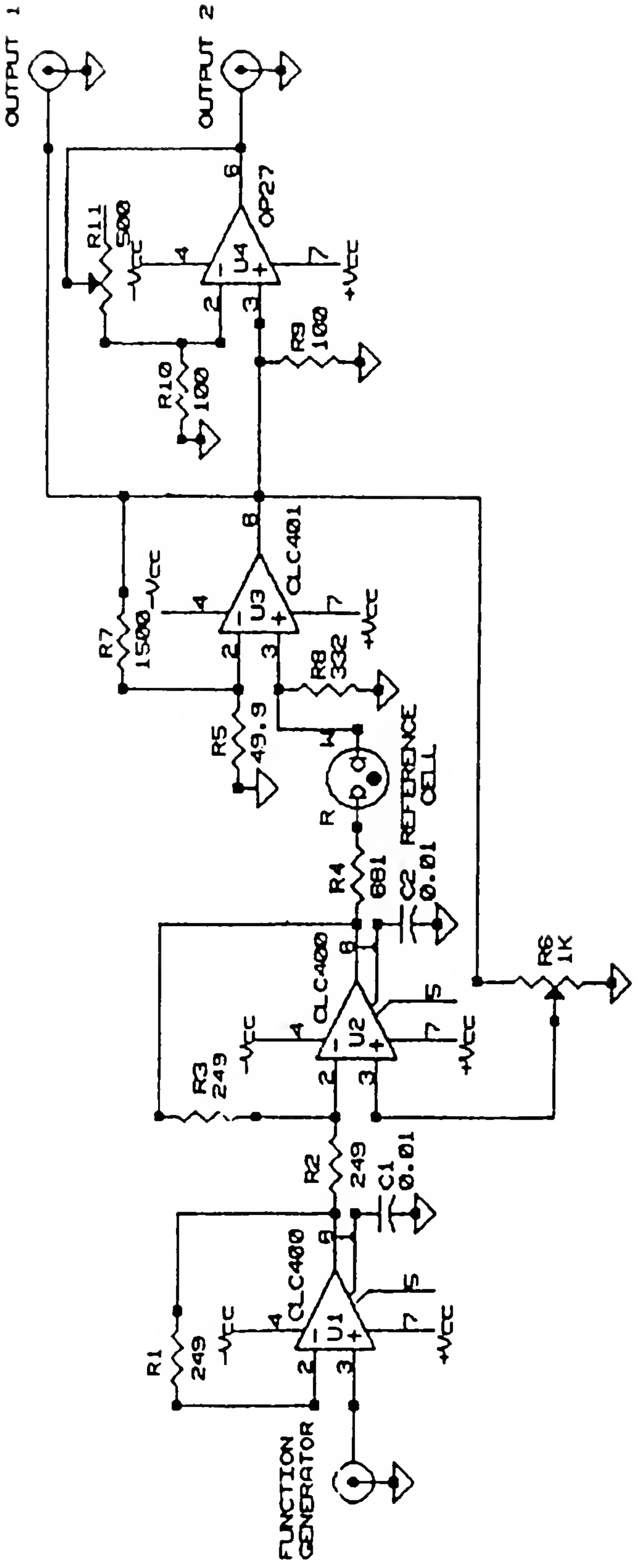
FUNCTION GENERATOR
U1
CLC400
R1
249
R2
249
C1
0.01
R3
249
U2
CLC400
R4
681
C2
0.01
R6
1K
R
W
REFERENCE CELL
R5
49.9
R7
1500
R8
332
U3
CLC401
R9
100
R10
100
R11
500
U4
OP27
-Vcc
+Vcc
2
3
4
5
6
7
8
OUTPUT 1
OUTPUT 2

current feedback iR compensation circuit. The potentiostat was based on two types of current feedback operational amplifiers (CLC 401 and CLC 400) obtained from the Comlinear Corporation.

Voltage at the positive input of the amplifier U3 equals to the current to be measured (i) times the sampling resistor (R_8). Voltage iR_8 is applied to the positive input of the amplifier U3 and is then amplified by a factor of $1 + R_7/R_5$ (R_7 and R_5 are the feedback and the gain resistors of the amplifier U3, respectively). Thus, the output voltage at output 1, U_s, to be measured by the digital oscilloscope, is:

$$U_s = R_8(1 + R_7/R_5)i \tag{2.1}$$

where U_s is the voltage output (V), R are the resistances (Ω) of the resistors in the circuit, and i is the current measured at the working electrode, W. The output voltage was monitored and recorded on the LeCroy 9310 digital oscilloscope.

The operational amplifiers used in the circuit, CLC 400 and CLC 401, are current feedback operational amplifiers. Unlike the conventional voltage feedback operational amplifiers, the bandwidth of the current feedback operational amplifiers depends only on the magnitude of the feedback resistance such as R_7 (see Fig 2.2). Therefore, the current feedback operational amplifiers have a larger bandwidth (at least of a factor of 5) which is very important for high speed experiments, such as fast scan voltammetry. The optimum value of R_7 is 1500 Ω for the CLC401 operational amplifier used in the current measurements.

The current to be measured crosses the sampling resistance R_8 (332 Ω), the value of which is chosen so as to be negligible compared to the input impedance of the amplifier U3 (ca. 200 kΩ). The output voltage, U_s, is fed back to the operational amplifier U2 through a variable resistor, R_6. The magnitude of the feedback is controlled by the fraction of the variable resistance which is applied (i.e. β; $\beta = (R_6 - x)/R_6$; $0 \leq x \leq R_6$). The summation of the positive feedback voltage, $\beta R_8(1+R_7/R_5)i$, with the voltage delivered by the function generator is carried out at the amplifier U2. Because the positive feedback is injected into the positive input of the amplifier U2, and the amplifier has an unit gain, the potential at the output of the amplifier U2 is thus:

$$U + 2\beta R_8(1 + R_7/R_5)i = U + R_c i \tag{2.2}$$

where U (V) is the voltage from the waveform generator (i.e. the original voltage on the reference electrode), β is the fraction of the positive feedback applied to the amplifier U2, i (nA) is the current to be measured, and $R_c = 2\beta R_8(1+R_7/R_5)$ is the "compensation" resistance. R_c can be change by adjusting β. A major concern in the design of an iR compensation circuit is to obtain an exact compensation, not an undercompensation nor an overcompensation. In other words, we need to ensure that the compensation resistance (R_c) is exactly equal to the uncompensated cell resistance (R_u). By doing so, the potential affected by the iR loss, iR_u, will be exactly compensated by the iR_c.

With conventional macroelectrodes, it is possible to design an instrument such that sustained oscillation of the output signal occur when the compensation and the cell resistances are practically equal. A simple determination of R_u is ensured, leading to a precise knowledge of the remaining uncompensated resistance in each experiment. This is so because the time constant of the instrument is much shorter than the cell time constant of a macroelectrode, R_uC_d. This is no longer true at a UME, because cell time constants with UMEs as working electrodes are comparable with the instrumental time constants. The following discussion shows how to compensate the iR drop with UMEs as working electrodes with on-line iR compensation.

The on-line iR compensation circuit can be analyzed in terms of a second order approximation as shown by the type of oscillations obtained upon increasing β (i. e. the fraction of the compensation resistance R_6) when it is connected to a resistor-capacitor dummy cell representing the solution resistance and the double layer charging in the absence of the faradaic current. The operational expression for the output voltage is thus:[83,84]

$$U_s = \frac{R_8(1+ R_7 / R_5)C_d v}{(R_tC_d/\omega)p^2+[R_t+(1/C_d\omega)-R_c]C_d\, p+1} \tag{2.3}$$

where p is the Carson-Laplace variable, C_d is the double layer capacitance (F), v is the scan rate (V/s), ω is the bandpass pulsation of the instrument and R_t is the total resistance to be compensated, i.e., $R_4 + R_u + R_8$. A sustained oscillatory behavior is obtained when:

$$R_t + (1/C_d\ \omega) - R_c = 0 \tag{2.4}$$

i.e., when:

$$R_t + R_o - R_c = 0 \tag{2.5}$$

The R_o is the "overcompensation resistance" which equals to $1/C_d\omega$. Thus, if we know R_o, exact compensation can be obtained by first increasing R_c until sustained oscillatory behavior is reached and then decreasing it by an amount equal to R_o. R_o can be derived from the value of the double layer capacitance (C_d) and from ω. C_d is obtainable from the height of the double layer charging current. The parameter ω can be obtained as follows. Dummy cells with known resistances (R_t) and capacitances (C_d) were used to simulate the electrochemical cell. The compensation resistances (R_c) were obtained by increasing β until sustained oscillations appeared. Since R_t, C_d, and R_c were known, the parameter ω can be obtained from equation 2.4. In our experiments, the value of ω was determined as 3.3×10^7 rad/s.

During the experiments, the ohmic drop compensation was performed by increasing the positive feedback (β) until sustained oscillations appeared on the cyclic voltammetric trace. The feedback was then decreased by $1/C_d\omega$ before recording the current-potential curve. The feedback should be carefully tuned to reach sustained oscillations but total oscillations should be avoided. Sustained oscillations are apparent when a noticeable oscillation appears in the beginning of the voltammogram as the compensation resistance increases. If the compensation resistance continues to increase, the magnitude of the oscillation will suddenly change from several mV to ± 7 V (same as the power voltage of the operational amplifiers) and will destroy the voltammogram. This type of oscillation is called total oscillation. The reason for avoiding total oscillations is that the total oscillations (magnitude +7 to -7V) feed back to the electrochemical cell and will cause pretreatment of the carbon fiber electrode. In our experiments, after total oscillations occurred a change in the ΔE_p of electrochemical probes, and the background current was observed.

Experiments were performed using iR compensation when the scan rates exceeded 1000 V/s. At scan rates up to 1000 V/s, iR compensation was not necessary, since the iR loss was insignificant. Because the current decreases as the scan rate decreases, at scan rates below 1000 V/s, the noise in the feedback circuit severely interferes with the small faradaic current. Thus, the circuit was modified to suit the experimental needs. An amplifier (OP27, 8 MHz bandwidth) was added to further amplify the current and filter out the high frequency noise when the scan rates were lower than 1000 V/s. The OP27 amplifier has a much narrower bandwidth (8 MHz) compared to the other two amplifiers (150 MHz for CLC 401 and CLC 400). The narrow bandwidth of OP 27 can function as a filter to eliminate the high frequency noise. Rechargeable Ni-Cd batteries (Radio Shack) were used as a power supply to avoid 60 Hz power line noise. An offset adjustment was used to adjust the offset of the output voltage due to the voltage drift of the operational amplifiers. All connections were made on printed circuit boards to minimize stray capacitances and crosstalk between leads. For the same reason, the leads connecting the digital oscilloscope, the working electrode, and the reference electrode were shortened as much as possible. At lower scan rates, majority of signals were acquired repeatedly 50 times, then averaged to improve signal-to-noise ratio. Data acquisition, signal averaging, background substraction and the measurements of the peak current and the peak potential were all performed on the LeCroy 9310 digital oscilloscope.

The cyclic voltammograms of the analytical species in fast measurements were repeatedly acquired, averaged and stored in the digital oscilloscope. Then the voltammograms of a blank solution were acquired, averaged and subtracted from the voltammograms of the analytical species. The data acquired by the LeCroy oscilloscope were transferred to a Northgate 386 PC for the display and the semi-integration. The data transfer is through an RS-232 interface on the oscilloscope and the communication port number two on the computer (Northgate 386 PC). Two QBasic programs were locally written to communicate with the digital oscilloscope and to perform the semi-integration (see Appendix A and B). A function generator (Model 182A, Wavetek) and an universal programmer (model 175 EG & G) were used to generate triangular waveforms for cyclic voltammetry. The function generator was used as a trigger source to simultaneously trigger the oscilloscope and the universal programmer.

The Current Transducer and the Potentiostat for the UME Experiments

The schematic of the current transducer is shown in Figure 2.3. The design of the current transducer was based on Faulkner's design.[85] We modified the circuit to make it more flexible in the instrumental time constant, and added an output (bypassing the OP27) for fast measurements. The power supply for this instrument was made from rechargeable batteries to minimize 60 Hz power line interference. Two 7.2 V Ni-Cd Turbo racing batteries (purchased from Radio Shack) were used because of their high current output (1200 mAh).

The input operational amplifier (AD515A, Analog Devices) was a monolithic, precision, low power, FET-input operational amplifier. It served as a current-to-voltage converter which amplifies and converts the input currents to voltages. This operational amplifier has a fast slew rate (3.0 V/μs), ultralow bias current (less than 50 fA with ± 5V

Figure 2.3 Schematic of the current transducer.

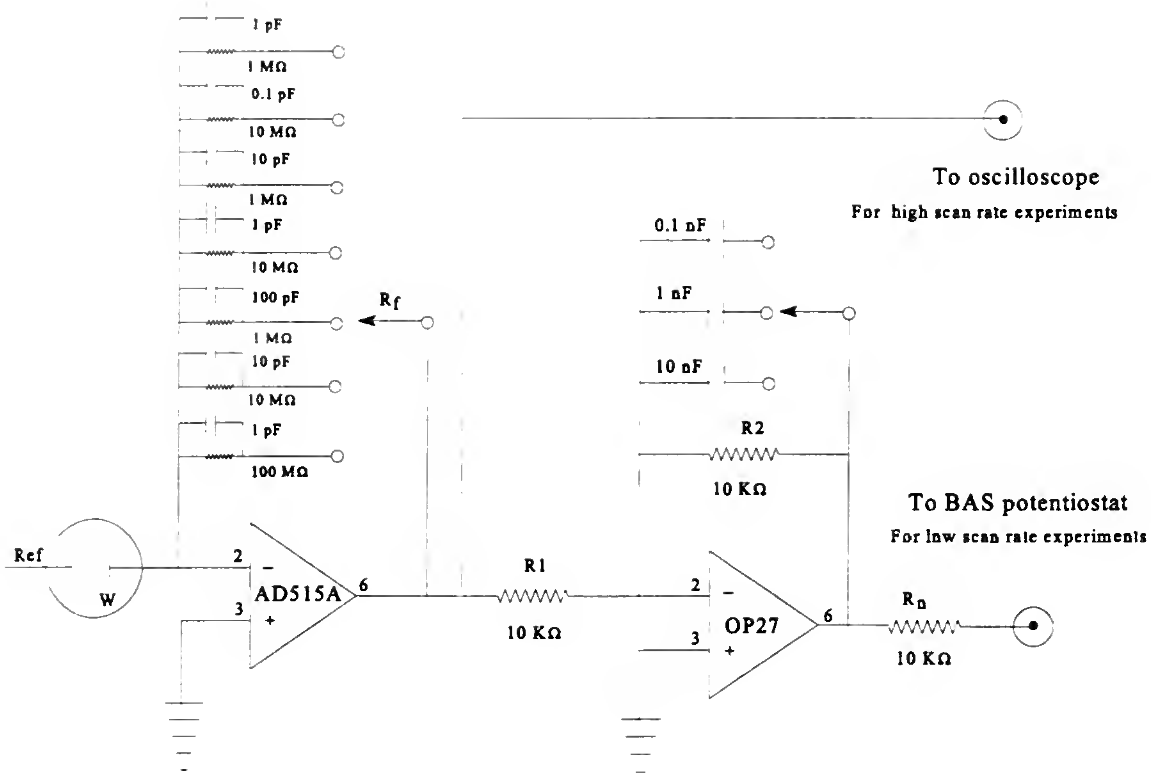
1 pF
1 MΩ
0.1 pF
10 MΩ
10 pF
1 MΩ
1 pF
10 MΩ
100 pF
1 MΩ
10 pF
10 MΩ
1 pF
100 MΩ
Rf
To oscilloscope
For high scan rate experiments
0.1 nF
1 nF
10 nF
R2
10 KΩ
To BAS potentiostat
For low scan rate experiments
Ref
W
2
3
AD515A
6
R1
10 KΩ
2
3
OP27
6
Rn
10 KΩ

power supplies), low input noise voltage (50nV/√Hz), and very low input noise current (0.01pA rms). The bandwidth of the operational amplifier (AD515A) is 1 MHz. The low bias current and the low noise make this operational amplifier suitable for low-level current measurements, yet the fast slew rate and the wide bandwidth make it adequate for fast scan voltammetry at scan rates of kV/s. Various resistors (1, 10 and 100 MΩ) and capacitors (0.1, 1, 10 and 100 pF) in the feedback loop control the gains (100, 1000 and 10000) and RC time constants (1 , 10 and 100 µs). Since the current-to-voltage converter (AD 515A) inverts the input signal phase, a second operational amplifier (OP27) with a unit gain is used as an inverter to invert the phase of the output signal back to normal. The capacitors and the resistor (R_2) on OP27 function as a first order filter, and the RC time constant should be adjusted not to exceed the RC time constant of AD 515A

The commercial potentiostat used in the experiments is Bioanalytical Systems (BAS100) Electrochemical Analyzer. When used with the BAS the output of OP 27 has a 10 kΩ (R_o) resistor connected to the working electrode lead of the BAS. In most commercial potentiostats such as the BAS the working electrode lead feeds a virtual-ground summing junction of a current to voltage converter. The current measured with the BAS in conjunction with the current transducer is $R_f \times (R_1/R_2) \times (R_{BAS}/R_o) \times i$, and is $R_{BAS} \times i$ without the current transducer. Because R_1 equals to R_2, the net gain of the current transducer will be the ratio of R_f/R_o (i.e. the ratio of the feedback resistance of OP AD515A to the output resistance of OP 27). For example, for a 10 kΩ value of R_o the gain is 100, 1000, and 10000 when R_f is 1 , 10 and 100 MΩ, respectively.

For stand alone use in fast scan measurements, the output of OP AD515A bypassed the OP27 and was directly connected to a digital oscilloscope (LeCroy 9310). The digital oscilloscope measures the output voltage (the transduced current). The ratio of the transduced current (output voltage) to the input current (i.e. the current flowing at the UME) was determined alone by the R_f on OP AD515A. The conversion factors for the potentiostat were 1, 10 and 100 V/µA when the resistors (R_f) in the feedback loop of the current transducer were 1, 10 and 100 MΩ respectively. Thus, for a conversion factor of 10V/µA a 10 mV of voltage measured by the oscilloscope corresponds to a 1 nA of the analytical current. The RC time constant of the current transducer was controlled by the feedback resistance (R_f) and the capacitance on OP AD515A. For example, a 1 MΩ of R_f and a 1 pF of a capacitor will give an 1µs of the RC time constant.

Instrumental Setup for Low and High Scan Rate Experiments

At low scan rates, the current amplifier is connected to the BAS. The ground of the instrument should be connected to the ground wire of the BAS to insure proper grounding (see Figure 2.4). The grounding is important for the output voltage of the circuit to be measured correctly by the BAS. A faraday cage was used to shield the circuit from noise and the faraday cage was also connected to the ground. At high scan rates the potential waveform is generated from the function generator and the waveform is applied to the SCE reference electrode. The current at the working electrode is transduced to voltage and amplified by OP AD515A. The transduced current bypasses OP27 and is directly measured with the digital oscilloscope (Figure 2.3). Simultaneously, the waveform applied to the reference electrode is measured at a separate channel of the digital oscilloscope (Figure 2.5). The stored waveform can be later transferred to a computer for plotting the cyclic voltammograms. Since the phase of the potential at the working electrode is reversed relative to the waveform potential at the reference electrode the phase of the potential waveform measured with the oscilloscope needs to be inverted. In addition, the phase of the current passed at the working electrode is inverted by the inverting input of OP AD515A. Thus, to obtain a correct plot of current vs potential (i.e. voltammogram), the phase of the potential waveform and the current stored in the digital oscilloscope are inverted by a computer program (Origin) before plotting the cyclic voltammograms on the computer.

Voltammetry at low scan rates

At low scan rates, the circuit shown in Figure 2.3 can be used as a current amplifier which allows pico ampere currents to be measured with the BAS. The minimum current range of the BAS is 0.1 μA. The gain of the current amplifier ranges from 100 to 10,000. Combing the BAS with the current amplifier, the minimum current range can be low to 100 pico amperes. To minimize noise, a first order filter is used in the circuit (Figure 2.3, OP AD515A). The time constant of the potentiostat is controlled by the time constant of the first order filter in the circuit (Figure 2.3).

Ideally, the time constant should be as large as possible if the experimental conditions allow it. Traditionally, for performing cyclic voltammetry a suitable time constant of a potentiostat is decided by the following equation,[86,87]

Figure 2.4 Instrumental setup for UME experiments at low scan rates.

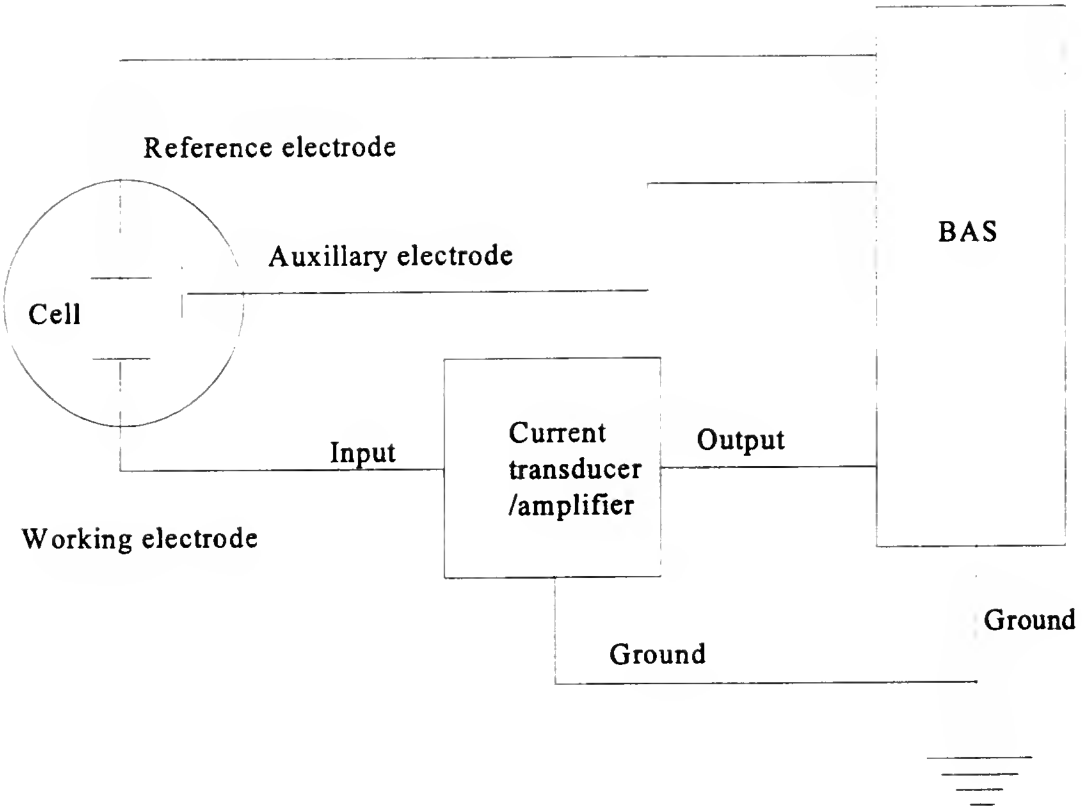

Reference electrode
Auxillary electrode
Cell
BAS
Input
Current transducer /amplifier
Output
Working electrode
Ground
Ground

Figure 2.5 Instrumental setup for UME experiments at high scan rates.

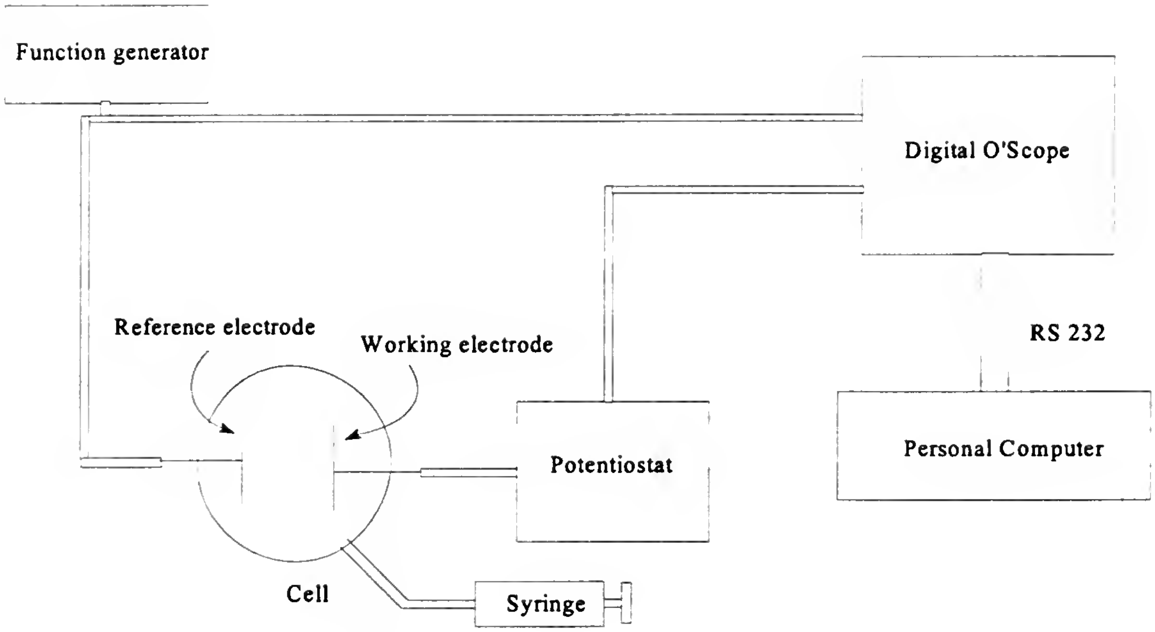
Function generator
Digital O'Scope
Reference electrode
Working electrode
RS 232
Personal Computer
Potentiostat
Cell
Syringe

$$RCn\nu \leq 4mV \qquad (2.6)$$

where the R is the resistance (Ω) of the first order filter (i. e. the feedback resistance R_f for OP AD515A), C is the capacitance (F) of the first order filter (i.e. the capacitance of the feedback capacitor for OP AD515A), n is of electrons number in the redox reaction, and υ is the scan rate (V/sec). At low scan rates (less than 40 V/s), the time constant of the system is set at 100 μs which allows use of scan rates up to 40V/s for one electron reactions (or 20 V/s for two electron reactions) with negligible distortion in the ΔE_p. Figure 2.6 shows the measured current (pico amperes) obtained from the BAS in conjunction with the amplifier.

Voltammetry at high scan rates

One of the advantages of using UMEs is that the current is small and thus there is no need to use an auxiliary electrode. Therefore, the circuit of the potentiostat can be simplified into a two-electrode configuration. The current transducer used for low scan rates can be used as a potentiostat for fast scan measurements in conjunction with a waveform generator and a digital oscilloscope. The potentiostat was designed to have a two-electrode configuration (one reference and one working electrode). The potential waveform generated from the function generator is applied to the reference electrode. Current passing through the UME working electrode is converted and is amplified to voltage through the current transducer. The output of the current transducer (voltage) and the potential waveform at the reference electrode are then simultaneously measured with the digital oscilloscope. The transducer is designed with flexibility and low noise in mind. Different gains (10^6 to 10^8 V/A) are obtained with different resisters (1 to 100 MΩ).

Figure 2.6 Cyclic voltammogram of 0.1 mM $Fe(CN)_6{}^{3-}$ in 70 mM pH 7.0 phosphate buffer obtained from the current transducer connected to the BAS. The scan rate is 10 mV/s. The gain of the current transducer is 10000 and the time constant of the first order filter is 100 µs. The working electrode is a carbon electrode (7 µm).

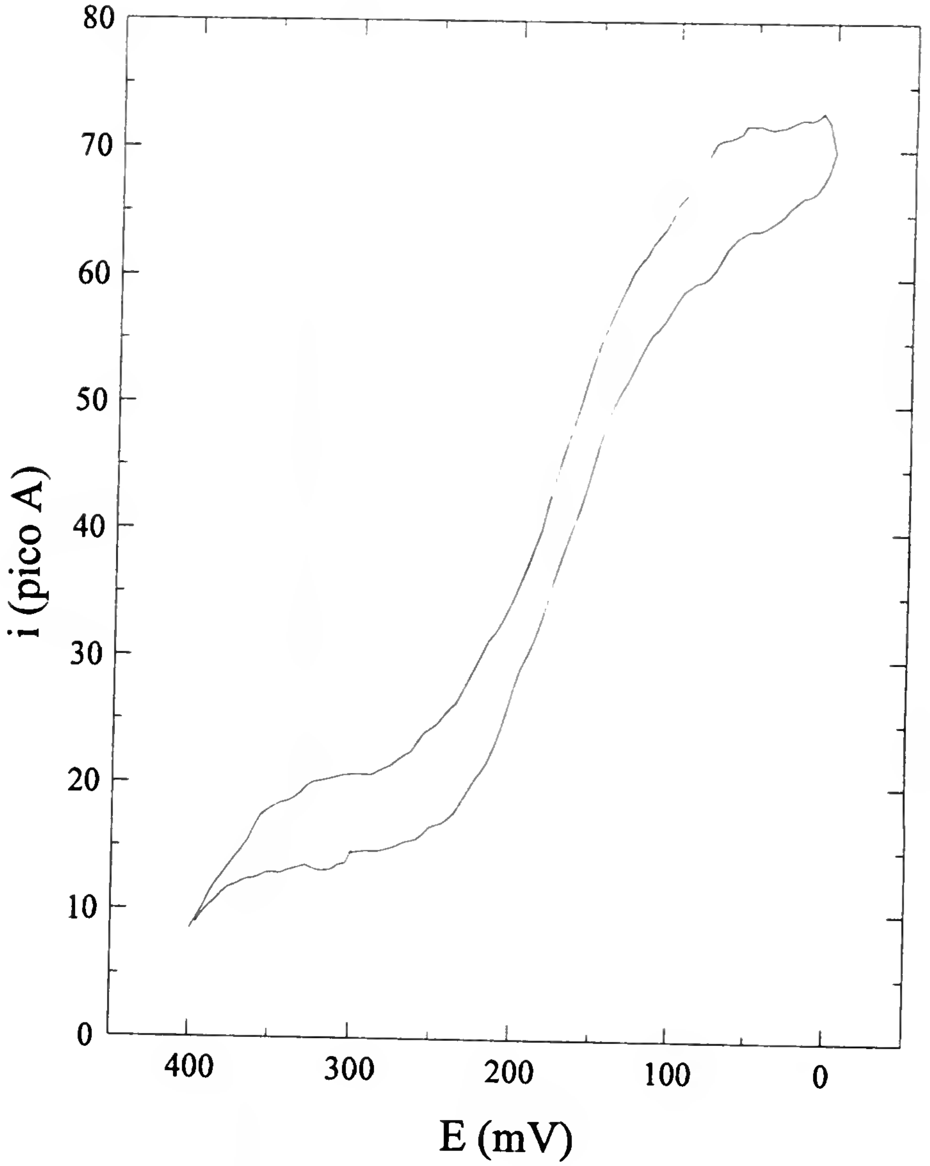
80
70
60
50
40
30
20
10
0
i (pico A)
400
300
200
100
0
E (mV)

As was described above, a first order filter with different time constants (1 to 100 μs) is used with OP AD515A (Figure 2.3) to minimize noise. Again, equation 1 can be used as a guide for setting the time constant of the potentiostat. A 10 μs time constant, for example, will allow a scan rate of 400 V/s to be used for one electron reactions with negligible distortion in the voltammogram. With 1 μs time constant, scan rate of 4,000 V/s will be the maximum scan rate allowed for obtaining undistorted voltammograms. Figure 2.7 shows the voltammogram of dopamine at a scan rate of 2,000 V/s. Since the large charging current can obscure the faradic current at high scan rates, the voltammogram needs to be background subtracted. The background voltammogram was obtained in a buffer solution and stored in the digital oscilloscope or in the computer. A buffer solution with analyte was then added and the voltammogram was acquired. The voltammogram was background subtracted to obtain a clear voltammogram.

The potentiostat design is not limited to fast scan voltammetry. It can be used in all electrochemical applications which need a fast instrumental time, such as fast potential step amperometry. The digital oscilloscope is the most expensive part of the potentiostat, because the digital oscilloscope has a very high bandwidth (150 MHZ) as well as other extra functions. However, a bandwidth of 10 MHZ is sufficient for all fast electrochemical measurements described above. Thus, the digital oscilloscope may be replaced with an analog-to-digital converter which has a narrower bandwidth but is much less expensive.

Figure 2.7 Voltammogram of 0.18 mM dopamine at 2,000 V/s in 70 mM pH 7.0 phosphate buffer with a carbon electrode (7 μm). The voltammogram is background subtracted and signal averaged 1000 times.

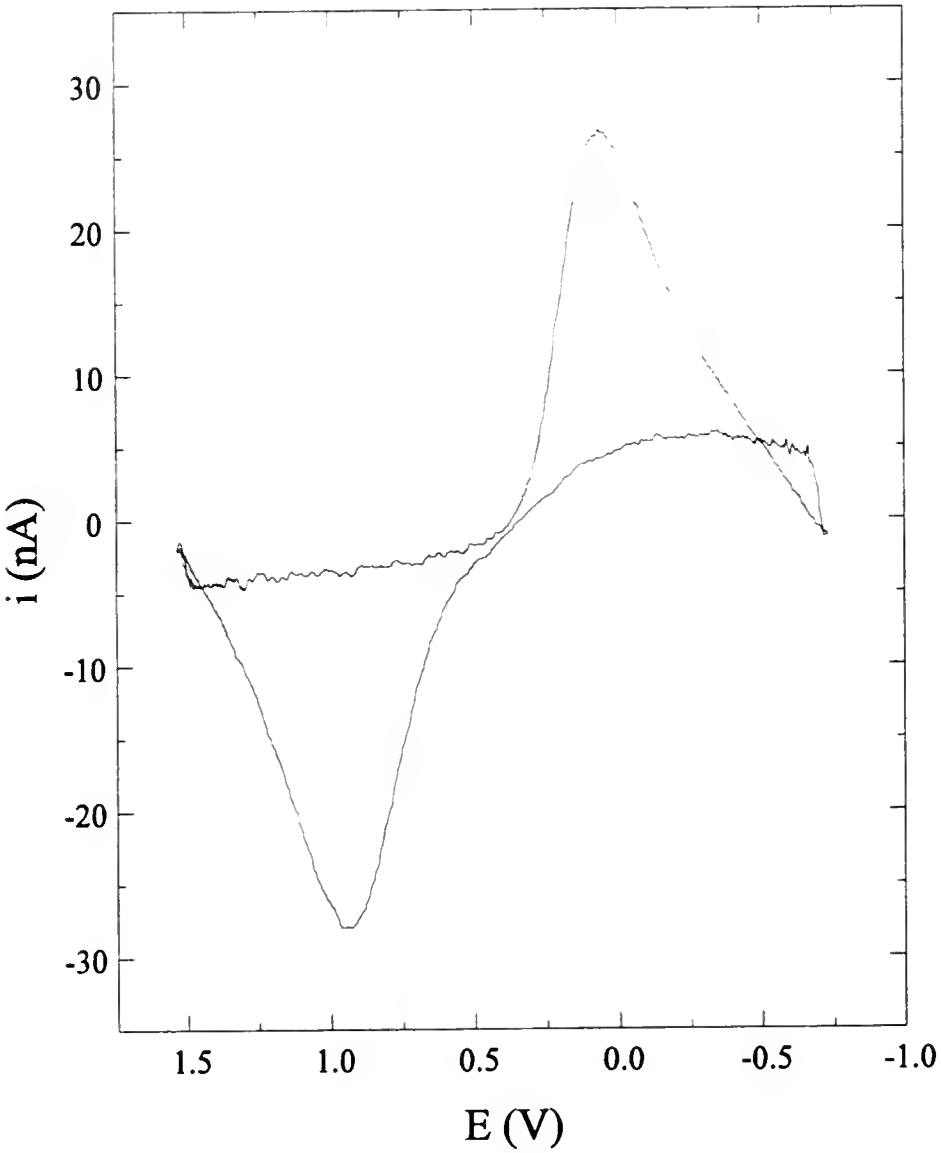
30
20
10
0
-10
-20
-30
i (nA)
1.5
1.0
0.5
0.0
-0.5
-1.0
E (V)

Fundamentals of Electrochemical Methods

Cyclic Voltammetry

In cyclic voltammetry (CV) experiments, the potential is scanned from an initial value where no reaction occurs to a final value where the reaction rate is limited by diffusion current. The potential is then swept back to the initial potential. The time scale of the experiment is expressed as scan rate, ν (V/s), which is the rate of potential sweep. The potential range between initial and final potential is called the potential window. In a cyclic voltammogram which is recorded, the current from the redox reaction gradually rises after the potential is swept past the potential where the electrochemical reaction occurs. The current then reaches a peak and then gradually decreases. The potential where the current reaches a maximum is called the peak potential, E_p. The potential difference between the reduction, E_{pc}, and the oxidation, E_{pa}, peak potentials is expressed as a $\Delta E_p = E_{pc} - E_{pa}$. Figure 2.8 illustrates the details of a voltammogram and the relationship of time scale , potential, and current.

The value of ΔE_p is an indication of a reversibility of a redox reaction. For an one electron reversible reaction, the ΔE_p value is around 58 mV.[88] For a quasi-reversible redox reaction, the ΔE_p is between 60 and 212 mV.[88] If the value of ΔE_p is above 212 mV, the reaction is considered irreversible.[88] The theoretical peak current for a diffusion controlled reversible reaction can be expressed as follows:[88]

$$i_p = (2.69\times10^5)n^{3/2}AD_o^{1/2}\nu^{1/2}C_o^* \tag{2.7}$$

and for a diffusion controlled irreversible reaction, the peak current is:

$$i_p = (2.99\times10^5)n(\alpha n_a)^{1/2}AD_o^{1/2}\nu^{1/2}C_o^* \tag{2.8}$$

where n is the number of electrons per mole oxidized or reduced, A is the electrode area (cm^2), D_o is the diffusion coefficient (cm^2/s), ν is the scan rate (V/s), C_o^* is the bulk concentration of the redox species (mol/cm^3), α is the transfer coefficient, and n_a is the number of electrons involved in the rate determining step.

Equations 2.7 and 2.8 define voltammetric peak currents for diffusing species. For adsorbed species, the peak current for a reversible reaction is:

$$i_p = \frac{n^2F^2A\nu\Gamma_o}{4RT} \tag{2.9}$$

and for an irreversible reaction is:

$$i_p = \frac{n\alpha n_aF^2A\nu\Gamma_o}{2.718RT} \tag{2.10}$$

where n is the number of electrons per mole oxidized or reduced, A is the electrode area (cm^2), ν is the scan rate (V/s), Γ_o is the surface excess of the redox species (mol/cm^2), α is the transfer coefficient, n_a is the number of electrons involved in the rate determining step,

Figure 2.8 A typical cyclic voltammogram.

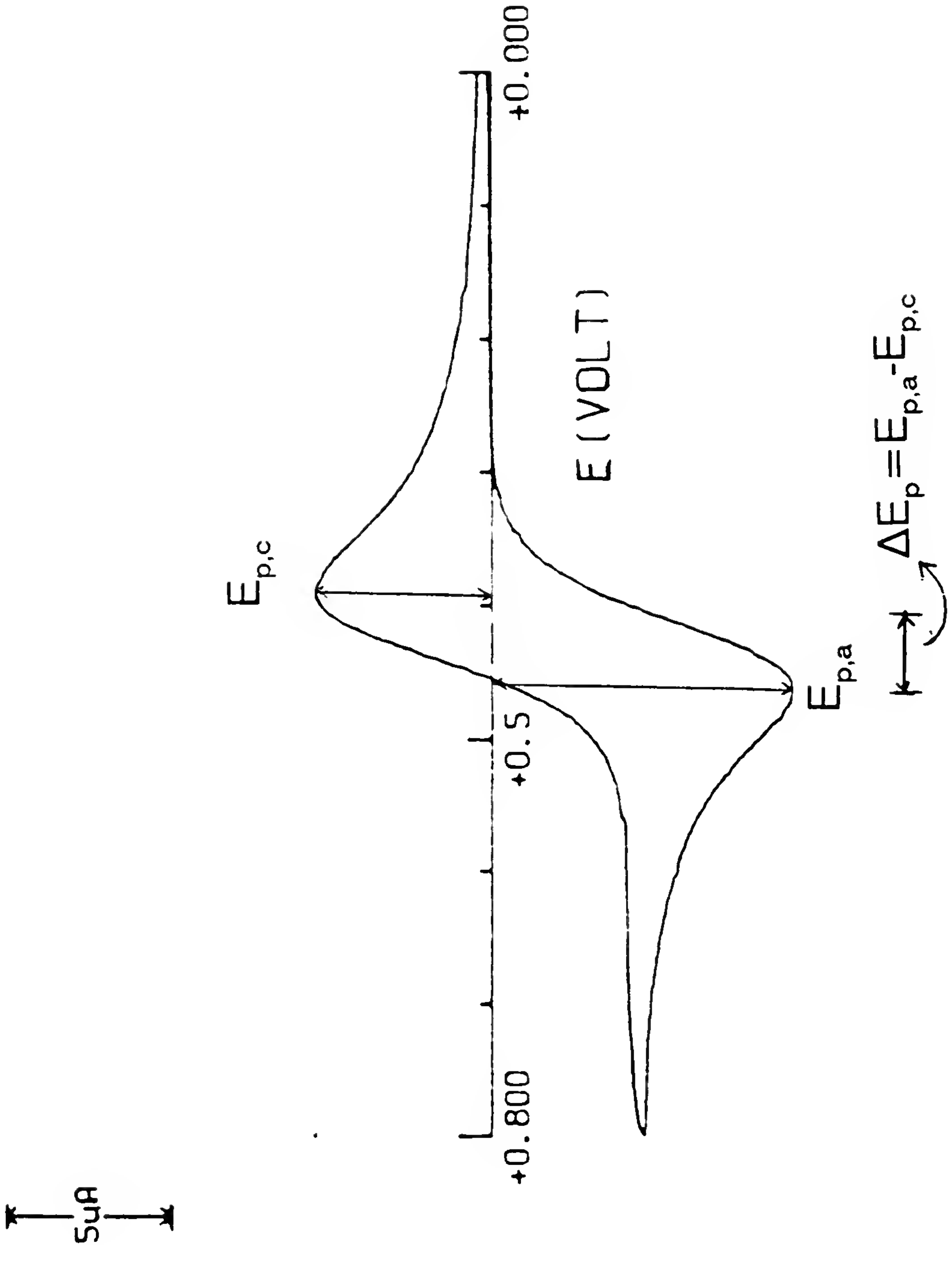
E(p,c)
E(p,a)
ΔE(p) = E(p,a) - E(p,c)
+0.000
+0.5
+0.800
E (VOLT)
5uA

R is the gas constant (J mol^{-1} K^{-1}), T is the temperature (K), and F is the Faraday constant (C).

Voltammograms at conventional electrodes (ca. mm in diameter) are peak-shaped and the peak currents depend on scan rate (equations 2.7 and 2.8). At UMEs, the voltammograms are sigmoidal in shape and the limiting current is independent of scan rate at scans up to ca. 1 V/s which results from an edge effect (radial diffusion). This effect has been described in Chapter One. Since the radius of UMEs is small enough compared to the thickness of the diffusion layer under common experimental conditions (i.e. scan rates of up to 1 V/s), radial diffusion can be established at a UME. Because radial diffusion is so efficient, steady state mass transport can be obtained. In the steady state, the current is time-independent and the scan rate does not affect the shape and the size of the voltammetric wave. For a disk UME, the limiting current at steady state is expressed by the following equation:[13]

$$i = 4nFDC^{*}r \tag{2.11}$$

where n is the number of electrons per mole oxidized or reduced, r is the electrode radius (cm), D is the diffusion coefficient (cm^2/s), C^{*} is the bulk concentration of the redox species (mol/cm^3) , n is the number of electrons involved in the reaction, and F is the Faraday constant (C).

It should be noted that the unique voltammetric response of UMEs exists only at low scan rates (less than 1 V/s) where the diffusion layer is thick compared to the electrode radius. As the scan rate increases (higher than 1V/s for a 5μm UME), the sigmoidal shape of the voltammograms is gradually transformed into a peak-shaped voltammogram. Eventually, at sufficiently high scan rates (above 100 V/s), the shape of a voltammogram obtained with a UME at high scan rates is the same as that with a conventional electrode. In fact, the diffusion behavior at a UME at high scan rates is the semi-infinite diffusion behavior as described for conventional size electrodes. Therefore, all theories for conventional size electrodes can be applied to analyze the response of UMEs at high scan rates.

Kinetic Measurements with Cyclic Voltammetry

Voltammetric ΔE_p (Fig. 2.8) is an indicator of the reversibility of a redox reaction. For a one electron reaction with no adsorption, ΔE_p between 58 and 212 mV is considered as a quasi-reversible behavior and from the ΔE_p values for a quasi-reversible reaction, kinetic information can be obtained for the reaction.[88]

The electrochemical redox reaction rate constants depend on the potential applied to the electrode surface. Therefore, a redox reaction with a low inherent reactivity may have a large reaction rate constant if a large overpotential is applied to the electrode. The electrochemical (heterogeneous) reaction rate constant can be expressed as follows:[88]

$$k_{ox} = k^0 e^{-\alpha n f(E-E^{0'})} \qquad (2.12)$$

$$k_{red} = k^0 e^{(1-\alpha)nf(E-E^{0'})} \qquad (2.13)$$

where k_{ox} (cm/s) is the heterogeneous oxidation rate constant at a potential E, k_{red} (cm/s) is the heterogeneous reduction rate constant at a potential E, k^0 (cm/s) is the standard reaction rate constant measured at $E^{0'}$, α is the transfer coefficient, f is equal to F/RT which is a constant ($38.92 V^{-1}$) at a temperature of 25 °C, n is the number of electrons involved in the redox reaction, $E^{0'}$ (V) is the formal potential for the redox reaction, and the term ($E-E^{0'}$) is the overpotential.

According to equations 2.12 and 2.13, k_{ox} and k_{red} are a function of the applied potential E (or the overpotential). At the potential of $E=E^{0'}$, both k_{ox} and k_{red} are equal to k^0. The k^0 is independent of the applied potential but depends on the inherent reactivity of the redox system. Thus, we can use standard reaction rate constant (k^0) as a reference point (an indicator) for the reactivity of a redox system without confusion caused by differences in the applied potential.

A method developed by Nicholson can be used to calculate standard reaction rate constants from cyclic voltammograms.[89] A kinetic parameter ψ is determined from the ΔE_p values in cyclic voltammograms of quasi-reversible systems. The k^0 is then determined from the value ψ and the scan rate. Their relationship is expressed by the following equation:[88,89]

$$\psi = \frac{k^0}{[D_o \pi v (nF/RT)]^{1/2}} \qquad (2.14)$$

where ψ is a function of ΔE_p. The larger the ΔE_p, the smaller the ψ. k^0 (cm/s) is the standard reaction rate constant. The value of ψ can only be obtained by numerical analysis. Figure 2.9 is a plot of ΔE_p vs ψ. It should be noticed that the coordinate of ψ is logarithmic, thus, a small error in ΔE_p will cause a large deviation in ψ (or in calculated k^0).

For redox reactions of adsorbed species, Nicholson's method is not valid. However, a method developed by Laviron can be used to calculate the standard reaction rate constant. According to Laviron's theory, the standard rate constant of an adsorbed species can be expressed by a following equation:[90]

$$\log k^0 = \alpha\log(1-\alpha)+(1-\alpha)\log\alpha-\log(\frac{RT}{nFv})-\frac{\alpha(1-\alpha)nF\Delta E_p}{2.3RT} \tag{2.15}$$

The equation is valid for $n\Delta E_p > 200$ mV. In the above equation, k^0 is the standard reaction rate constant (s^{-1}), α is the electron transfer coefficient, n is the number of electrons involved in the reaction, R is the gas constant (J mol^{-1} K^{-1}), T is the temperature (K), F is the Faraday constant (C), v is the scan rate (V/s), and ΔE_p is the peak separation measured from a cyclic voltammogram.

Semi-Integration Analysis

Voltammetric current (i vs E(t)) can be integrated as a function of square root of time to produce a steady state response and the method is referred to as semi-integration analysis. Semi-integration analysis is useful for obtaining kinetic information and in verification of

Figure 2.9 A plot of ΔE_p vs kinetic parameter ψ (reference 88 and 89).

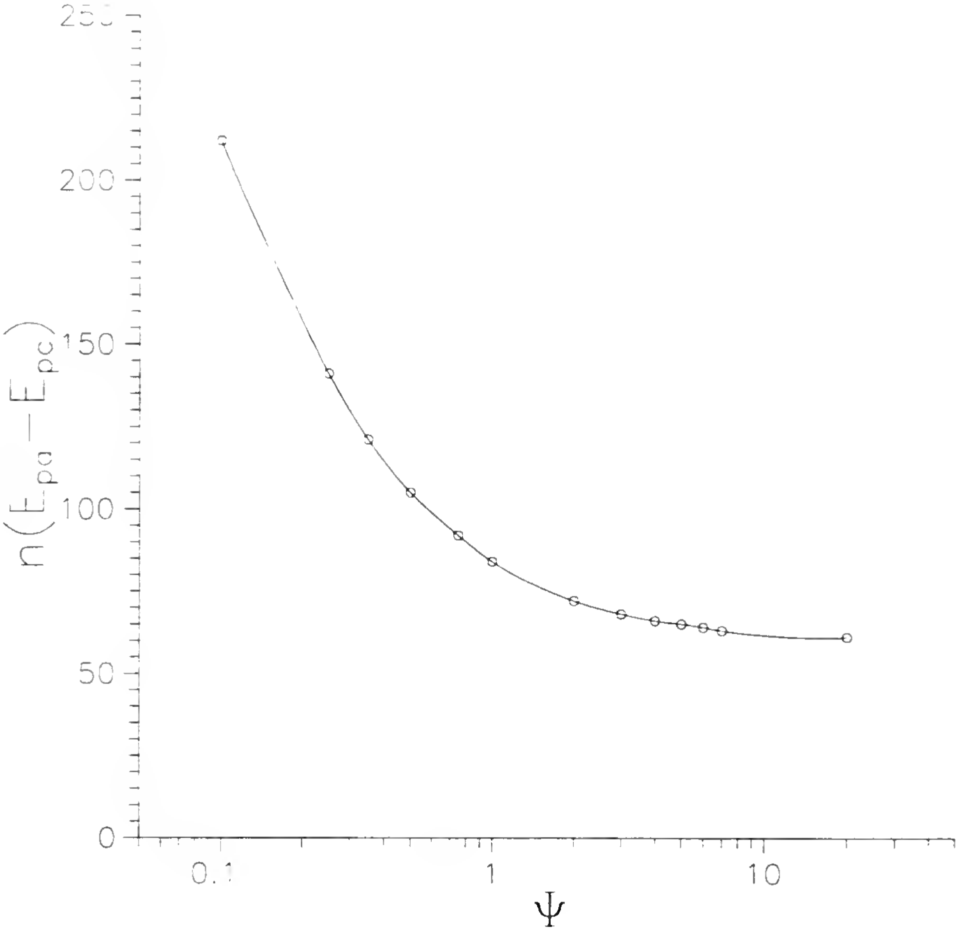
250
200
150
100
50
0
0.1
1
10
Ψ
$n(E_{pa} - E_{pc})$

weak adsorption.[91,92] Semi-integration analysis was used in this work to verify the presence of weak adsorption at high scan rates. If the redox reaction involves only diffusing probes, semi-integrated current will have a sigmoidal shape. If there is weak adsorption of the probe on the electrode surface, semi-integrated current will be peak-shaped. Therefore, semi-integration is a very sensitive method for identification of weak adsorption.

Semi-integration analysis can be performed by a numerical integration technique with a help of a computer. The integration algorithm can be described as following. The i-t data are divided into N equally spaced time intervals between t = 0 and $t=t_f$ and indexed by j (Figure 2.10). The integrated current, I(t), becomes I(kΔt) (where k varies between 0 and N, representing t= 0 and t = t_f; $\Delta t = t_f/N$). The following is the mathematical expression for the semi-integration algorithm:[93]

$$I(k\Delta t) = \frac{1}{\pi^{1/2}} \Sigma \frac{\Gamma(k-j+\frac{1}{2})}{(k-j)!} \Delta t^{1/2} i(j\Delta t) \tag{2.16}$$

where I, the semi-integrated current ($\mu As^{1/2}$), is a function of time (kΔt), i is the faradic current (μA), and $\Gamma(k-j+1/2)$ is the so called Gamma function of (k-j+1/2). The summation Σ is from j=1 to j=k, where j and k are the indexing numbers for the numerical integration. The Gamma function is expressed in the form:[93]

$$\Gamma(n+\frac{1}{2}) = \sqrt{\pi}\frac{1\cdot 3\cdot 5\cdot 7\ldots(2n-1)}{2^n} \tag{2.17}$$

A computer program has been written in our laboratory using the above algorithm (Appendix B) to perform semi-integration analysis.

Figure 2.10. Division of experimental i(t) vs. t [or vs. E(t)] curve for semi-integration.

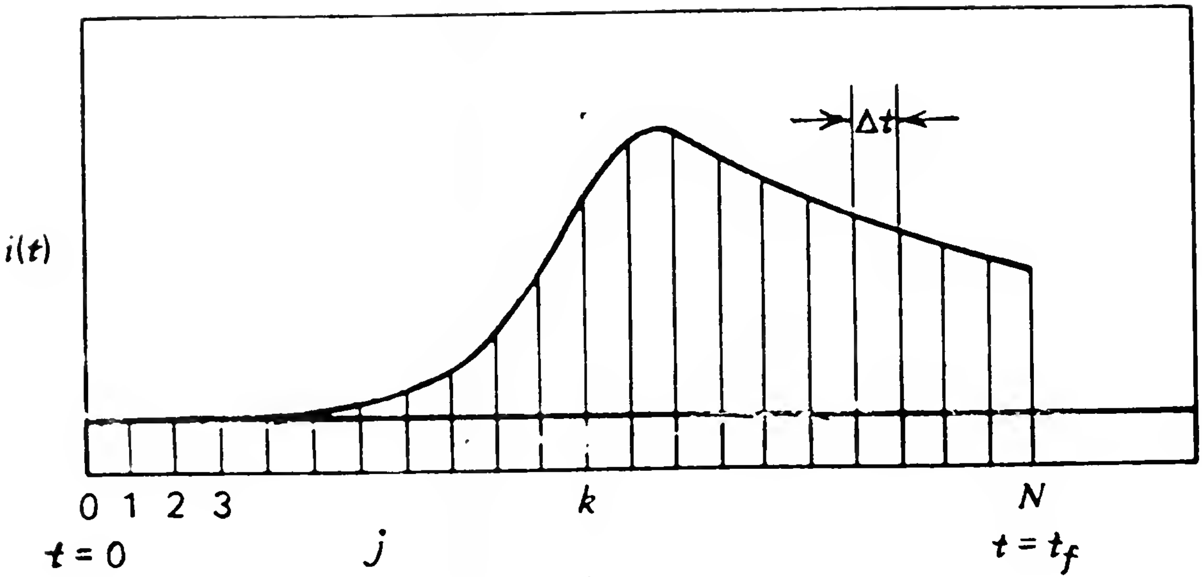
i(t)
Δt
0
1
2
3
t = 0
j
k
N
t = t_f
t

Measurement of Diffusion Coefficients with Rotating Disk Electrodes

Diffusion coefficients of probes in films can be measured with the rotating disk electrode (RDE). With the RDE, the diffusion limiting current (i_d) is proportional to the square root of the rotation rate ω (s^{-1}).[94] The intercept of a plot of i_d^{-1} versus $\omega^{-1/2}$ (Koutecky-Levich plot) gives i_d^{-1} at the infinite rotation rate.[94] At infinite rotation rate, the effect of diffusion of the probe in solution becomes negligible, and i_d simply depends on the diffusion of the probe through the film.[94,95,96] For a membrane covered RDE, the membrane diffusion limiting current, i_d, at an infinite rotation rate, is given by:

$$i_d = nFAC^{*}P_m = nFAC^{*}D_{app}/\delta_m \qquad (2.18)$$

where A (cm^2) is the electrode area, P_m (cm/s) is the permeability of the film, and C^* (M) is the bulk concentration of the probe. D_{app} (cm^2/s) is the apparent diffusion coefficient of the probe in the film and δ_m (cm) is the thickness of the film. D_{app} can be obtained from equation 2.18 since i_d can be obtained from the Koutecky-Levich plot of the experimental data with n, F, A, C^* and δ_m as knowns. The above method can be used to determine D_{app} of probes at macroelectrodes modified with films. For an ultramicroelectrode, it is difficult to measure D_{app} of a probe with the above method because an ultramicro rotating disk electrode is extremely difficult to make.

Chronocoulometry

Chronocoulometric (CC) experiments are performed by stepping the potential of a working electrode from a potential where the rate of the redox reaction is negligible to a potential where the reaction rate is diffusion limited. The charge passed is monitored as a function of time, and can be expressed as:[97]

$$Q(t) = \frac{2nFAD^{1/2}C^{*}t^{1/2}}{\pi^{1/2}} \tag{2.19}$$

where Q is the charge as a function of time (C), n is the number of electrons per mole oxidized or reduced, F is the Faraday constant (C), A is the electrode area (cm^2), D is the diffusion coefficient (cm^2/s), C^* is the bulk concentration of the redox species (mol/cm^3), and t is the pulse width (s).

Based on equation 2.19, a plot of Q(t) vs. $t^{1/2}$ should produce a straight line with a slope of $2nFAD^{1/2}C^{*}/\pi^{1/2}$. The values of the slope can be used to determine electrode areas (A) or diffusion coefficients (D). In this work, chronocoulometry was used to determine the electrode areas. In the experiments with polypyrrole films, chronocoulometry was used to determine the amount of pyrrole polymerized on the electrode surface by measuring the charge used in the polymerization reactions.

CHAPTER 3
FAST KINETIC MEASUREMENTS IN AQUEOUS SOLUTIONS WITH ON-LINE IR COMPENSATION

Background

Many fast heterogenous electron transfer reactions have been characterized since UMEs have been introduced for the fast scan cyclic voltammetry.[42,43,44] Most research has focused on pushing the upper limit of scan rate (up to MV/s) to investigate faster reactions where majority of the experiments have been performed in nonaqueous solvents at metallic ultramicroelectrodes (Au, Pt or Hg).

Compared to metallic electrode, carbon electrodes in aqueous solutions have a large and irregular background current due to faradaic processes of surface bound redox couples which make fast kinetic measurements very difficult. Because background current is proportional to scan rate (equation 1.1), it severely interferes with signal of interest unless background subtraction is performed. There are a few reports of fast scan cyclic voltammetry measurements (up to 300 V/s) at carbon fiber electrodes in aqueous solutions for quantitative purposes (such as low detection limit measurements).[52,1] To our knowledge, there is no report on kinetic measurements with carbon electrodes in aqueous solutions at scan rates above 5000 V/s.

Measurements of fast electron transfer reactions at carbon electrodes are important in aqueous solutions because carbon electrodes have wider useful potential window than useful metallic material, which means more redox reactions can be observed at carbon electrodes than at metallic electrodes. Moreover, many redox reactions, especially of significant biomolecules, show faster electron transfer rates at carbon electrodes than at metal electrodes. The other reason that makes carbon electrodes of interest is that carbon electrodes can be manipulated relatively easily. Carbon surface can be directly modified, and electrochemical pretreatment, heat pretreatment or laser activation can also change the properties of carbon surfaces and promote faster electron transfer.[78]

In this work we demonstrate that measurement of rate constants of very rapid redox reactions can be done up with fast cyclic voltammetry to 11,000 V/s on carbon fiber electrodes with on-line iR compensation and background subtraction. We also investigate how carbon surface changes affect electron transfer rates. We investigated redox reaction kinetics of $Ru(NH_3)_6^{(3+/2+)}$ and $Fe(CN)_6^{(3-/4-)}$ which are two well known rapid outer-sphere redox reactions. We were also interested in proton-coupled redox reactions of a biomolecule. The compound chosen for the study was uric acid which undergoes a $2H^+$, $2e^-$ redox reaction in aqueous solutions. A rapid follow up reaction makes the cathodic peak undetectable unless the scan rate is higher than 20 V/s.[2] In our laboratory, the acquired data show that uric acid is weakly adsorbed on the carbon fiber surface. In such a case, kinetic information is difficult to extract since the faradaic current is produced by diffusing and adsorbing species. However, the current from adsorbed species is proportional to scan rate (equations 2.9 and 2.10) and the current from diffusing species is proportional to a square root of scan rate (equations 2.7 and 2.8). At sufficiently high scan rates adsorption current should be the major current. Under such conditions the effect of diffusion current on peak current and peak potential is negligible. Therefore the ΔE_p is determined by adsorbed species alone. The standard rate constant of adsorbed species can then be easily calculated (equation 2.15). In this chapter, the determination of the standard redox rate constants of $Ru(NH_3)_6^{(3+/2+)}$, $Fe(CN)_6^{(3-/4-)}$ and uric acid will be discussed as well be the role of surface in the redox reactions.

Signal Averaging and its Effect on Surface Properties

Signal averaging is frequently used to improve the ratio of sinal-to-noise for quantitative purposes. It can also be used in fast electrochemical kinetic measurements to improve the accuracy of measurement of peak potentials by reducing the interference of noise.[3] Signal averaging seems adequate when a metal electrode is used. However, when applying signal averaging to an untreated carbon fiber electrode in aqueous solutions caution is necessary since surface properties can be changed dramatically due to repeated cycling which is needed for signal averaging. The extent of change in surface properties depends on cycling potential limits and scan rate. High positive potential limit (e.g. +1.1 V vs. SCE in the case of uric acid) will speed up the formation of surface oxide. The amount of surface oxide increases more rapidly when high positive potential limit and slower scan rates (e.g. +1.1 V vs. SCE and a scan rate of 200 V/s in the experiments with uric acid) are used since the time of potential sweep through the positive region is increased.

For example, background current and the k^0 of $Ru(NH_3)_6^{(3+/2+)}$ were not significantly changed after averaging 1000 cycles when the upper potential was 0.16 V vs. SCE at a scan rate of 11000 V/s. However, the k^0 of $Fe(CN)_6^{(3-/4-)}$ was greatly reduced after 1500 cycles at a scan rate of 500 V/s with an upper potential of 0.6 V vs. SCE. The background current and the peak current of uric acid changed significantly after 1000 cycles when the upper potential was 1.1 V vs. SCE at a scan rate of 200 V/s.

Surface Properties of Carbon Fiber and Their Effect on Response of $Ru(NH_3)_6^{(3+/2+)}$, $Fe(CN)_6^{(3-/4-)}$ and Uric Acid

Semiintegral analysis of the cyclic voltammetric response (Figure 3.1) shows a sigmoidal response which indicates that $Ru(NH_3)_6^{(3+/2+)}$ does not adsorb on freshly cut carbon fiber electrode.[4,5] However, the condition of the surface plays an important role in the kinetics of this redox reaction. Faradaic background currents are often observed at a potential of 0.2-0.3 V vs SCE on carbon electrodes.[6] Because of this, two different upper potential limits (0.17 and 0.4 V) were used in the experiments with $Ru(NH_3)_6^{(3+/2+)}$ to observe the effect of the surface on kinetics of the redox reaction. At a scan rate of 11000 V/s, ΔE_p for the cyclic voltammetric peaks of $Ru(NH_3)_6^{(3+/2+)}$ is 110 mV and no significant increase in the ΔE_p is observed after 200 cycles when the upper potential is 0.17 V. When the upper potential limit is above 0.4 V, ΔE_p increases more than 30 mV after the same number of cycles. With this upper potential limit the background current also increases and its shape changes which indicates surface changes. When the electrodes are treated electrochemically as described earlier in the Experimental section, the peak width and the ΔE_p are greatly increased. Those

Figure 3.1. Semiintegrated cyclic voltammetric current of 10 mM $Ru(NH_3)_6^{(+2/+3)}$ in 1 M KCl solution at a freshly cut carbon fiber electrode (7 μm). Scan rate is 5000 V/s.

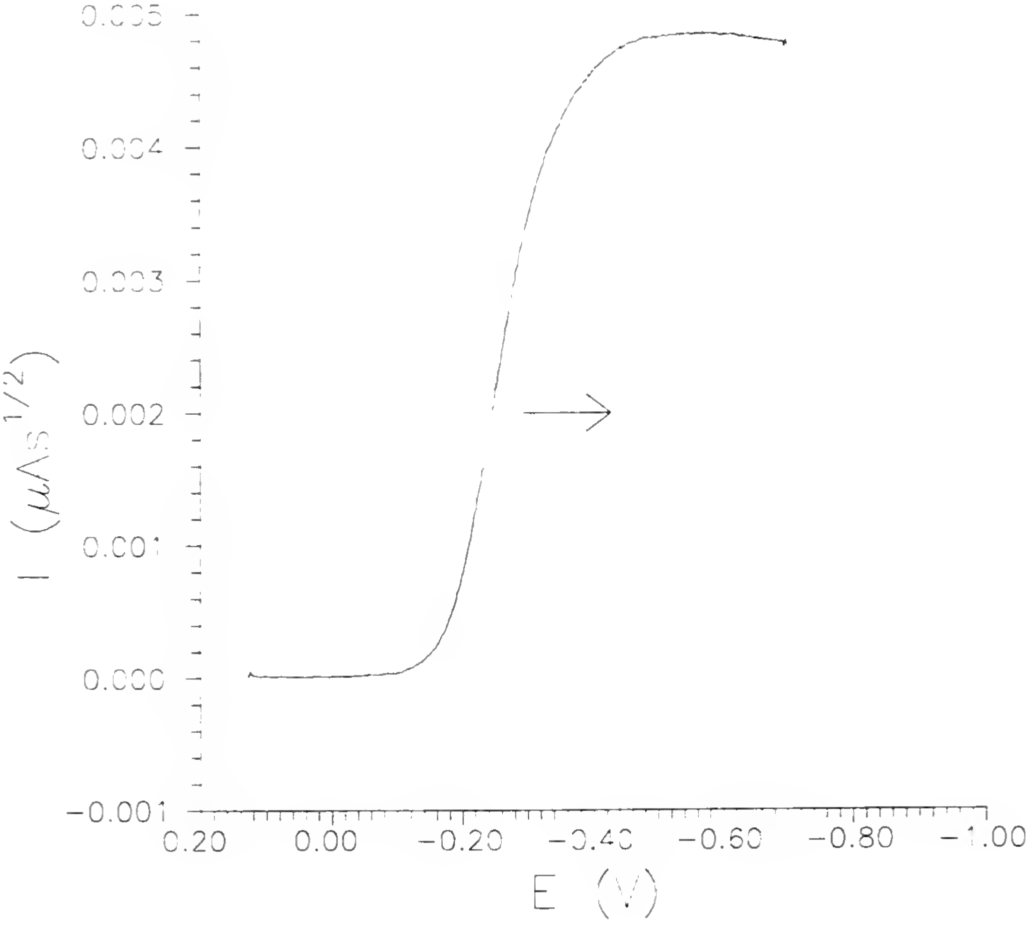
0.005
0.004
0.003
0.002
0.001
0.000
-0.001
I (μAs^1/2)
0.20
0.00
-0.20
-0.40
-0.60
-0.80
-1.00
E (V)

results indicate that changes in surface properties of carbon fiber, most likely formation of surface oxides at positive potentials, slow down the redox reaction of $Ru(NH_3)_6^{(3+,2+)}$.

Semiintegral analysis of cyclic voltammetric response indicates that $Fe(CN)_6^{(3-/4-)}$ does not adsorb on freshly cut carbon fiber. However, the ΔE_p of $Fe(CN)_6^{(3-/4-)}$ increases from 111 to 253 mV after 1500 cycles at a scan rate of 500 V/s with an upper potential limit of 0.6 V. The results show that $Fe(CN)_6^{(3-/4-)}$ response deteriorates similarly to that of $Ru(NH_3)_6^{(3+/2+)}$ when the carbon surface is exposed to positive potentials.

Electrochemical pretreatment has been reported to improve the kinetics of the redox reaction of uric acid on carbon fiber electrodes. After the carbon fiber was pretreated as described in the Experimental Section, a significant enhancement of the voltammetric response was reported at low scan rates (50 mV/s).[81] The same pretreatment was repeated in our laboratory to improve the kinetics of the redox reaction of uric acid with fast scan cyclic voltammetry. However, after pretreatment at scan rates of 400 V/s peak currents were greatly decreased (Figure 3.2). Before pretreatment semiintegral analysis of the cyclic voltammetric data shows a clear peaked response which indicates uric acid adsorption (Figure 3.3). After pretreatment, semiintegral analysis shows a nearly sigmoidal response which indicates no adsorption or very low adsorption current (Figure 3.3). Reasonable explanation for this phenomena is that pretreatment changes the properties of the surface hence the surface excess due to the adsorbed species is dramatically decreased. At high scan rates, peak currents are greatly decreased when adsorption becomes less favored.

Figure 3.2. Cyclic voltammograms of 1 mM uric acid in 1 M pH 7.0 phosphate buffer at a carbon fiber electrode (7 μm). Scan rate 400 V/s. Solid line - freshly cut; dashed line - electrochemically pretreated. (For pretreatment procedure see the Experimental Section)

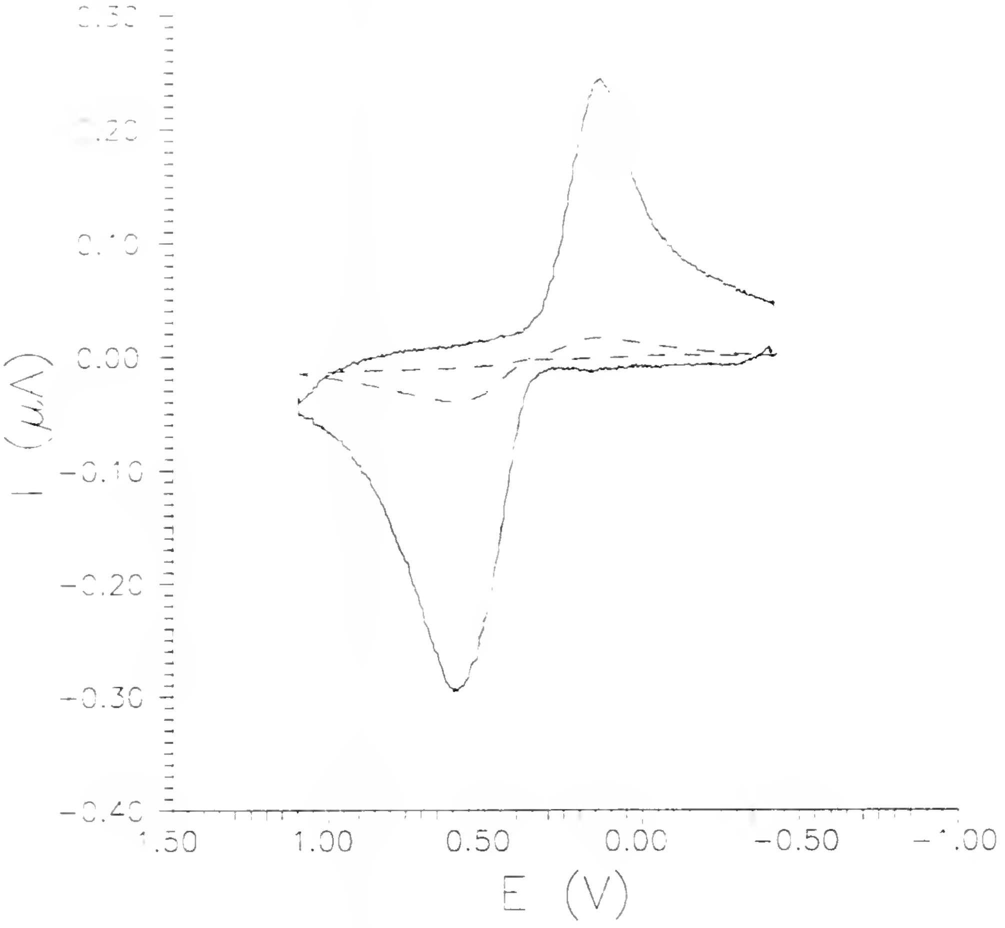
0.30
0.20
0.10
0.00
−0.10
−0.20
−0.30
−0.40
I (μA)
1.50
1.00
0.50
0.00
−0.50
−1.00
E (V)

Figure 3.3. Semiintegrated cyclic voltammetric currents of uric acid in Figure 3.2. Solid line - freshly cut; dashed line - electrochemically pretreated.

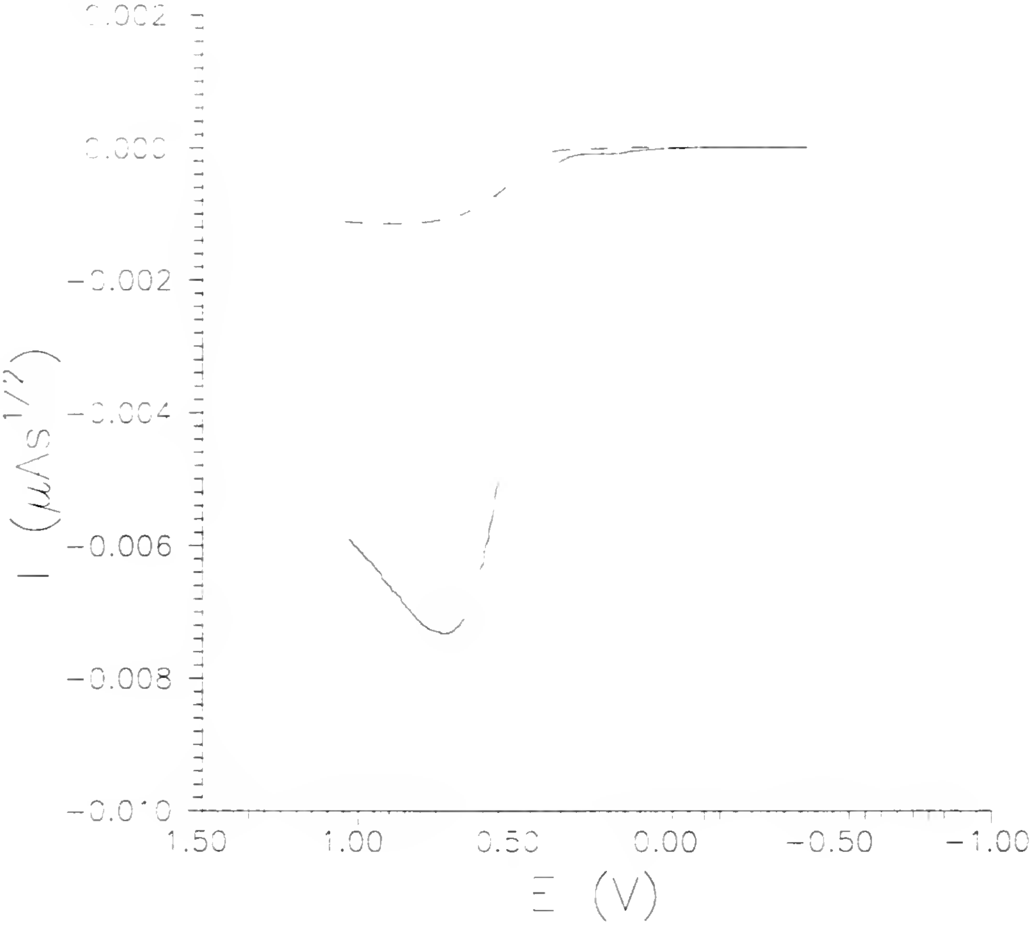
0.002
0.000
−0.002
−0.004
−0.006
−0.008
−0.010
I (μAs$^{1/2}$)
1.50
1.00
0.50
0.00
−0.50
−1.00
E (V)

Kinetics of $Ru(NH_3)_6^{(3+/2+)}$ on Freshly Cut Carbon Fiber

Redox reaction of $Ru(NH_3)_6^{(3+/2+)}$ is a fast, outer-sphere, one-electron transfer reaction. Kinetics of $Ru(NH_3)_6^{(3+/2+)}$ had been measured on Hg ultramicroelectrode by fast scan voltammetry and a standard reaction rate constant k^0=0.45 cm/s had been reported.[23] Using an AC impedance technique at a chemically modified gold electrode, k^0=1.8 cm/s had been reported.[7] The theoretical electrochemical outer-sphere heterogeneous rate constant can be derived from the Marcus equation:[8]

$$k^0 = \sqrt{\frac{k_{ex}}{10^3}} \qquad (3.1)$$

where k^0 is the heterogeneous standard rate constant (corrected for the double layer effect) and k_{ex} is homogeneous self-exchange rate constant ($M^{-1}s^{-1}$). Values of k_{ex} found in the literature for $Ru(NH_3)_6^{(3+/2+)}$ are 8.2×10^2 (direct determination) in aqueous solution and 4×10^3 $M^{-1}s^{-1}$ (indirect determination).[9] The expected values of the standard reaction rate constant calculated from equation 3.1 are 0.92 and 2.0 cm/s. From our experimental results following iR compensation, the standard reaction rate constant is $k^0=1.22 \pm 0.07$ cm/s (N= 15) at freshly cut carbon fiber electrode at a scan rate of 11000 V/s, using the following values in the calculation: electron transfer coefficient α=0.5 and diffusion coefficient $D_{ox}=5.48\times10^{-6} cm^2s^{-1}$.[10] Due to the lack of data for carbon electrodes, experimental k^0 was not corrected for the double layer effects. Only reproducibilty errors are considered in the accuracy of the detemination of k^0. Systematic errors (e.g. residual ohmic drop) are not taken into account.

Nicholson method was used to calculate the standard reaction rate constant (equation 2.14). A value of the parameter ψ is determined by ΔE_p. Then k^0 is determined from ψ and the scan rate. However, at high scan rates (11,000V/s) used to measure k^0, adsorption, if present, will greatly decrease ΔE_p and would cause the calculated k^0 to be much higher than its true value. To check if adsorption current contributes to the measured voltammogram, semiintegral analysis was performed. A sigmoidal semiintegrated current curve indicates that $Ru(NH_3)_6^{(3+/2+)}$ does not adsorb on freshly cut carbon fibers .[18,24](Fig. 3.1)

Figure 3.4 shows voltammograms of $Ru(NH_3)_6^{(3+/2+)}$ obtained at 11000 V/s showing the difference in response before and after on-line iR compensation. Without iR compensation, the peak separation is larger and peak current is smaller since the scan rate at the working electrode is decreased by the iR drops.

The results show that $Ru(NH_3)_6^{(3+/2+)}$ exhibits faster electron transfer kinetics (k^0=1.22 cm/s) on a freshly cut carbon fiber than on a mercury ultramicroelectrode. For outer-sphere electron transfer, apparent reaction rates are usually much slower on carbon electrodes than on metal electrodes unless the carbon electrode is treated.[78] The redox reaction of $Ru(NH_3)_6^{(3+/2+)}$ on untreated glassy carbon is usually a quasi-reversible reaction (typical k^0 equal to ca. 0.014 cm/s).[11]

The redox reaction of $Ru(NH_3)_6^{(3+/2+)}$ is very rapid on the freshly cut carbon fiber compared to glassy carbon, which indicates that the activity of the freshly cut carbon fiber surface may be much higher. The high activity of freshly cut carbon fiber could be due to the following factors. First, the density of edge planes on the surface may be higher at carbon fiber. Secondly, the roughness of the surface which increases the active area available for

Figure 3.4. Cyclic voltammograms of 10 mM $Ru(NH_3)_6^{(+2/+3)}$ in 1 M KCl solution at a freshly cut carbon fiber electrode (7 μm). Scan rate is 11,000 V/s. The solid line is the current response with iR compensation (Compensated resistance R_c=6.9 KΩ). The dashed line is the current response without iR compensation.

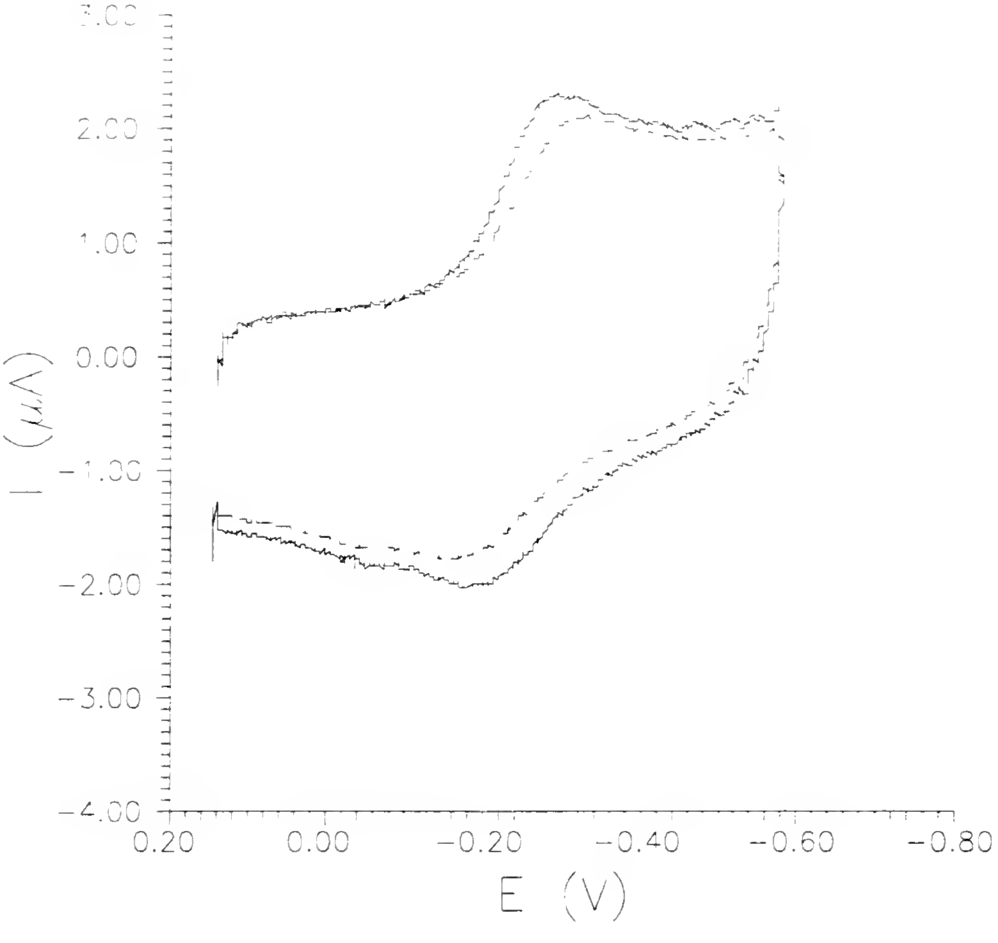
3.00
2.00
1.00
0.00
-1.00
-2.00
-3.00
-4.00
I (μA)
0.20
0.00
-0.20
-0.40
-0.60
-0.80
E (V)

electron transfer is higher at a cut carbon fiber, because the carbon fiber is cut without any subsequent polishing. An additional reason that could contribute to the high activity of the freshly cut fiber electrode is the cleanness of the surface. Since the fiber electrode is made without relying on any polishing procedure, the electrode surface can avoid contaminants which may be introduced during surface treatment.

Kinetics of $Fe(CN)_6^{(3-/4-)}$ on Freshly Cut Carbon Fiber

Redox reaction of $Fe(CN)_6^{(3-/4-)}$ is a fast outer-sphere, one electron reaction. However, it shows a quasi-reversible response at untreated glassy carbon. The standard reaction rate constant is usually reported in the 0.005 cm/s range at untreated glassy carbon following polishing.[78,108] When special treatment (such as ultraclean polish, high speed polish and surface fracturing) are applied, the standard reaction rate constants are 0.14, 0.098 cm/s and 0.5 cm/s respectively.[12, 13, 14] Our results show that the kinetics of the redox reaction of $Fe(CN)_6^{(3-/4-)}$ at freshly cut untreated carbon fibers are much faster than at untreated glassy carbon . The standard reaction rate constant of $Fe(CN)_6^{(3-/4-)}$ determined by the Nicholson method is $k^0=0.13 \pm 0.02$ cm/s (N=12) on freshly cut carbon fiber. A diffusion coefficient $D^0=7.17 \times 10^{-6} cm^2/s$ and electron transfer coefficient $\alpha=0.5$ were used in the calculation. The apparent high activity of cut carbon fiber electrode in this reaction must be due to the same reasons that were described earlier - high density of edge plane, roughness and cleanness of the surface. Compared to the ultraclean polished glassy carbon ($k^0=0.14$ cm/s), the freshly cut carbon fiber exhibits the same high activity ($k^0=0.13$ cm/s). The cleanness of the surface could be the most important factor which affects the activity in this case.

Redox Reaction of Uric Acid

The oxidation of uric acid is a 2 e^- and 2 H^+ reaction. The oxidation product, a diimmine, is an unstable intermediate with a half-life of less than 22 ms.[15] A follow up hydration reaction converts the diimmine to an imine-alcohol. Figure 3.5 shows the redox reactions and follow up reactions of uric acid in aqueous solutions. Using fast scan cyclic voltammetry, follow up reaction can be out run and the cathodic peak and potential will not be affected by the follow up reaction.

Semiintegral analysis (Figure 3.2) shows that uric acid is adsorbed on a freshly cut carbon fiber electrode. In this case Nicholson's method cannot be applied to calculate the standard reaction rate since the reaction involves both diffusing and adsorbed species. It is difficult to extract kinetic data from the voltammogram which is comprised of diffusion and adsorption components. However, at sufficiently high scan rates, the faradaic current comes primarily from adsorbed uric acid since diffusion peak current and adsorption peak current are proportional to square root of scan rate and scan rate respectively (equations 2.7-2.10).

The predominance of adsorption current of uric acid at high scan rates can be confirmed by the following calculation. Diffusion peak current of a totally irreversible system is given by euqation 2.8 in Chapter 2. Diffusion peak current of uric acid was calculated using the following values: $n=2$, $\alpha n_a= 0.5$, $A=3.8\times10^{-7}cm^2$ for a 7 μm diameter disk electrode, $C^*=1mM=1\times10^{-6}mole/cm^3$, $D=5\times10^{-6}$ cm^2/s and $v=400$ V/s. The calculated $i_p=7.2\times10^{-9}A$ is far below the experimental value ($i_p= 2.8\times10^{-7}$ A, Figure 3.2). The large

Figure 3.5. Redox and follow-up reactions of uric acid in aqueous solutions.

Redox and follow-up reactions of uric acid

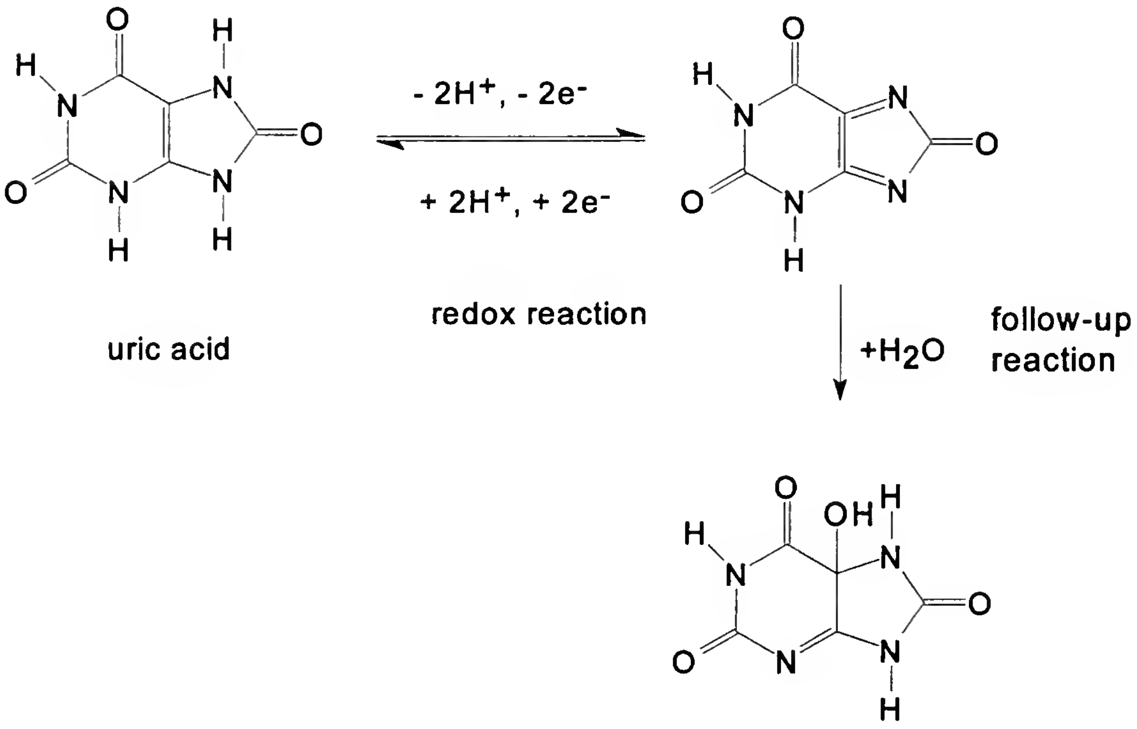
- 2H+, - 2e-
+ 2H+, + 2e-
redox reaction
uric acid
+H2O
follow-up reaction

experimental peak current is due to adsorption. Contribution from diffusing species to this peak current as calculated from equation 2.8 is less than 3%. The calculations support the statement that in this case adsorption predominates at high scan rates.

Under these conditions, peak potential difference (ΔE_p) is mainly determined by adsorbed species and an equation (equation 2.15) describing adsorbed system can be used to acquire the standard reaction rate for adsorbed uric acid.

Based on equation 2.15 and using α=0.5 in the calculation, the standard rate constants of adsorbed uric acid were determined with values ranging from 12 to 80 s^{-1}. The average value of the standard reaction rate constant is 54 s^{-1}. The poor reproducibility of the standard rate constant may reflect greater sensitivity of this system to the structure condition of the surface which could change when the electrode is cut. The reaction may be sensitive to changes in the ratio of edge to basal planes, since edge and basal planes exhibit different adsorption strength and activities. The small change in the ratio could cause large changes in the ΔE_p. The peak currents are also not reproducible and show no dependence on ΔE_p.

Since $2H^+$ and $2e^-$ are involved in the redox reaction of uric acid, the mechanism involves several steps (i.e. intermediates with various number of e^- and H^+). It may be possible to observe split peaks from different intermediates at high scan rates. However, we only observed a single peak current even though the scan rate was as high as 5,000 V/s. The lack of split peaks on the experimental time scale could result from more negative formal potential of the second electron transfer than of the first and the rapid kinetics of H^+ transfer.

Conclusions

The task of acquiring kinetic information on carbon fiber electrodes by fast scan voltammetry has been accomplished and is reported in the work. The results show that, with on-line iR compensation and background subtraction, determination of standard reaction rate constants at scan rates of 11000 V/s is possible in aqueous solutions even though the background current is large. A freshly cut carbon fiber electrode exhibits very high activity in the redox reactions of $Ru(NH_3)_6^{(3+/2+)}$ and $Fe(CN)_6^{(3-/4-)}$. The high activity of the cut carbon fiber could be due to the high density of the edge plane on the electrode surface and the procedure of preparing the electrodes. Electrode activity decreases after electrochemical pretreatment or after continuing cycling to high positive potentials which likely indicates that surface oxides block activity of the electrode.

Redox reactions which involve weak adsorption and diffusion are usually difficult to characterize since the peak potentials are affected by both adsorption and diffusion. However, using fast scan cyclic voltammetry, the effect of diffusion current on peak potential can be minimized. Hence, the redox reaction of weakly adsorbed species can be characterized. As shown above, at sufficiently high scan rates, the redox reaction rate constants of adsorbed species can be obtained. Thus, extracting kinetic information for weakly adsorbed species cab be esaily achieved.

The relationship between adsorption peak current and surface properties could be useful for quantitative purpose. Fast scan cyclic voltammetry can be used as an analytical tool in trace detection of biocompounds. To increase sensitivity, carbon electrode are usually electrochemically pretreated. However, our results show that pretreatment could reduce adsorption strength and, therefore, the sensitivity. Hence for some compounds, a freshly cut carbon fiber electrode may gain more analytical advantage in fast measurements.

CHAPTER 4
ELECTROCHEMICAL PREPARATION OF ULTRATHIN OVEROXIDIZED POLYPYRROLE FILMS AND THEIR ANALYTICAL APPLICATIONS

Background

Our previous investigations showed that overoxidized polypyrrole (OPPy) films can be made quite permeable, and have ionic conductivity, although the electrical conductivity of polypyrrole (PPy) is lost after overoxidation.[71,72,73] Figure 4.1 shows the structures of Py, PPy and OPPy. The high electron density of the carbonyl groups can act as a barrier hindering diffusion of anions through the OPPy film (Figure 4.2).

In an attempt to decrease thickness of the OPPy film so a better response can be obtained, we found that as the thickness of the film was decreased, the pin holes and defects in the film made anion diffusion though the film possible, and the film lost its ability to impede anion diffusion. To solve this problem, a new strategy for preparing ultrathin films was designed. A procedure of repeatedly polymerizing pyrrole (Py) and overoxidizing it to OPPy was used to obtain a compact and relatively pin hole free ultrathin film.

A monolayer PPy film is first polymerized on an electrode, then overoxidized in phosphate buffer. The electrode is then transferred back to PY solution for a second polymerization step. Since the first layer loses its conductivity after overoxidation, the second layer can only grow on the bare substrate. Therefore, the pin holes become partially

Figure 4.1. Chemical structures of Py , PPy, and OPPy.

pyrrole

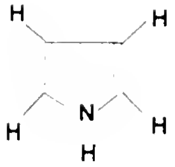

electrochemically
polymerized
pyrrole

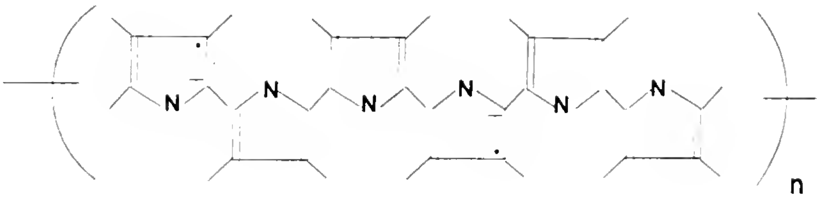

polypyrrole
overoxidized

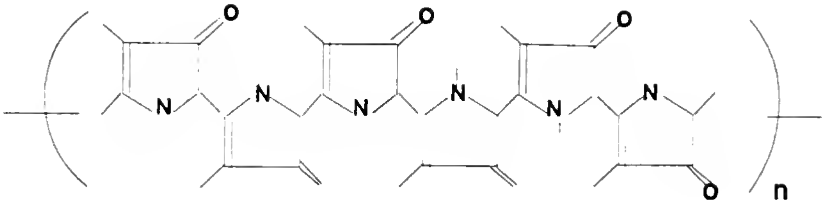
O
O
O
N
N
N
N
N
N
O
n

Figure 4.2. A cartoon representation of the proposed carbonyl group in OPPy films hindering anion diffusion.

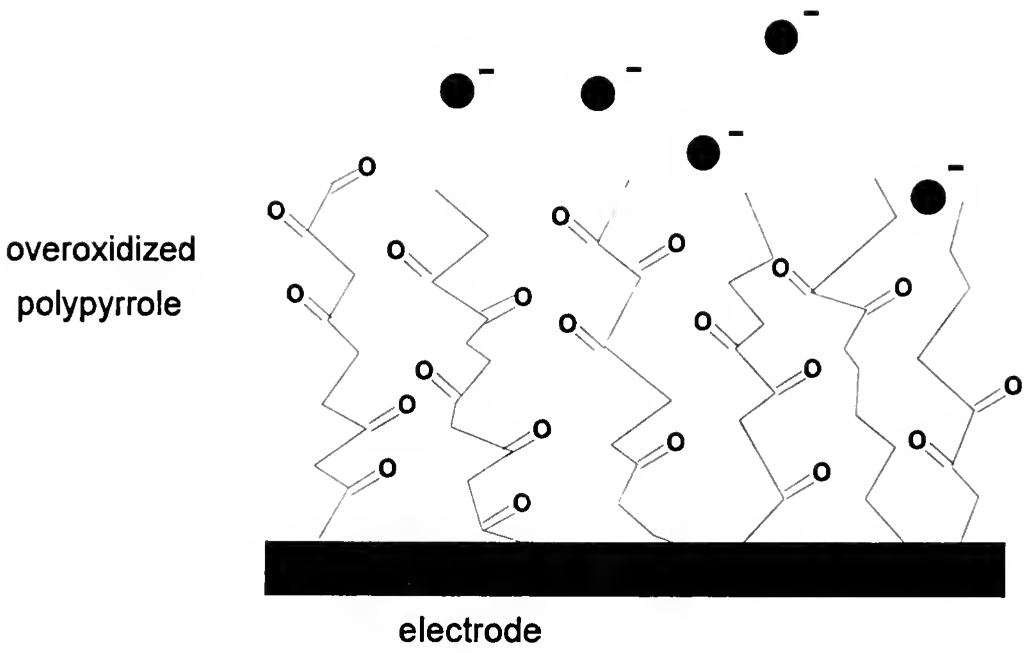
overoxidized
polypyrrole
electrode

Low permeability of anion in OPPy film

filled. By repeating the above procedure, an OPPy ultrathin film which still has excellent ability to impede anion diffusion can be coated on carbon electrodes.

Another approach to obtain an ultrathin film was tested in which a monolayer of PY is adsorbed on an electrode and then polymerized and overoxidized. In this procedure, platinum electrodes were used due to the effective adsorption of PY on platinum.[113] Monolayer OPPy films that show good permselectivity towards cations were made using this approach. The methods of coating ultrathin OPPy films on different substrates and the permselectivity analysis of these films are presented in this chapter.

Ultramicroelectrodes have been widely used for in vivo experiments due to their small size. A common application is to use ultramicroelectrodes to monitor the concentrations of neurotransmitters in the central nervous systems (e.g., the detection of dopamine (DA) in vivo).[53,54] However, voltammetric responses of the neurotransmitters usually suffer from the interference of ascorbic acid (AA) which usually coexists in vivo at high concentrations.[114] Microelectrodes coated with Nafion are usually used to solve this problem since Nafion can repel AA (an anion in vivo). Here we describe the use of microelectrodes coated with OPPy ultrathin films to improve selectivity of the electrodes. The interference by anions is lessened with electrodes coated with ultrathin OPPy film. Practical use of OPPy ultrathin films for detection of catechols in the presence of ascorbic acid is demonstrated.

A derivative of Py, pyrrole-2-carboxylic acid (Py-2-COOH), was also investigated for its ability to form cation permselective films. The Py-2-COOH can be polymerized at 1.7 V *vs.* Ag wire in acetonitrile (MeCN). This polymer layer also shows cation permselectivity at pH 7 due in part to the negative charge of the deprotonated carboxylic group (pK_a = 4.453).[115] The cation permselectivity of polypyrrole-2-carboxylic acid (PPy-2-COOH) is discussed and compared to that of OPPy films.

Procedure of Ultrathin OPPy Film Formation by Polymerization and Overoxidation

Carbon electrodes were modified by electropolymerizing PY at +0.950 V *vs.* Ag wire. The solution used for polymerization was 20 mM PY and 0.1 M TBAP in MeCN. A small amount (1.5×10^{-10} mole/cm^2, a typical monolayer coverage)[116] of PY was polymerized by holding the potential at +0.950 V for a short time (about 40 ms for GC and 10 ms for carbon fiber ultramicroelectrode). The charge passed at the GC electrode at each coating was controlled at ca. 3.5×10^{-5} C/cm^2 (corresponds to 1.5×10^{-10} mole/cm^2 surface coverage) which is about a monolayer coverage. Due to the edge effect, the current density is higher at an ultramicroelectrode than at a macroelectrode.

The time required to polymerize a PY monolayer on an ultramicroelectrode is very short and it is more difficult to control the surface coverage by controlling the time of polymerization. Therefore, a higher surface coverage (3×10^{-10} mole/cm^2) was used at ultramicroelectrodes for each coating, which allows longer times for polymerization of Py.

The PPy modified electrode was rinsed with deionized water and then transferred to 0.5 M pH 7.0 phosphate buffer solution and overoxidized at +0.950 V *vs.* SCE. During overoxidation, the current was monitored. Initially, a large current was passed, but this rapidly decreased as the oxidation progressed. The current eventually leveled off and began to fluctuate slightly around one value. This was taken to indicate complete overoxidation. This process usually took about two minutes. The electrode was left to dry and then put back to Py/MeCN solvent for another coating of PPy film. The procedure was repeated several times until the cyclic voltammogram (CV) of $Fe(CN)_6^{(3-/4-)}$ was completely suppressed. For the GC electrode, six times of repeated coating with $9x10^{-10}$ mole/cm^2 total surface coverage is sufficient. For carbon fiber ultramicroelectrodes, four times of repeated coating with $1.2x10^{-9}$ mole/cm^2 of total surface coverage are satisfactory.

Procedure for Coating Ultrathin OPPy Films on Pt

Pt ultramicroelectrodes (5 µm in diameter) were used as working electrodes. The Pt electrodes were put in 20 mM Py/ MeCN solvent for 5 minutes to allow Py adsorption on the surface. Then the electrodes were taken out and rinsed with deionized water. The electrode with adsorbed Py was placed in phosphate buffer to be polymerized and overoxidized at +0.950 V *vs.* SCE. During the process, current was monitored until it leveled off and fluctuated only slightly. This indicated that the polymerization and overoxidation were completed.

Preparation of Ultrathin OPPy Films

It has been found that the major route of forming conducting polymers (such as PPy) is through "continual electroprecipitation".[117] The monomers form oligomeric chains in solution, then precipitate on the bare substrate. Further growth of the polymer occurs not only by addition of monomers to the polymer chain end, but largely by the precipitation of other oligomeric moieties on top of the nuclei already formed. Precipitation on top of the polymeric nuclei, rather than on the bare substrate, has been found to be favored.[117] Therefore, a very thin film will have a lot of pin holes and defects since the growth of the film is favored on top of the polymer instead on the bare substrate.

A repeated coating and overoxidation procedure was used to fill the pin holes and defects in the thin PPy film while the thickness of the film was maintained. Fig. 4.3 is a conceptual drawing of how the pin holes and defects are filled by repeated polymerization and overoxidation of PPy. An ultrathin film of PPy (ca. 1.5×10^{-10} mole/cm^2 surface coverage) is first coated on a GC electrode following a potential step from +0.500 to +0.950 V in 20 mM Py/MeCN solution. This first thin layer of PPy is overoxidized by holding the potential at +0.950 V in phosphate buffer (pH 7.0) until the current is less than 1 μA, and becomes stable, which insures that the overoxidation is complete. This step causes loss of conductivity of the film.[118] When the electrode is transferred back to Py/MeCN solvent for the second coating of PPy film, the second coating does not grow on top of the first layer. Since the first layer of OPPy has no electronic conductivity and the pin holes insure exposure of the electroactive surface, the most likely place the second coating can form is on the bare substrate, and in the process the pin holes and defects in the first layer become partially filled. By repeating this procedure several times, the pin holes and defects are eventually filled. A thin but virtually pin hole free OPPy film can be made using this approach. The procedure can be used to form ultrathin films on macro and ultramicro graphite electrodes.

Figure 4.3. A cartoon representation of pin holes gradually filled with OPPy by a repeated coating procedure.

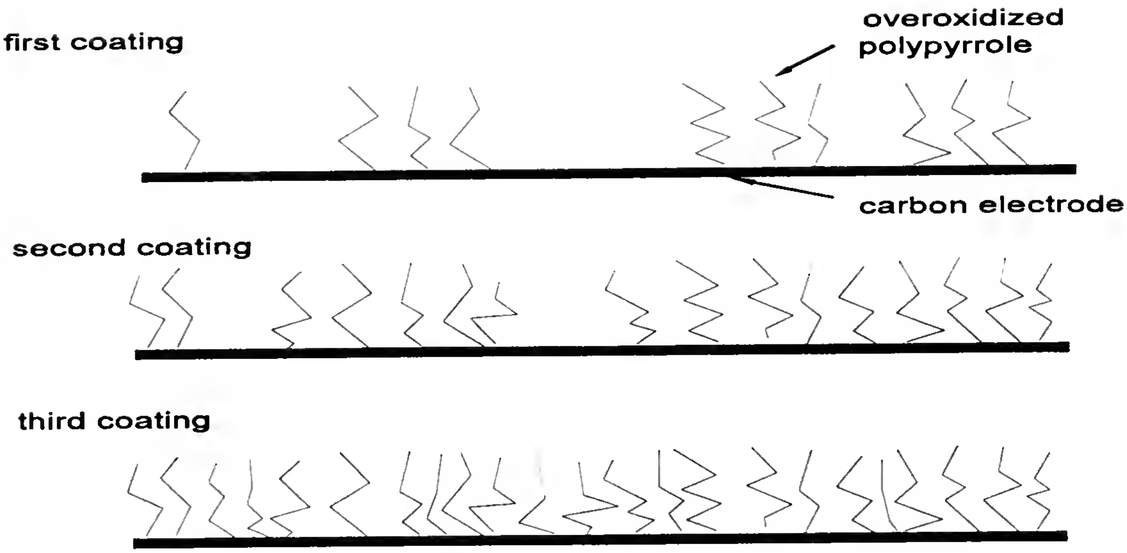
first coating
overoxidized polypyrrole
carbon electrode
second coating
third coating

Cation Permselectivity of Ultrathin OPPy at GC Electrodes

An ultrathin film can be coated on GC by polymerizing a small amount of Py (ca. 1.5×10^{-10} mole/cm^2, a typical monolayer surface coverage) in 20 mM Py/MeCN solvent. However, as was already discussed, this film has a limited permselectivity due to the pin holes and defects in the film; therefore, a procedure was developed in which the electrode was repeatedly treated by a polymerization/overoxidation to fill the pin holes. After repeated treatment, the response of the anionic $Fe(CN)_6^{(3-/4-)}$ redox couple is totally suppressed while the response of the cationic $Ru(NH_3)_6^{(3+/2+)}$ redox couple decreased slightly.

Fig. 4.4A shows the responses of the anion before and after repeated coating. The response of $Fe(CN)_6^{(3-/4-)}$ anion gradually decreases until it almost disappears after six coating (curve 7). Compared to the bare electrode, the response decreases 95% after coating six times. The total surface coverage of OPPy coated on the electrode is $9\text{x}10^{-10}$ mole/cm^2, which corresponds to a multilayer coverage (3~6 layers) since typical monolayer coverage is between $1.5\text{x}10^{-10}$ to $3\text{x}10^{-10}$ mole/cm^2.[67]

The thickness of this film was roughly estimated at about 16 Å (assuming 4 layers and each layer has 4 Å thickness). The value of the thickness for each layer is based on the size of Py (ca. 4 Å). The bond lengths on Py are 1.34, 1.48, 1.07 , and 1.01 Å for C=C, C-N, C-H, and N-H respectively. Considering the angles between the bonds, the diameter of PY is estimated at ca. 4 Å. Since this thickness value is based on some assumptions, it has to be viewed as a rough estimate. Consequently, the other values obtained in this paper which are based on the thickness of the film (such as apparent diffusion coefficients and permeability) are also rough estimates.

Fig. 4.4B shows the responses of a cationic redox couple before and after coating. The electrode is the same as that used in Fig. 4.4A. The response of the $Ru(NH_3)_6^{(3+/2+)}$ cation decreases only 16% after six times of coating (dashed line). The value of $1/P_m$ (δ_m/D_{app}) obtained by the method of Gough and Leypoldt (see Charpter 2) for $Ru(NH_3)_6^{(3+/2+)}$ in this film is 22.1 s/cm. Rough estimate of the thickness of this film based on the surface coverage is ca. 16 Å, therefore, D_{app} of $Ru(NH_3)_6^{(3+/2+)}$ is 7.2×10^{-9} cm^2/s. This apparent diffusion coefficient is slightly lower than that measured on a thick OPPy film (0.1 μm) on the same GC electrode substrate (2.8×10^{-8} cm^2/s),[119] which may be due to the greater compactness of the thin film. The ultrathin film obtained by repeated coating and overoxidation has filled pin holes; therefore, the thin film may be more compact than the thick film, although the electrode substrates used are the same (polished GC electrode).

Despite the fact that D_{app} for the thin film is smaller than that for the thick film, CVs of $Ru(NH_3)_6^{(3+/2+)}$ obtained at the thin film modified electrode show peak currents that are 30% higher than for the electrodes modified with the thick film. This is because the response of the electrode is determined by film permeability (D_{app}/δ_m) and not only by D_{app} (equation 1.20). Since the δ_m of the thin film is much smaller than that of the thick film, the permeability of the thin film is higher. A thinner film with higher permeability will allow redox species to approach the electrode surface readily thus producing a higher redox current.

We observed that the ΔE_p of $Ru(NH_3)_6^{(3+/2+)}$ at an ultrathin film modified electrode is smaller than the ΔE_p at a thick film modified electrode. A possible reason is that the cell

Figure 4.4. Cyclic voltammograms: (a) 10 mM $Fe(CN)_6^{3-}$ in 0.5 M phosphate buffer (pH 7.0) at OPPy modified glassy carbon electrode. Curve 1 is the response of the bare electrode. Curves 2-7 are the responses after first time (curve 2) to sixth time (curve 7) of repeated coating; (b) 10 mM $Ru(NH_3)_6^{3+}$ at the same electrode and buffer as in (a). Solid line is the response before coating. Dashed line is the response after coating six times. Scan rate is 20 mV/s. Electrode area is 0.067 cm^2.

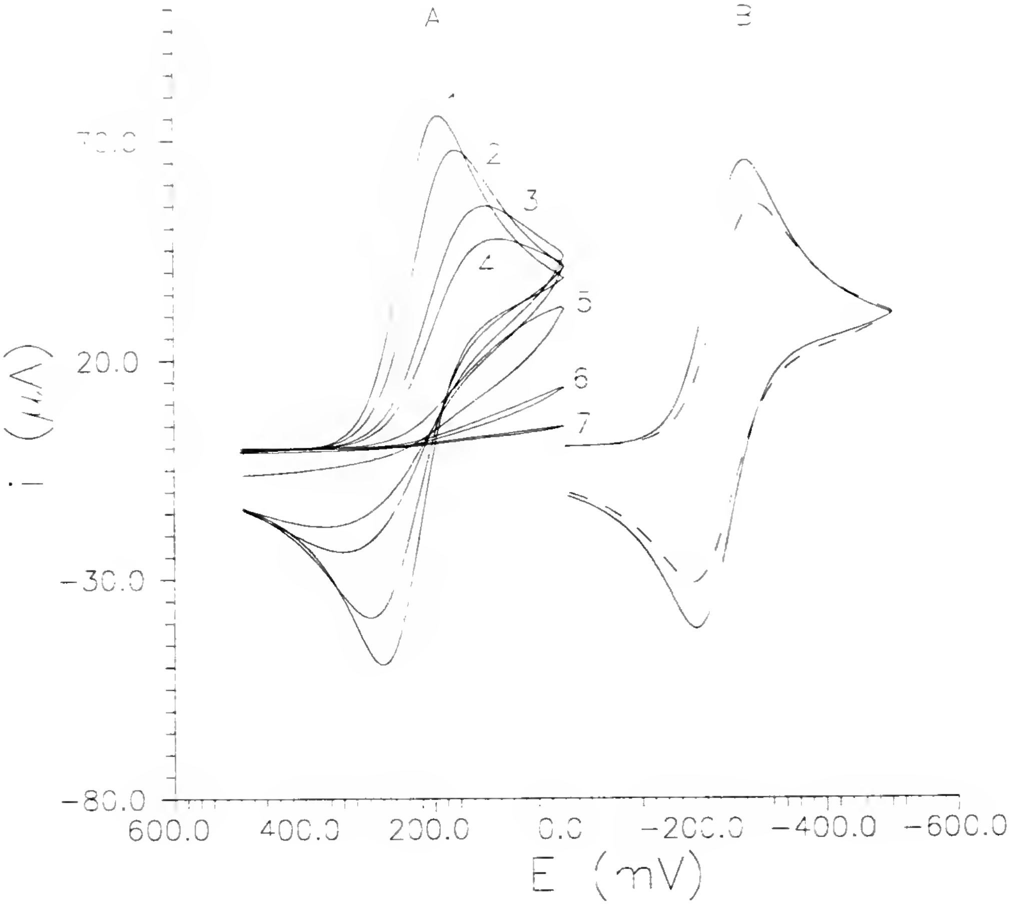
A
B
1
2
3
4
5
6
7
70.0
20.0
-30.0
-80.0
i (μA)
600.0
400.0
200.0
0.0
-200.0
-400.0
-600.0
E (mV)

resistance increases when the film becomes thicker and larger ΔE_p may be due to larger iR drop at a thicker electrode.

Permselectivity of Ultrathin OPPy Films at Carbon Fiber Electrodes

Carbon fiber ultramicroelectrodes were modified using the same procedure as was used to modify large area GC. Fig. 4.5A shows the responses of $Fe(CN)_6^{3-}$ anion before and after four times of repeated coating. For each coating, the amount of deposited PPy is about $3x10^{-10}$ mole/cm^2 which is calculated from the amount of charge for each coating divided by the electrode area. The amount of deposited PPy during each coating corresponds approximately to a monolayer surface coverage. The total amount of deposited Py after coating four times is $1.2x10^{-9}$ mole/cm^2.

The response of $Fe(CN)_6^{3-}$ gradually decreases while the procedure is repeated as the pin holes in the film are being filled. The sigmoidal current of $Fe(CN)_6^{3-}$ at the bare electrode rises after the electrode is modified with OPPy film, which shows that the kinetics of $Fe(CN)_6^{3-}$ slow down greatly. The same effect was observed at large electrodes (Fig. 4.4A) where the ΔE_p increased as the pin holes were being filled. Eventually, the response of the $Fe(CN)_6^{3-}$ is totally suppressed presumably due to the repulsion between $Fe(CN)_6^{3-}$ and the film (Fig. 4.5A, curve 5).

Fig. 4.5B shows the responses of the $Ru(NH_3)_6^{(3+/2+)}$. The sigmoidal current decreases 30% after the electrode is coated four times. Compared to a large GC electrode, at modified carbon fiber a more drastic decrease in both anion and cation response is observed. This is

Figure 4.5. Cyclic voltammograms: (a) 10 mM $Fe(CN)_6^{3-}$ in 0.5 M phosphate buffer (pH 7.0) at OPPy modified carbon fiber ultramicroelectrode. Curve 1 is the response of the bare electrode. Curves 2-5 are the responses after first (curve 2) to four times (curve 5) of repeated coating; (b) 10 mM $Ru(NH_3)_6^{3+}$ at the same electrode and buffer as in (a). Solid line is the response before coating. Dashed line is the response after coating four times. Scan rate is 20 mV/s. Electrode diameter is 7 μm.

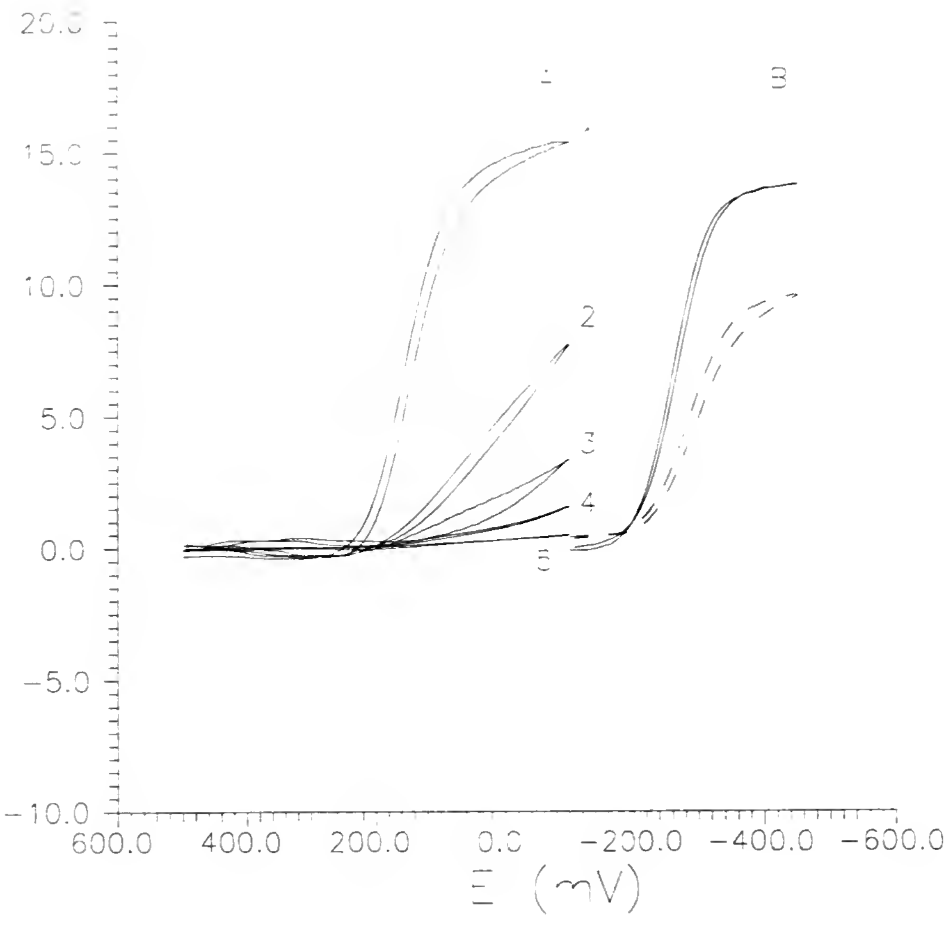
20.0
15.0
10.0
5.0
0.0
−5.0
−10.0
i (nA)
600.0
400.0
200.0
0.0
−200.0
−400.0
−600.0
E (mV)
1
B
2
3
4
5

probably due to the higher surface coverage at each coating and different surface properties of GC and carbon fiber. However, both types of electrodes exhibit excellent ability to impede anion diffusion after repeated coating. At both electrodes, the ability to impede anion diffusion can be enhanced by repeatedly coating with a polymer film at a small expense of a small decrease in cation response.

Applications of OPPy-Coated Ultramicroelectrodes

Ultramicroelectrodes (such as carbon fiber electrodes) have been widely used in sensors for in vivo measurements. There is considerable interest in their use as detectors for microcolumn HPCL and CZE because of their extremely small size (less than 10 μm) and higher signal-to-noise ratio (up to one decade higher) compared to macroelectrodes (see Chapter 1). In spite of these merits of microelectrodes, the selectivity of microelectrodes is not improved as the size of the electrode decreases. The results obtained here show that the ability to impede anion diffusion by the OPPy film can improve the selectivity of carbon fiber electrodes without significantly sacrificing the sensitivity of the electrode towards cations.

Practical applications of the new selective films were tested with two biological compounds - one is dopamine (DA) which is a cation at physiological pH ($pK_a = 8.92$) and the other is ascorbic acid (AA) which is an anion ($pK_a = 4.10$).[120,121] AA has a redox potential ($E^{0'}$ of +0.20 V vs. SCE) close to that of DA ($E^{0'}$ of +0.12 V vs. SCE) at pH 7.0.[122] In vivo, the concentration of AA can be three to four orders of magnitude higher than the concentration of DA.[123] To detect DA in the presence of AA, OPPy was used to modify carbon fiber electrodes in order to reduce the interference of AA.

Figure 4.6 shows the responses of 10 mM AA and DA in pH 7 buffer on an ultrathin OPPy film modified carbon fiber electrode (coated four times with total surface coverage of ca. 1.2×10^{-9} mole/cm^2). The solid line is the CV of DA. The dashed line is the CV of AA, which is almost totally suppressed. In our previous investigation of thick OPPy films, the ability to impede anion diffusion was shown to be affected by the hydrophobicity of the anions.[72,73] The structure of AA made it permeable in thick OPPy films on GC electrodes. Therefore, the film has low permselectivity against AA. However, the response of AA is suppressed quite effectively with the ultrathin film. This may be due to the fact that the thinner film obtained by repeated coating is more compact because of the effective filling of pin holes and defects. A more compact OPPy film has higher density of carbonyl groups and thus a higher electron density to repel anions and possibly may also be less hydrophobic. Since AA has four OH functional groups and a carbonyl group, which have high electron density, these groups can make AA less permeable in a more compact film with high electron density.

Permselectivity of Ultrathin OPPy Films at Pt Ultramicroelectrodes

Py adsorption on Pt electrodes has been characterized.[124] A monolayer of Py has been found to irreversibly adsorb on Pt(111).[124] Py can adsorb on the Pt(111) surface in the horizontal or vertical orientation through either N or C=C, respectively, but the horizontal

Figure 4.6. Cyclic voltammograms of 10 mM dopamine (solid line) and ascorbic acid (dashed line) in 0.5 M phosphate buffer (pH 7.0) at carbon fiber electrode modified four times with the same film as in Figure 4.5. Scan rate is 20 mV/s. Electrode diameter is 7 µm.

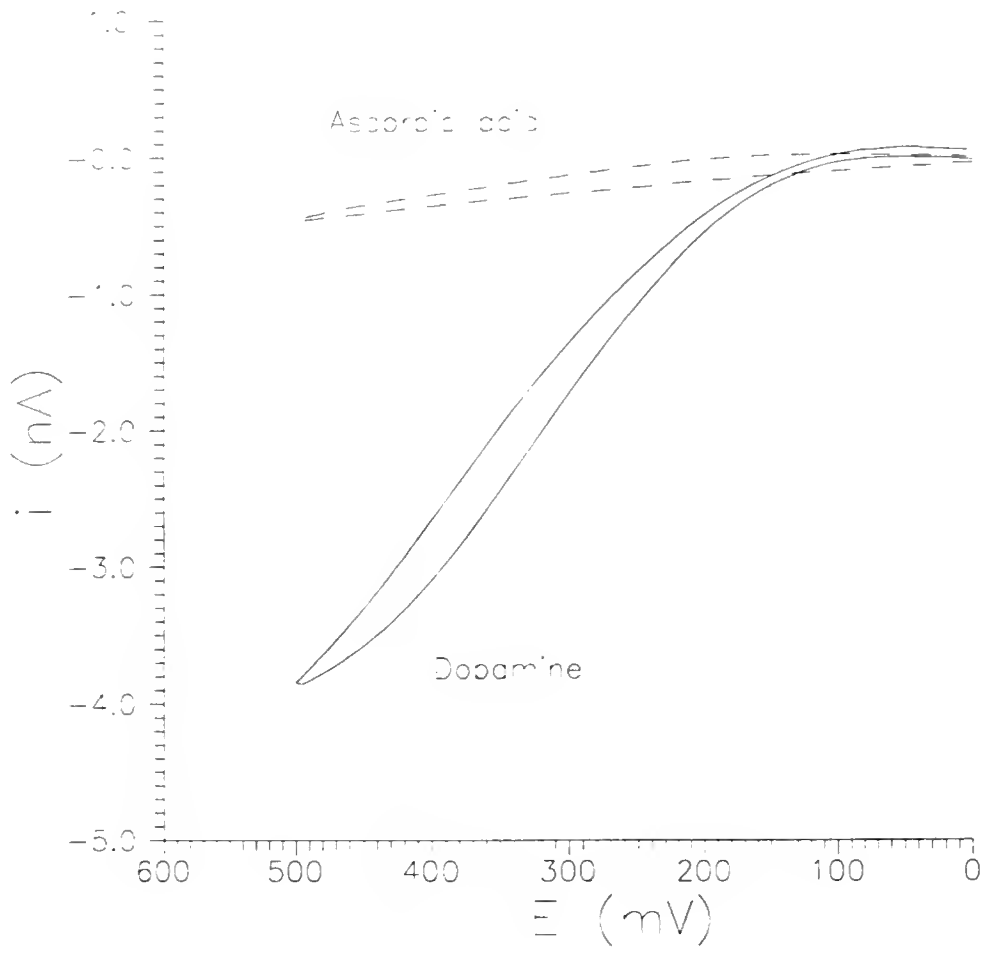
1.0
−0.0
−1.0
−2.0
−3.0
−4.0
−5.0
i (nA)
600
500
400
300
200
100
0
E (mV)
Ascorbic acid
Dopamine

orientation is predominant.[124] It should be possible to form a monolayer of OPPy on a polycrystalline Pt ultramicroelectrode since Py adsorbed on a Pt electrode can be first polymerized and then overoxidized into a monolayer of OPPy at a potential of +0.950 V (the polymerization potential for Py on Pt begins at ca. +0.400 V). Surface coverage of adsorbed Py may be obtained by performing a CV from 0.000 to +0.600 V in phosphate buffer. We tried to obtain surface coverage of such monolayer by integrating the current under the oxidation peak of the CV, but there is no observable peak in the CV to allow this. However, the value of the monolayer surface coverage is available from the literature.[125] Calculated from the Auger spectra, the surface coverage of PY adsorbed on Pt(111) from aqueous solution has been reported as 4.16×10^{-10} mole/cm^2.

We expected this monolayer to exhibit an ability to suppress anion response. Figure 4.7A shows that the responses of $Fe(CN)_6^{(3-/4-)}$ is decreased about 90% after the Pt ultramicroelectrode is modified with the monolayer OPPy film, while the response of $Ru(NH_3)_6^{(3+/2+)}$ is decreased only about 20% (Figure 4.7B). Compared to the results on GC and on carbon fiber electrodes, the ability to impede anion diffusion (90% of the anion response is suppressed) by the monolayer film coated on Pt is not as good as that of the films obtained using the repeated coating procedure at graphite electrodes (anion response totally suppressed). Py adsorbed on Pt might not fully cover the surface. Following polymerization and overoxidation, the polymer may have some pin holes and defects. The permselectivity of the modified Pt electrode should improve when a more ordered adsorbed monolayer is formed before polymerization and overoxidation.

Figure 4.7. Cyclic voltammograms: (a) 10 mM $Fe(CN)_6^{3-}$ obtained at Pt ultramicroelectrode in 0.5 M phosphate buffer (pH 7.0). Solid line is the response at the bare electrode. Dashed line is the response at an electrode modified with adsorbed/polymerized monolayer of OPPy film; (b) 10 mM $Ru(NH_3)_6^{3+}$ at the same electrode and buffer as in (a). Solid line is the response at the bare electrode. Dashed line corresponds to the conditions for dashed line in (a). Scan rate is 20 mV/s. Electrode diameter is 5 μm.

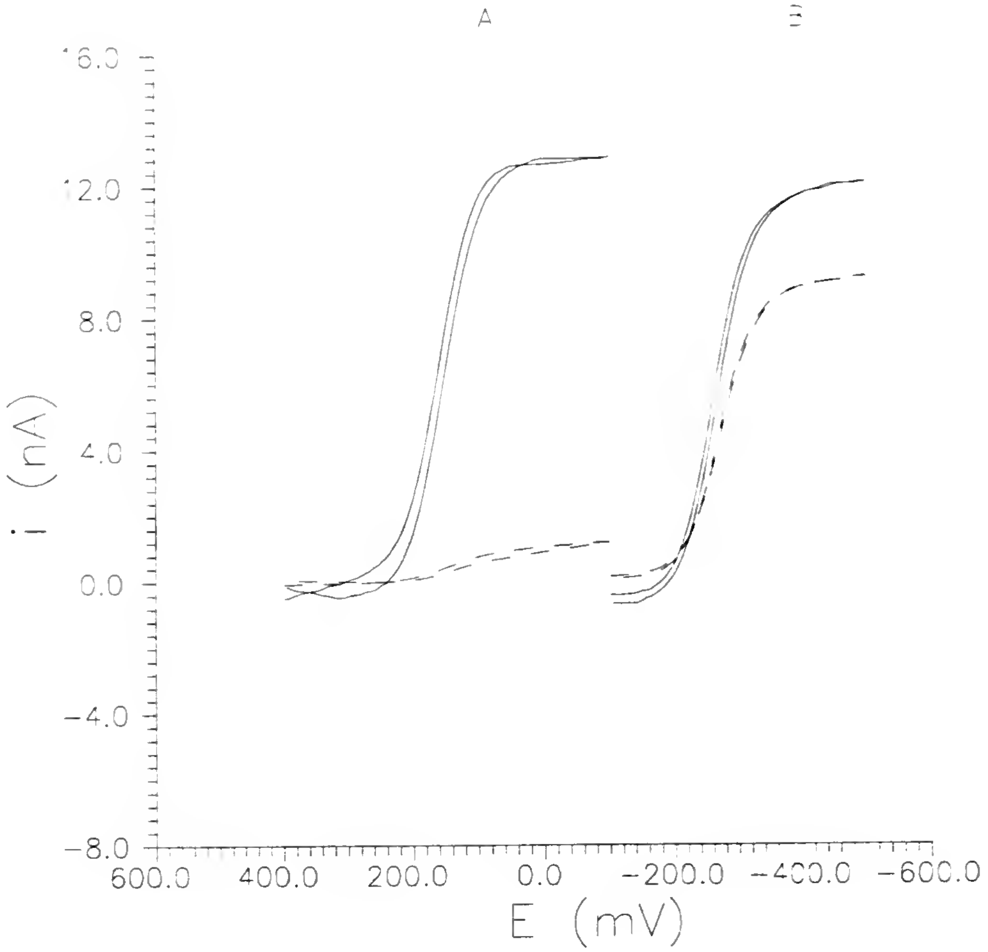
A
B
16.0
12.0
8.0
4.0
0.0
−4.0
−8.0
i (nA)
600.0
400.0
200.0
0.0
−200.0
−400.0
−600.0
E (mV)

Stability of the OPPy Films

The stability of the OPPy on GC, carbon fiber and Pt was tested by storing the modified electrodes in phosphate buffer (pH 7.0) for 5 days. The responses of OPPy film coated electrodes were virtually unchanged after the electrodes were stored in phosphate buffer for 5 days, which demonstrates that the deposited film is stable in a quiescent solution. However, the mechanic stability is not quite as good. It was noticed during the rotating disk experiments that high rotating speeds (higher than 1000 rpm) partially damaged the OPPy film on GC. However, at lower speeds, the permselectivity of the film remained intact. The stability of the monolayer OPPy on Pt was also tested. Its permselectivity is maintained after the electrode is stored in phosphate buffer for 5 days.

Coating Polymer Films of PPy-2-COOH on Pt Electrodes

We also investigated the ability of PPy-2-COOH to form permselective films. The ability to impede anion diffusion by these films can come from the deprotonated carboxylic groups ($pK_a = 4.453$)[126] which can repel anions with the fixed negative charge. Only the polymerization is needed to form a permselective film. Unlike the formation of the OPPy film, the overoxidation of the film and the introduction of the carbonyl groups during the overoxidation is not needed here. It has been reported that Py-2-COOH can be polymerized at +1.700 V vs. SSCE in MeCN.[127] Because of the effective adsorption of Py and the carboxylic group on Pt, we expected that Py-2-COOH should adsorb on Pt.[128]

Figure 4.8A shows consecutive voltammetric cycles in the 50 mM Py-2-COOH/MeCN solution. The first cycle shows a sharp peak with no diffusional tailing even though the cyclic voltammogram was obtained in 50 mM Py-2-COOH/MeCN with an ultramicroelectrode. The second and third cycles show a drastic decrease in peak currents. The symmetric and adsorption-like peak on the first scan can not simply come from adsorbed monomers since the total charge under the peak is enormous for an adsorption peak (ca. $1.2\text{x}10^{-10}$ C which corresponds to ca. $4.5\text{x}10^{-5}$ mole/cm^2 surface coverage). In contrast to Pt, the cyclic voltammograms of 50 mM Py-2-COOH on a GC electrode show diffusion behavior (Fig. 4.8B). A reasonable explanation is that Py-2-COOH is adsorbed on Pt and polymerizes during the first scan. The polymer film which adheres to the electrode must have a very low electronic conductivity and must passivate the electrode during the first scan, so that the current rapidly decreases and causes a symmetric peak instead of a diffusional peak. The passivation of the electrode also prevents continuing growth of the film during the second and third scans. Adsorption of PPy-2-COOH on GC may not be as strong, so the polymer diffuses away instead of passivating the surface. Therefore, a normal diffusional tailing appears in CVs on GC electrodes.

Pt electrode coated with the polymer shows the ability to impede anion diffusion in phosphate buffer since the deprotonated carboxylic groups can repel anions with their negative charge. Figure 4.9 shows CVs at a Pt ultramicroelectrode before and after the electrode is modified with PPy-2-COOH. The sigmoidal current of $Fe(CN)_6^{(3-/4-)}$ decreases ca. 84% but the current of $Ru(NH_3)_6^{(3+/2+)}$ decreased only ca. 15%. Compared to the CVs obtained on Pt, the response of $Fe(CN)_6^{(3-/4-)}$ at the modified GC electrode is suppressed only

Figure 4.8. (a) Cyclic voltammograms of three consecutive scans at Pt ultramicroelectrode in 50 mM Py-2-COOH and 0.1 M TBAP in MeCN. Scan rate is 50 mV/s. The reference electrode is a Ag wire. Electrode diameter is 5 μm. The peak potential is ca. +1.5 V vs. Ag wire; (b) Cyclic voltammograms of three consecutive scans at a glassy carbon electrode in 50 mM Py-2-COOH and 0.1 M TBAP in MeCN. Scan rate is 100 mV/s. Electrode area is 0.067 cm^2. The peak potential is ca. +1.65 V vs. Ag wire.

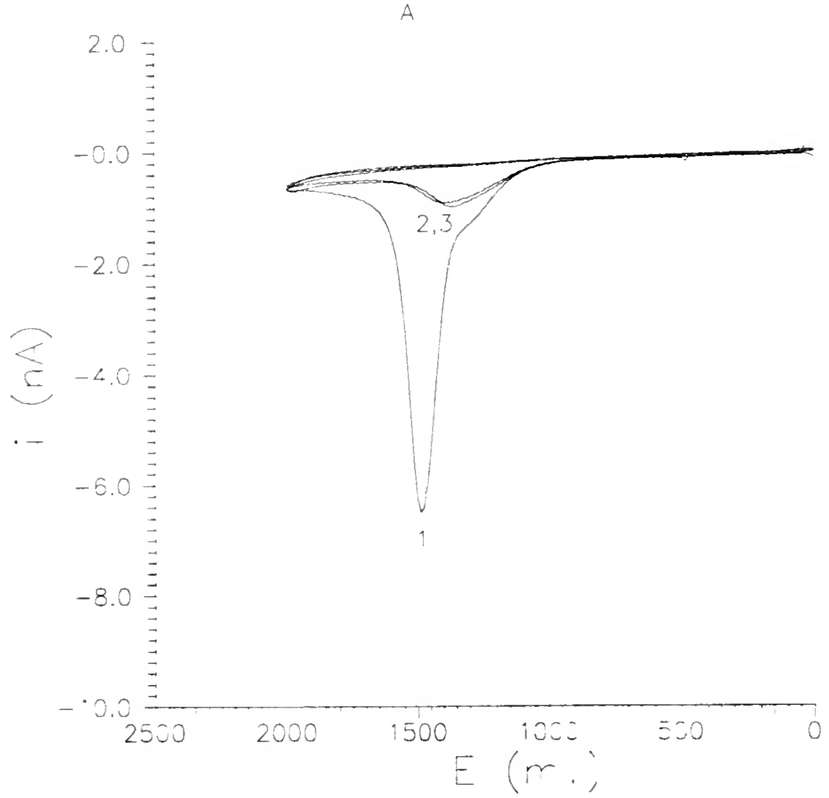
A
2.0
−0.0
−2.0
−4.0
−6.0
−8.0
−10.0
i (nA)
2,3
1
2500
2000
1500
1000
500
0
E (mV)

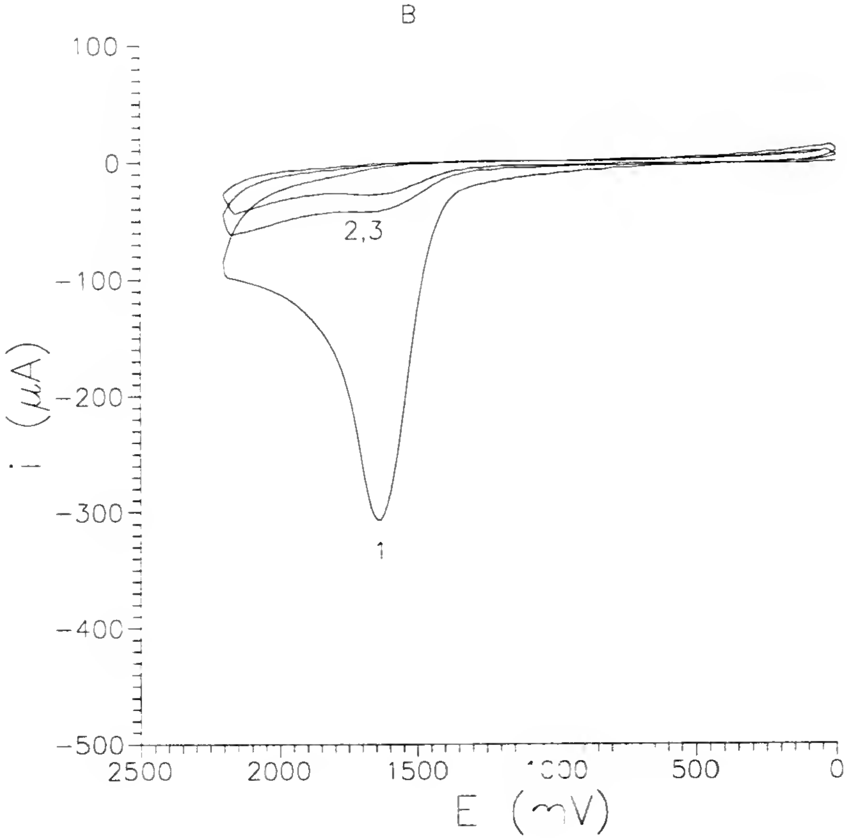
B
100
0
−100
−200
−300
−400
−500
i (µA)
2,3
1
2500
2000
1500
1000
500
0
E (mV)

Figure 4.9. Cyclic voltammograms: (a) 10 mM $Ru(NH_3)_6^{3+}$ and (b) 10 mM $Fe(CN)_6^{3-}$ in 0.5 M phosphate buffer (pH 7.0) at a Pt ultramicroelectrode before and after coating with PPy-2-COOH in one CV scan. Solid lines are the voltammograms at the bare electrodes. Dashed lines are the voltammograms at the modified electrodes. Scan rate is 20 mV/s. Ultramicroelectrode diameter is 5 μm.

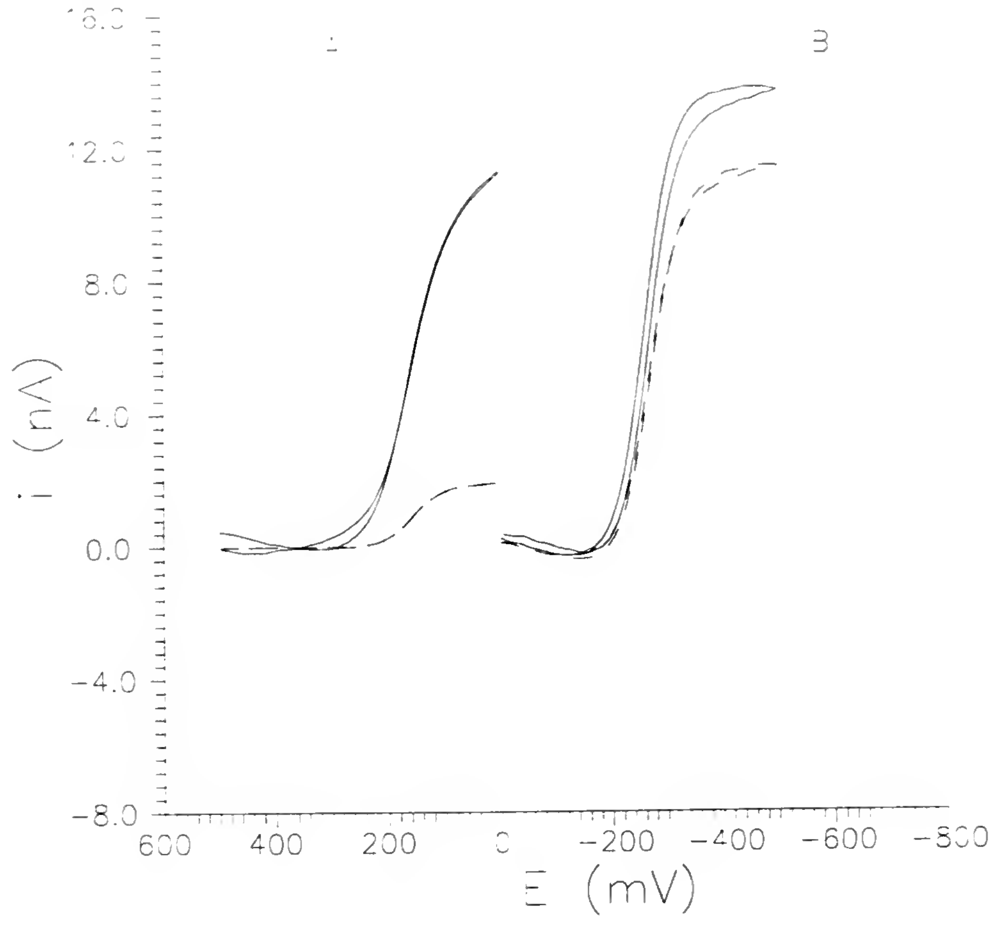
A
B
16.0
12.0
8.0
4.0
0.0
−4.0
−8.0
i (nA)
600
400
200
0
−200
−400
−600
−800
E (mV)

40%. This shows that the ability to impede anion diffusion by the modified GC electrode is not as good as that of Pt. Adhesion and precipitation of the polymer on GC may be not as good as on Pt because of the lack of effective adsorption to form a thin and compact layer that can accelerate polymer precipitation.

Surface coverage of PPy-2-COOH at Pt is ca. 4.5×10^{-5} mole/cm^2 based on the charge passed at the electrode during polymerization. This surface coverage is four orders of magnitude higher than the surface coverage (ca. 10^{-9} mole/cm^2) of OPPy on Pt and carbon electrodes. Besides the high surface coverage, the anion repulsion strength of the $-COO^-$ group in the PPy-2-COOH should be greater than that of the -CO group of the OPPy. Based on the much higher surface coverage and the expected stronger anion repulsion, we expected that the PPy-2-COOH should have much better permselectivity than the OPPy film. However, compared to the monolayer OPPy-modified Pt and ultrathin OPPy films modified GC, the permselectivity of PPy-2-COOH modified Pt is about the same. This may be due to the fact that the permselectivity of the film depends not only on the repulsion strength and the surface coverage by the film, but also on the structure (compactness) of the film. In spite of the higher surface coverage and the greater inherent repulsion strength of the PPy-2-COOH, the OPPy films must have a more compact structure. Thus OPPy should work more effectively in impeding anion diffusion.

Conclusions

Different methods of modifying electrodes with ultrathin permselective films are presented in this chapter. This work demonstrates that a monolayer or multilayer ultrathin film can effectively suppress the responses of anions as long as the films are compact and relatively pin hole free. As the above results show, compact ultrathin films can be obtained by taking advantage of repeated polymerization, or adsorption and polymerization, of a monolayer on electrodes.

Self-assembled alkanethiol monolayers formed on well-defined gold electrode substrates have been found to show cation permselectivity at pH higher than 7.0 due to the electrostatic effect of the carboxyl group of the monolayer preventing close anion access to the gold surface.[129,130,131] The previous results as well as the results presented here indicate that permselectivity of a film should occur regardless of the thickness of the film. The reason for using well defined electrodes is to form a uniform and pin hole free monolayer. Present results show that ultrathin films coated on not so well-defined substrates (such as GC, carbon fiber and Pt wire) can also be permselective as long as the films are relatively pin hole free.

Preparation of ultramicroelectrodes modified with ultrathin permselective films is also demonstrated in this chapter. The permselectivity of the OPPy thin films suggests that ultramicroelectrodes coated with such films may be useful for in vivo measurements to lessen the interference of biological anions. Hydrophobic substrates have been used to control or promote the growth of conducting polymers. This ultrathin OPPy film may be used to precoat electrodes to promote or control the growth of conducting polymers since the ultrathin OPPy film is sufficiently hydrophobic to permit monomers to accumulate in the film and be polymerized.

CHAPTER 5
NEW STRATEGIES FOR IMPROVING SENSITIVITY AND SELECTIVITY WITH FAST SCAN VOLTAMMETRY

Background

Small dimensions of UMEs permit in-vivo detection with high spatial resolution and minimal tissue damage. Because of these properties small dimensions of UMEs have been exploited by electrochemists and neuroscientists. In-vivo detection of neurotransmitters with UMEs has been extensively studied since 1980.[132]

One of the most important neurotransmitters, dopamine (DA), has been under intensive investigation by electrochemist and neuroscientists due to its important role in neurology and its ease of electrochemical detection due to its low oxidation potential ($E_{1/2} \sim 0.12$ V at graphite electrodes).[133] Despite of the successful detection of dopamine in aqueous buffers, detection of dopamine in-vivo remains challenging. The major problem has come from the interference by ascorbic acid (AA). AA has similar oxidation potential ($E_{1/2} \sim 0.2$V at graphite electrodes) to DA but its concentration is 10^2 to 10^3 times higher than that of DA in extracellular fluid of the brain where the in-vivo measurements of DA are done. Thus, attempts at selective detection of DA in the presence of AA have become a major challenge in in-vivo detection.

In the 1980's, Adams group introduced coating Nafion (a cation selective polymer) on the electrode surface to increase the selectivity of DA detection in the presence of AA.[134,135] At physiological pH of 7.4 DA is protonated and is present as a cation while AA is an anion at pH 7.4. Anion diffusion dramatically decreases at electrodes coated with anion excluding Nafion films. Thus, the selectivity of DA over AA can be enhanced on Nafion coated electrodes because of the permselectivity of Nafion to anions.

However, the enhancement in selectivity provided by Nafion is not sufficient to allow DA detection in the presence of high concentrations of AA. An additional improvement in selectivity is needed for successful analysis. One possible approach to further enhance the selectivity is to use fast scan voltammetry at scan rates of 100 to 300 V/s. This approach has originally been developed in Millar's group and has later been improved by Wightman's group.[136,137] One of the advantages of fast scan cyclic voltammetry is that the analyte and the interferant may be resolved by exploiting the differences between electrochemical kinetics of the analyte and the interferant.[138] At Nafion coated electrodes, the electrochemical kinetics of AA are very sluggish. Fast scan voltammetry enhances the effect of kinetic differences between DA and AA measurements, where the oxidation peak potential of AA shifts away from the oxidation peak potential of DA as the scan rate increases. Thus, the selectivity of DA over AA can be improved further.

Another advantage of fast scan voltammetry is that it can contribute to the stability of the working electrodes. Many redox reactions of biological species (such as DA, uric acid and NADH) are followed by chemical reactions which produce side products. Those products can adsorb on the electrode surface leading to a gradual loss of electrode activity. Consequently, electrode activity can decrease significantly after several scans. This problem can be partially resolved by adding surfactants to solution to act as molecular spacers at the surface to prevent surface fouling but in in-vivo detection, addition of surfactants is not practical.[139] However, because of the short time span of fast scan voltammetry, before the products can undergo chemical reactions in solutions, they can be converted back to the original analyte. Consequently, surface fouling caused by the products of the follow-up reactions can be prevented.

Another advantage of fast scan voltammetry compared to other fast techniques (such as chronoamperometry) is that fast scan voltammetry can provide qualitative information about the analyte which may used to confirm the identity of the analyte of interest in complex samples. Since different redox reactions occur at unique redox potentials and have unique waveforms, identification of potentials and waveforms can add more confidence that the analyte of interest is being detected in a complicated environment. In addition, at high scan rates, thickness of the diffusion layer of analytes such as DA will be greatly reduced, therefore, the chance of the diffusion been blocked by , for example, the brain tissue in the in-vivo experiments, and distorting the shape of the voltammogram is greatly reduced. This can insure that qualitatively voltammograms of DA obtained in-vivo will be identical to the voltammograms of DA in buffer.

Despite the improved selectivity of DA over AA at Nafion coated electrodes when combined with fast measurements, there are drawbacks to Nafion-coated electrodes. First, thickness and quality of Nafion films is difficult to control and reproduce. In addition, thin Nafion films cast on electrodes tend to have pin-holes which decrease the film permselectivity. On the other hand, thick Nafion films may have fewer pin-holes, but the extremely low diffusion coefficients of DA inside Nafion decrease the sensitivity and increase the response time.

In this chapter, we demonstrate that further significant increase of scan rate to above 1,000 V/s may considerably improve selectivity and sensitivity in analysis. In our laboratory we have investigated the possibility of using fast scan voltammetry to improve selectivity of DA detection in the presence of AA at bare electrodes without Nafion coatings. By pushing scan rates to above 1,000 V/s, the most obvious advantage gained is that the voltammograms of DA and AA may be resolved because of the kinetic differences in their response without the need for permselective film on the electrode. Some additional advantages are also obtained by increasing the scan rates. These include higher temporal resolution, higher peak currents and lower detection limits made possible by the use of signal averaging. These advantages, and some of the limitations of increasing scan rates to above 1,000 V/s are discussed in this chapter.

Effects of Surface Oxides on Sensitivity and Selectivity

Surface functional groups including oxide groups usually play an important role in electrochemical reactions because of the heterogeneous nature of electrochemical redox reactions in which the surface of the electrode has to participate. In fast scan voltammetry, the contributions to background current result from charging current which is due to physical charging of the electrical double layer at the electrode surface and from faradaic current due to the redox reactions of surface functional groups such as surface quinones. Because formation of surface functional groups can occur during the experiment and it can consequently change the surface roughness and the amount of surface oxygen, background current may significantly change during experiments. It is, of course, important to obtain a fairly stable background from run to run.

A stable background will facilitate background subtraction which is necessary in fast scan voltammetry. We have established experimentally that after 30 minutes of repeated cycling of the carbon fiber electrode in pH 7.4 phosphate buffer in the potential window of -0.8 to +1.2 V, background current will become fairly stable (Figure 5.1). The cycling potential window was chosen because all experiments were performed within this window, and the upper potential of +1.2 V is usually used for mild electrochemical pretreatments.[78] Comparison of voltammograms 1 and 2 indicates a significant change in the voltammograms following initial 30 minutes of cycling. A small peak grows at ca. 0.2 V as a result of cycling while the charging current in the entire potential window increases. This indicates that changes in the structure of the surface are occurring and supports formation of surface redox active functional groups. The surface wave at ca. 0.2 V may be due to a redox reaction of surface quinones because of the coincidence in the redox potential.[140,141]

After additional 30 minutes (total of one hour) of cycling in the same potential window, changes in the surface wave at 0.2 V and in charging current throughout the potential window are minimal. This was taken as an indication that a stable background has been reached. Surface coverage of the surface redox groups was estimated by integrating the current due to the surface wave at 0.2 V after 30 minutes of cycling by dividing the moles of the reactant producing this charge by the electrode surface area. The surface

Figure 5.1. Background currents after repetition of fast cycle scans. Cyclic voltammogram obtained: (line 1) with a freshly polished carbon fiber electrode (7 µm diameter); (line 2) after 30 minutes of repeated cycling, at a scan rate of 100 V/s, in the potential window of -0.8 to +1.2 V vs SCE; (line 3) after one hour of cycling; (line 4) after one and a half hour of cycling.

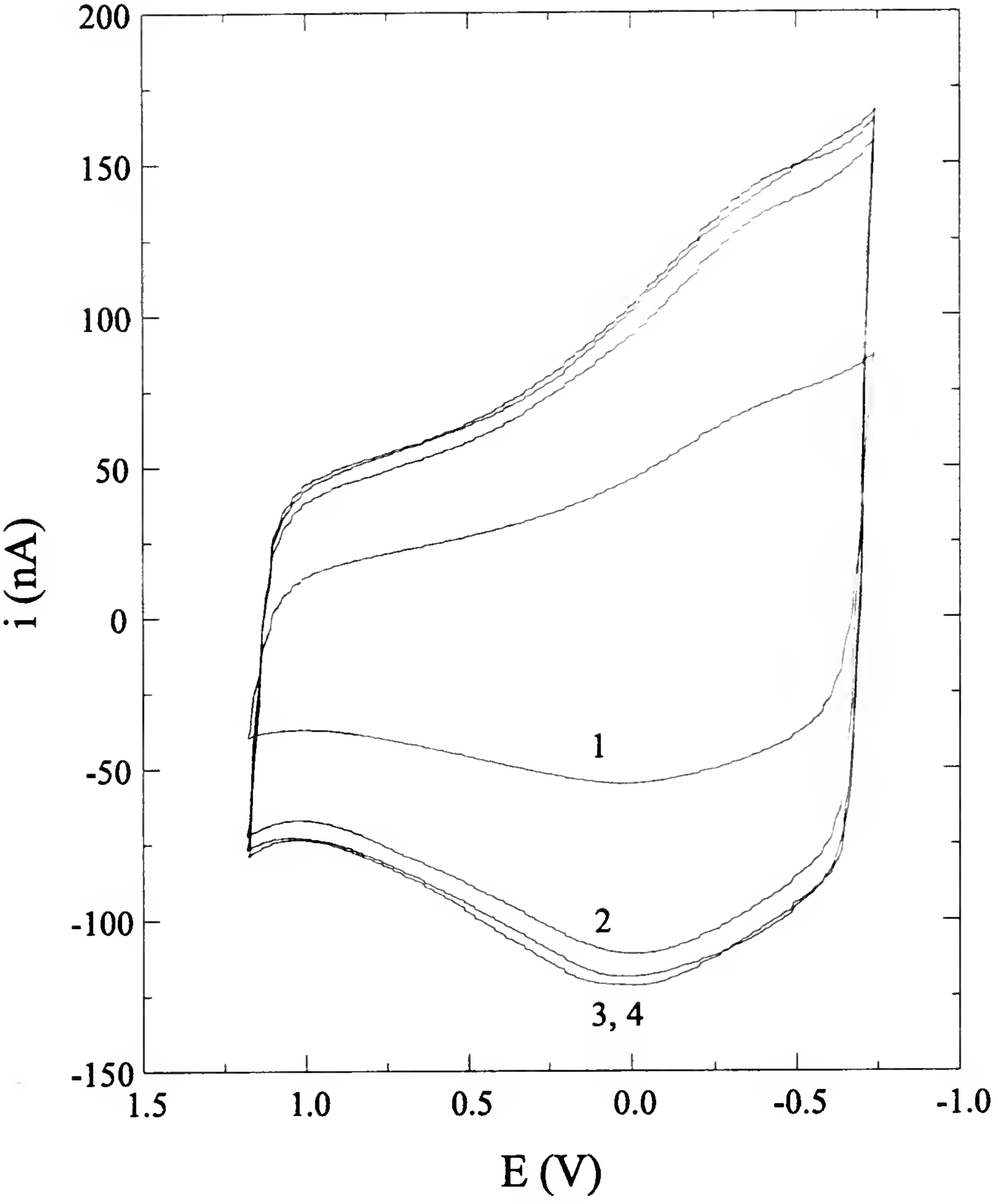
200
150
100
50
0
-50
-100
-150
i (nA)
1.5
1.0
0.5
0.0
-0.5
-1.0
E (V)
1
2
3, 4

coverage due to this particular surface wave ranges from 7.2×10^{-10} to 8.8×10^{-10} mole/cm^2 which indicates a ca. monolayer coverage by the redox active functional groups.

Besides affecting the background current, surface functional groups can play an important role in redox reactivity of analytes. For example, surface oxides have been found to improve the electrochemical kinetics of proton coupled redox reactions.[78] A most likely mechanism which can explain the observed improvement in electrochemical kinetics is one in which the surface functional groups (such as surface quinones) facilitate proton transfer during the redox reactions. Because the electrochemical oxidation of DA involves two electrons and two protons, this reaction may be assisted by the presence of surface functional groups.[78] Another benefit to the redox reaction of DA from surface functional groups may come from the fact that DA which is a cation at physiological pH will tend to adsorb and , therefore, be preconcentrated at the electrode surface due to the interactions with the negatively charged surface functional groups.[142,143,144] Adsorption of DA may not be apparent at low scan rates. However, at higher scan rates (> 100V/s), adsorption can start to dominate the electrochemical response because the adsorption peak current is proportional to scan rate.[145]

Cyclic voltammetric peak current is directly proportional to scan rate for an adsorbed species and is proportional to the square root of scan rate for a diffusing species as shown by equations 2.9 and 2.8, respectively.

For weakly adsorbed species such as DA where adsorption is not apparent at low scan rates, diffusional current dominates the electrochemical response at low scan rates.[92] However, because of adsorption, the adsorption current will become more important as the scan rate increases since the adsorption current increases faster with the increase in scan rate than does the diffusional current (equation 2.9 vs equation 2.8). At sufficiently high scan rates, adsorption current will dominate the electrochemical response as has been illustrated. The peak current for analytes such as DA will be roughly proportional to scan rate at high scan rates when the adsorption current becomes dominating. Thus, the detection limit can be improved by simply increasing the scan rate.

The effect of adsorption of DA on peak current as a function of scan rate was verified by plotting the logarithm of peak current vs the logarithm of scan rate. For purely adsorption controlled process (equation 2.8), the peak current should increase proportionally with scan rate and the slope of the plot should be 1. For purely diffusion controlled process (equation 2.9), the peak current will increase proportionally with square root of scan rate and the slope of the plot should be 0.5. For a weakly adsorbed species (such as DA), adsorption and diffusion will contribute to the measured current. Thus, the slope of the plot should be between 0.5 and 1 and should increases as the scan rate increases.

The slope of the plot calculated from the experimental data at the electrodes which were treated by 30 minute cycling in the potential window of -0.8 to +1.25 V is equal to 0.65 in the scan rate range from 50 to 10,000 V/s. This slope value indicates that adsorption significantly influences the measured current at high scan rates. When the slopes of the plots for the scan rate ranges of 50 to 500 V/s and 1000 to 10,000 V/s were calculated separately, the respective values were 0.59 and 0.70 (Figure 5.2). The significant increase in the value of the slope in the higher scan rate range further confirms that adsorption current starts to dominate the response at the higher scan rates. Based on the slope value of 0.65, peak

Figure 5.2. Plots of log of 0.1 mM DA peak current, log i_p vs log scan rate. Scan range is from 50 to 10,000 V/s. Working electrode is a carbon fiber electrode (7 μm diameter) and buffer solution is 70 mM pH 7.4 phosphate buffer.

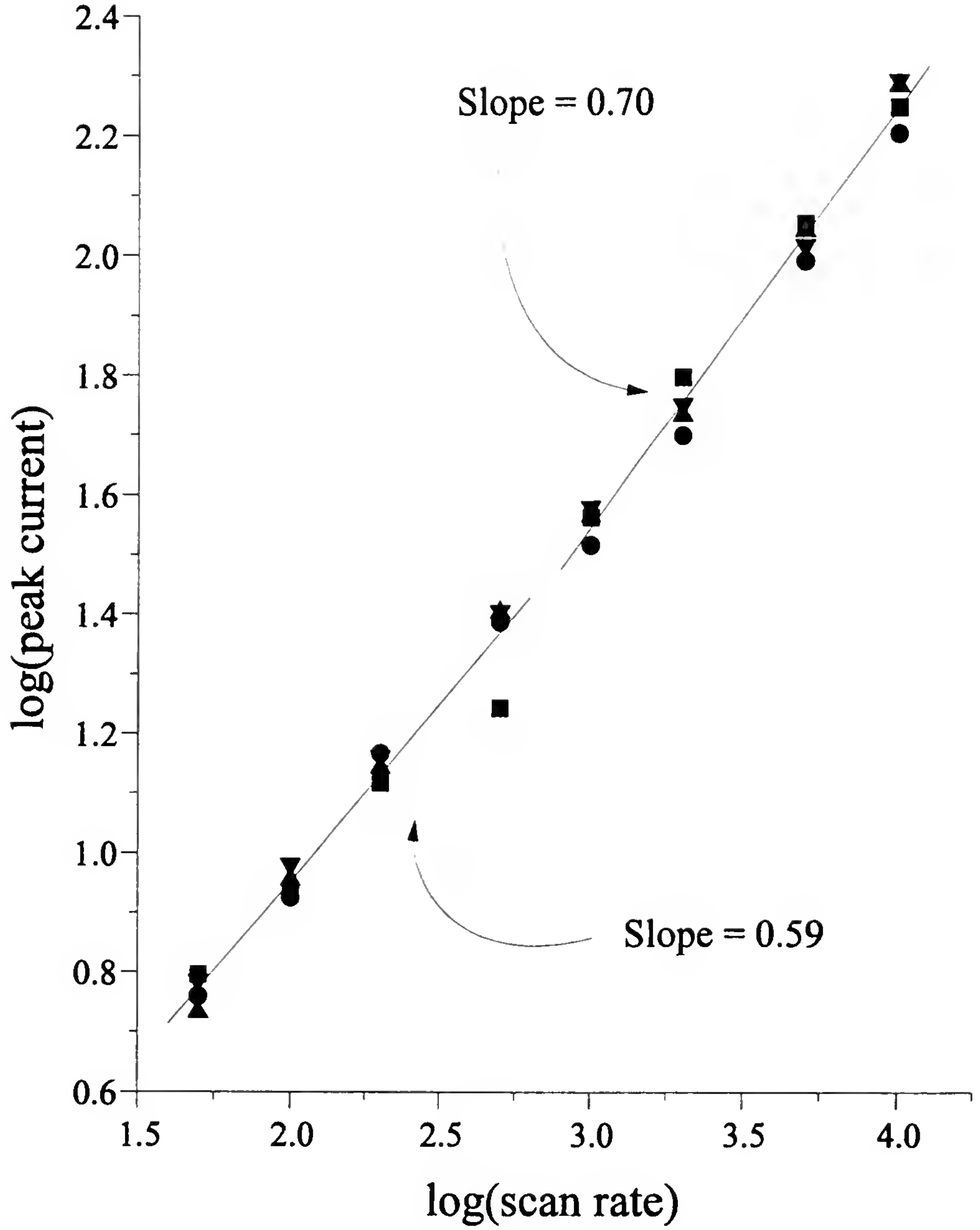
2.4
2.2
2.0
1.8
1.6
1.4
1.2
1.0
0.8
0.6
log(peak current)
1.5
2.0
2.5
3.0
3.5
4.0
log(scan rate)
Slope = 0.70
Slope = 0.59

current at a scan rate of 10,000 V/s can be expected to be 20 times greater than the peak current at a scan rate of 100 V/s where the slope value is 0.59. Such increase in peak current can significantly contribute to improved detection limits.

On the other end, surface functional groups can also have a negative effect on the redox reactions. For example, they can deter redox reactions because of electrostatic effects on negatively charged analytes such as AA. The surface functional groups which can include phenols and carboxylic acid groups (Figure 1.10) which can contribute to the negative charge of the electrode surface thus decreasing the ability of the anion (such as ascorbate anion present at physiological pH) to approach the electrode surface. Consequently, the kinetics of AA can be slowed down further by the surface. Thus DA and AA will have a very different response due to the kinetic differences which will be most apparent at high scan rates.

Detection of DA Without the Interference of AA

Figures 5.3A and B show cyclic voltammograms of 10^{-4} M DA and 10^{-2} M AA at scan rates of 100 and 10,000 V/s. At a scan rate of 100 V/s, the peak current for AA is much greater than that for DA because of the higher concentration of AA than of DA. As shown in Figure 5.3B, when the scan rate is increased to 10,000 V/s, the current due to AA is significantly suppressed relative to the current of DA and no redox peaks from AA is observed. In contrast to the behavior of AA, DA exhibits a well defined peak at this scan rate and its peak current is enhanced up to 30 times compared to the peak current at a scan rate of 100 V/s.

Figure 5.3b. Cyclic voltammograms of 10^{-4} M DA (solid line) and 10^{-2} M AA (dashed line) at a scan rate of 10,000 V/s. Same electrode and solution conditions as in Figure 5.3A.

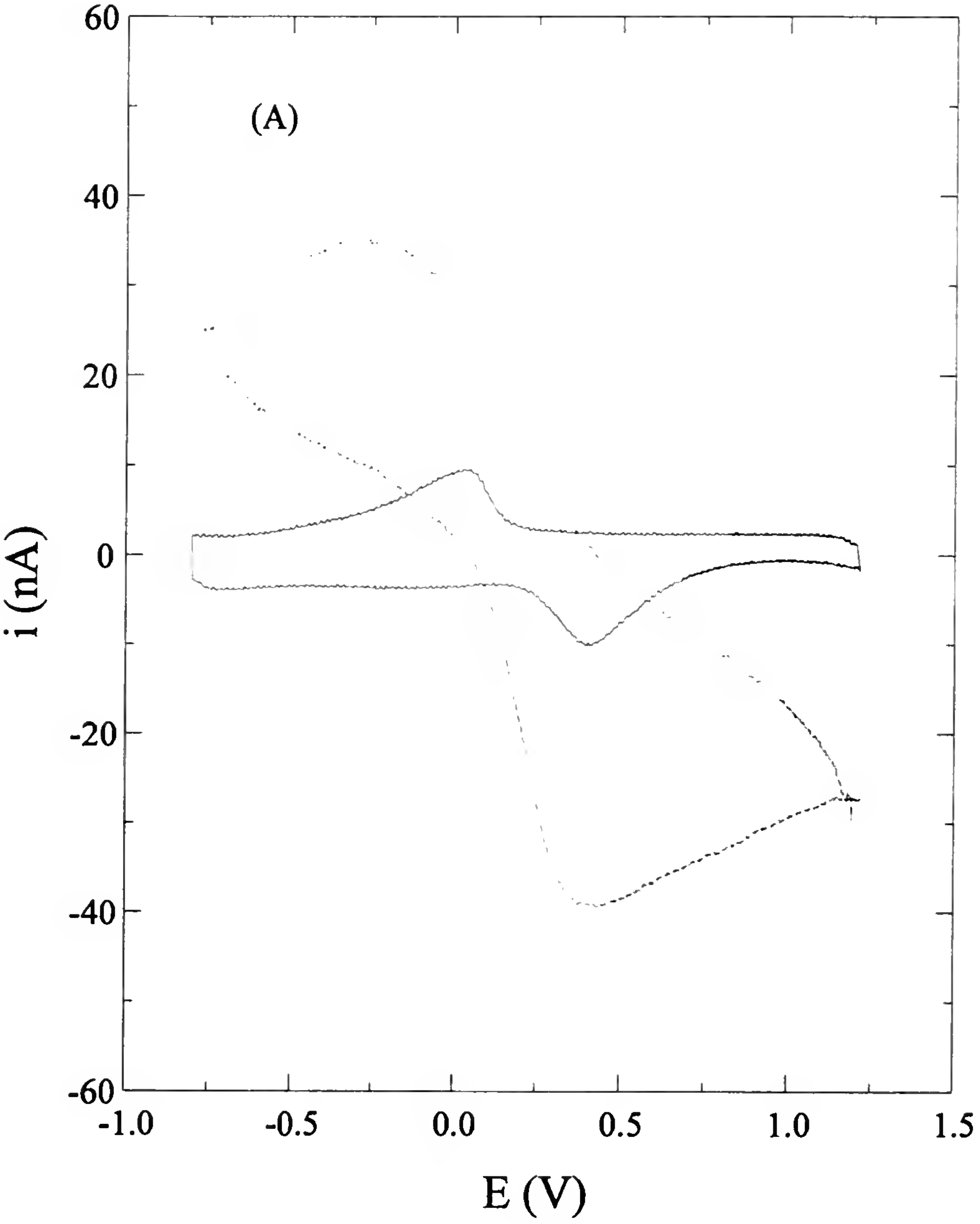
(A)
60
40
20
0
-20
-40
-60
i (nA)
-1.0
-0.5
0.0
0.5
1.0
1.5
E (V)

Figure 5.3b. Cyclic voltammograms of 10^{-4} M DA (solid line) and 10^{-2} M AA (dashed line) at a scan rate of 10,000 V/s. Same electrode and solution conditions as in Figure 5.3A.

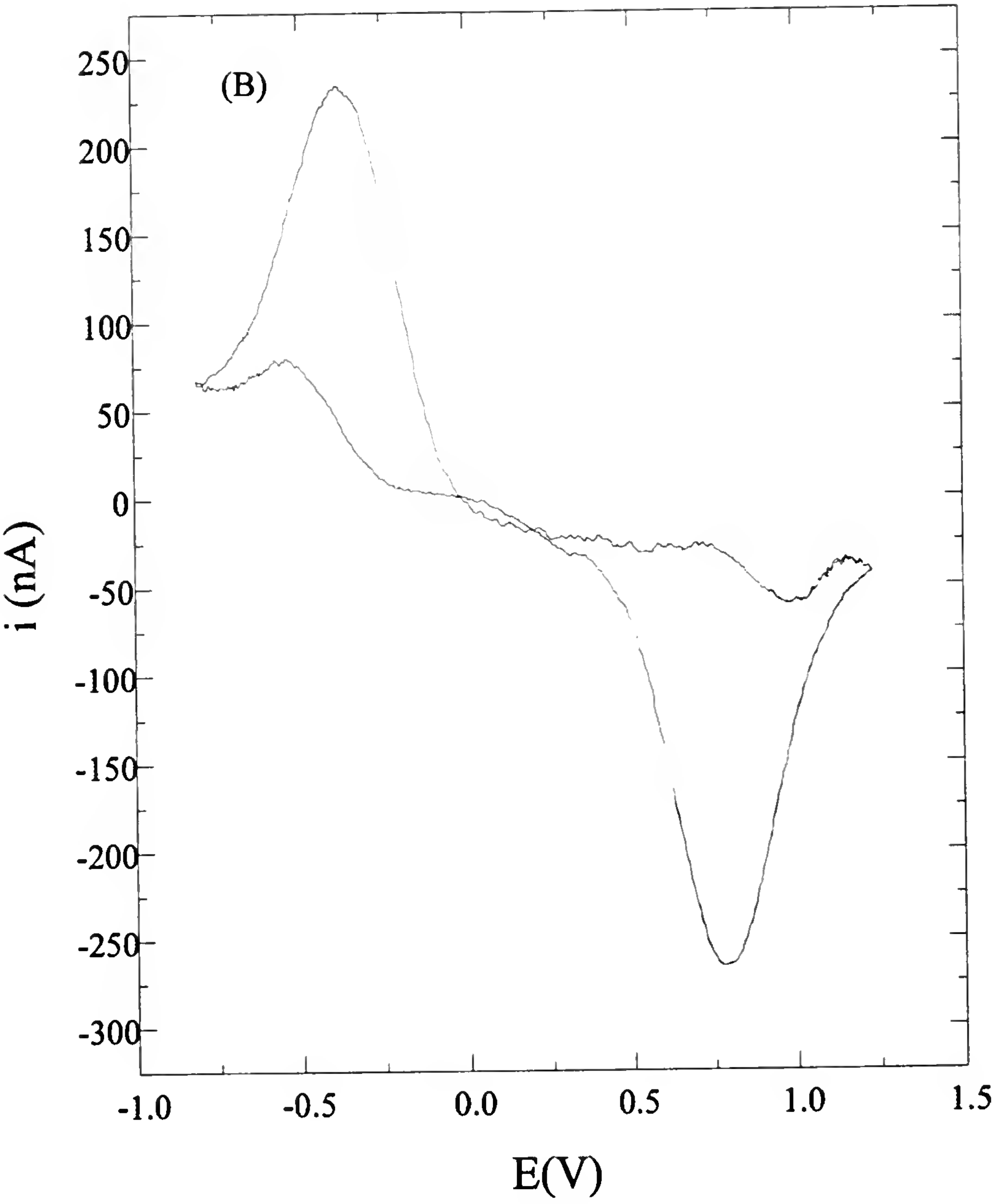
(B)
250
200
150
100
50
0
-50
-100
-150
-200
-250
-300
i (nA)
-1.0
-0.5
0.0
0.5
1.0
1.5
E(V)

The magnitudes of the peak currents of DA at scan rates of 100 and 10,000 V/s are ca. 7 nA and 240 nA, respectively. Both of these currents are much higher than the calculated peak currents (0.122 nA and 1.2 nA respectively) which are based on purely diffusional process (equation 2). This enhancement of peak current is an indication of adsorption and preconcentration of DA on the electrode surface. Peak current-to-bulk concentration ratios (i_p/C^*) for 10^{-4} M DA and 10^{-2} M AA at a scan rate of 100V/s are 73 and 3.5 nA/mM , respectively. The much larger i_p/C^* of DA is another strong indication of DA adsorption and preconcentration on the electrode surface.

Figure 5.4 shows cyclic voltammetry results for 5 μM DA in the presence of 1.2 mM AA obtained at a scan rate of 2,000 V/s. At this scan rate, in spite of high concentration of AA, voltammogram of DA is practically identical to the voltammogram of DA alone which shows the freedom from interference by AA. It is worth noting that the concentration of AA is 240 times higher than the concentration of DA, and that the selectivity is obtained without the need for electrode coating with a permselective polymer film. In other words, by simply increasing the scan rate the selectivity of DA over AA can be greatly improved at carbon fiber electrodes. Another advantage of the increased scan rate results from fast electrochemical regeneration of reduced DA which contributes to the stability of the electrode.

Figure 5.4. Cyclic voltammogram of 5 μM DA in the presence of 1.2mM AA in 70 mM pH 7.4 phosphate buffer. Scan rate is 2,000 V/s, electrode diameter 7 μm . The voltammogram was averaged 1000 times.

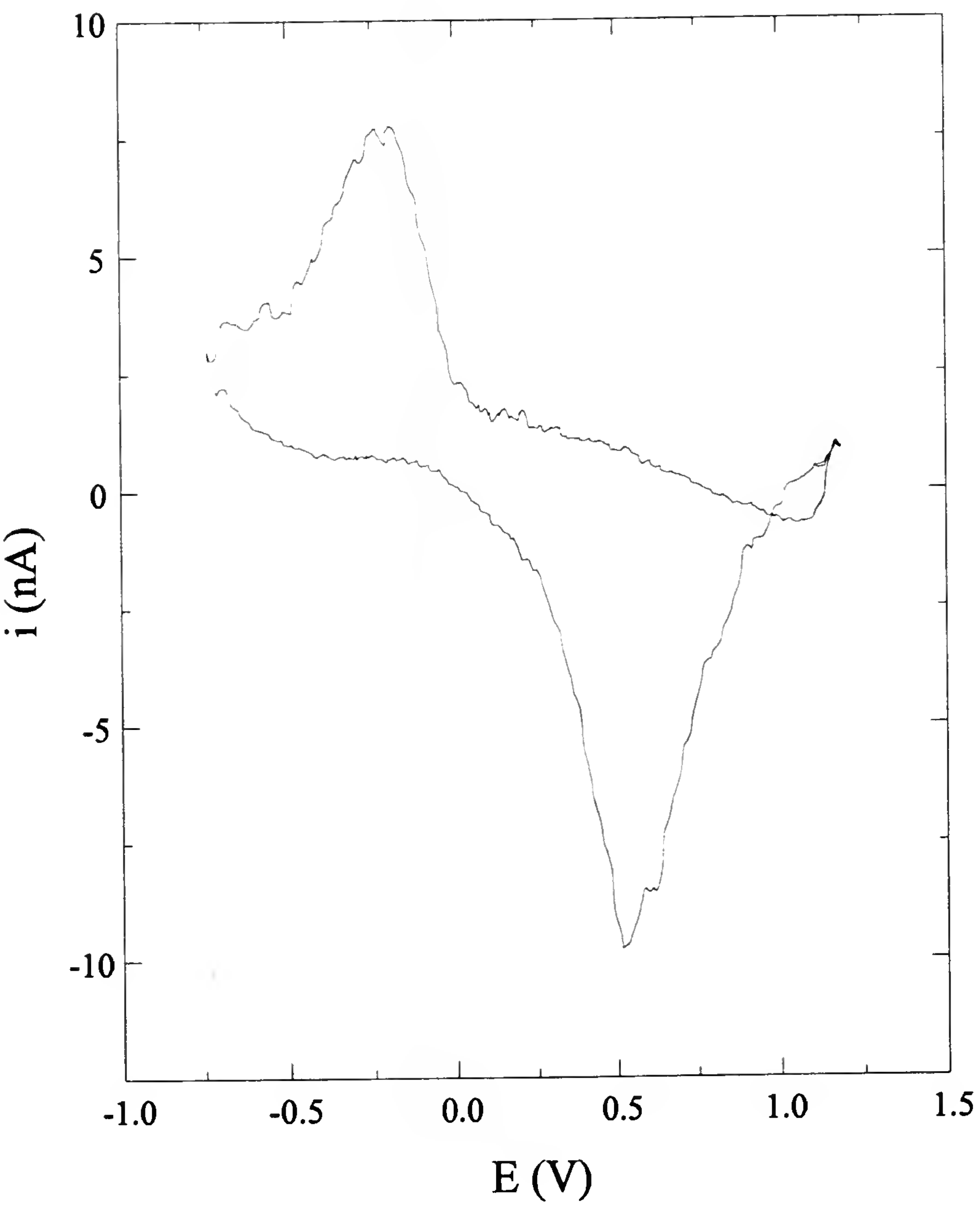
10
5
0
-5
-10
i (nA)
-1.0
-0.5
0.0
0.5
1.0
1.5
E (V)

Fast Scan Voltammetry with Signal Averaging

An additional significant advantage of increased scan rates results from shorter time required to complete a voltammogram which has an effect of improving temporal resolution of the measurements. For a scan rate of 10,000 V/s with a potential window from -0.6 to 1.0 V, the time required to complete a cyclic voltammogram is 320 μs which is 100 times shorter than the time required to complete the same cycle at a scan rate of 100 V/s.

If the fast detection allowed by this temporal resolution is not of major interest, the shorter measurement time can be taken advantage of in signal averaging and in improving signal-to-noise ratio (S/N). Wightman's group has investigated various techniques - such as analog and digital filtering, and signal averaging - to improve detection limits (i.e. increase S/N).[146] The combined use of these techniques allowed 100 nM of DA to be detected in vivo. Forty voltammograms collected at a scan rate of 300 V/s were averaged to improve S/N in their experiment. The numbers of voltammograms which could be collected and signal averaged was limited by the scan rate and experimental time scale. The shorter cycling time in fast scan voltammetry means that more cycles (or more cyclic voltammograms) can be acquired in a specific time. Each acquired voltammogram can then be added and averaged to improve the signal-to-noise ratio (S/N). The expected enhancement in S/N is given by following equation:

$$S/N \propto \sqrt{n} \tag{5.1}$$

where n is the number of cyclic voltammograms acquired and averaged.

For a scan rate of 10,000 V/s, with a potential window from -0.6 to 1.0 V, the maximum number of scans per second in cyclic voltammetry is 3125 if the time of digitizing and trigger delay of the digital oscilloscope is neglected. For 3125 averaged signals, the S/N can be expected to improve 56 times. The improvement of S/N at 10,000 V/s is 10 times greater than for a scan rate of 100 V/s. Figure 5.5 shows the single scan cyclic voltammogram and the signal averaged results where 10, 100, and 1000 cycles are shown. For the sake of clarity, only forward scans are shown in the Figure 5.5. The acquired signals were added together and then divided by the numbers of scans and the resulting data are plotted in the Figure. As Figure 5.5 shows, the high frequency noise is rapidly reduced by signal-averaging as the numbers of scans increases. However, the low frequency noise tends to remain even after 1000 scans. The reason for that may be that the low frequency noise is harmonic with, or close to, the frequency of cycling.

Limitations of Fast Scan Voltammetry

Although increased scan rate in cyclic voltammetry can produce many advantages, a major inherent limitation has to be addressed. Because charging current, i_c , increases proportionally to scan rate, most of the resolution resources of the digital oscilloscope or digitizer are consumed by the higher charging current which accompanies all electroanalytical signal at high scan rates. The resolution that is left can not adequately reflect the shape of the analytical signal because of the noise introduced by the lack of the resolution of the digitizer, i.e. the digitized noise. This noise will prevent low concentrations

Figure 5.5. Signal averaged cyclic voltammograms of 50 µM DA in 70 mM phosphate buffer, scan rate 2,000 V/s. Only the oxidation peaks are shown. Lines 1,2, 3, and 4 averaged 1, 10, 100, and 1000 times, respectively.

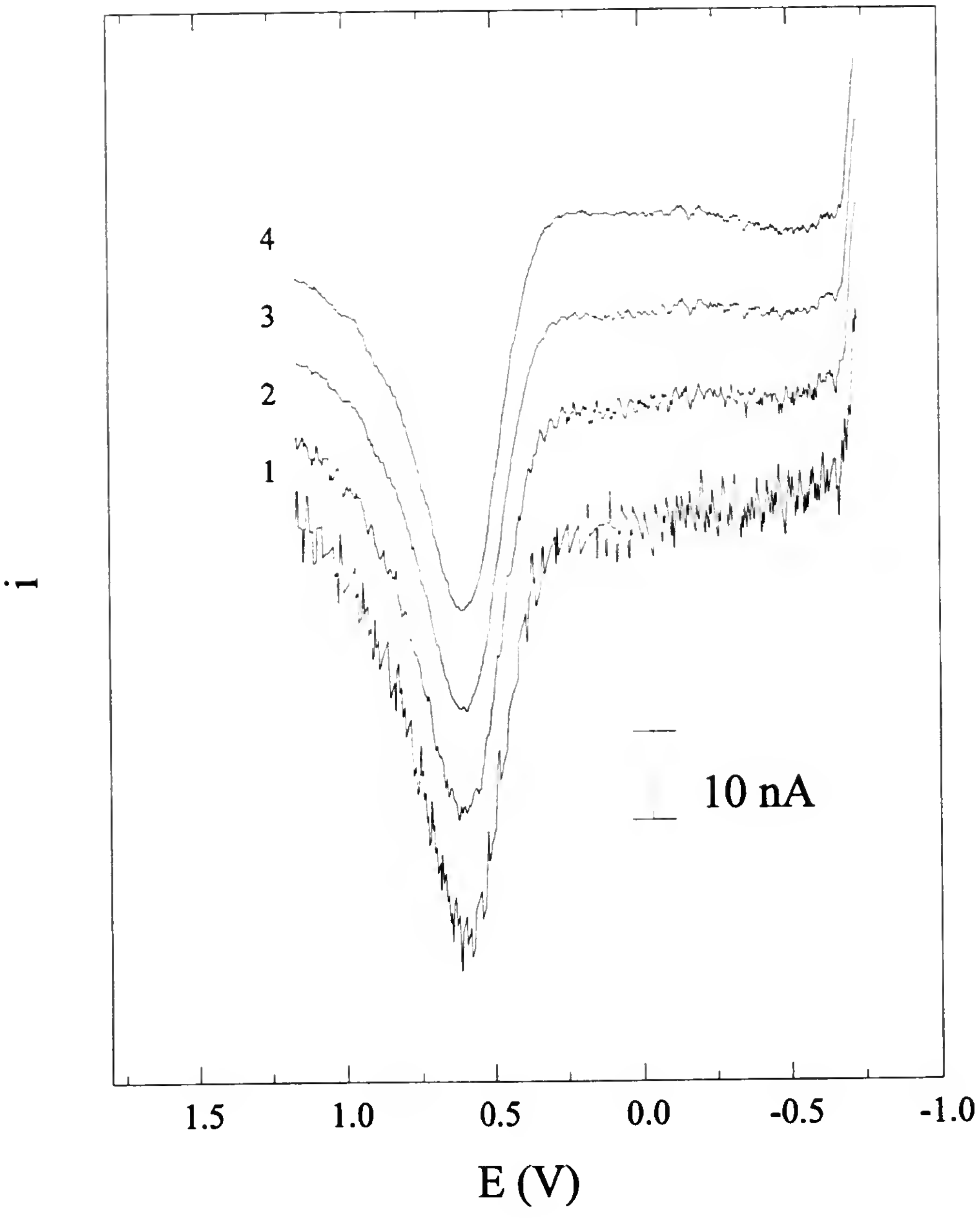
4
3
2
1
i
10 nA
1.5
1.0
0.5
0.0
-0.5
-1.0
E (V)

of analyte from being detected even if all of the noise from the electrochemical cell and the current measuring circuit could be eliminated. Before the benefit of pushing scan rates to higher values can be further pursued this obstacle must be removed.

An additional problem is that the high frequency noise becomes more difficult to eliminate as the scan rate increases, especially the noise with frequencies close to the cycling frequency. This problem can be reduced by adequate circuit design (such as the use of high order filters) or digital filtering and smoothing after the data are digitized.

Conclusions

By increasing the scan rates in fast scan voltammetry up to 10,000 V/s, we demonstrated that the detection of low concentrations of DA (ca. 5 μM) in the presence of higher concentrations of AA (ca. 1 mM) can be accomplished at graphite electrodes without a need for permselective polymer coatings. Differences in electrochemical kinetics between DA and AA contribute to the observed selectivity where the apparent kinetics of AA (ΔE_p = 710 mV at 100 V/s) are significantly lower than those of DA (ΔE_p = 360 mV at 100 V/s). The selectivity and sensitivity might be further improved by optimizing the electrochemical pretreatment of graphite electrodes. Research has shown that electrochemical pretreatment of graphite electrodes causes enhancement in adsorption of cations (such as DA) and the suppression of anions (such as AA). However, extensive pretreatment may also cause formation of thick graphite oxide films (up to 1 μm) which can increase cell resistance and may have drawbacks related to those of thick electrically insulating polymer films (such as

Nafion).[147] Optimization of surface pretreatment methods for fast scan voltammetry needs further investigation.

Temporal resolution can significantly benefit from the increase in scan rate. The magnitude of the peak signal is also greatly increased. Moreover, the repeated signals can be signal-averaged to improve S/N. However, the enormous background currents under fast scan conditions need to be taken into account. At high scan rates, this background current consumes most of the resolution resources of the digital oscilloscope, which ultimately limits the detection limit. Based on the evidence presented in this work, pushing the scan rate to above 10,000 V/s can produce significant analytical advantages if the problems of large background currents are solved.

To address this problem, an on-line background subtraction circuit is being constructed in our laboratory. This circuit will be capable of performing fast scans above 10 kV/s and subtracting the background current on-line. The output will contain only faradic current, thus, the resolution of the digital oscilloscope will be conserved. Fast scan experiments (above 10 kV/s) with this circuit are ongoing in our laboratory.

CHAPTER 6
CONCLUSIONS AND FUTURE WORK

The work described in this dissertation can be summarized as follows. Fast redox reactions of a bio-analyte and two outer sphere inorganic complexes have been characterized with fast scan voltammetry. Significance of fast scan voltammetry with on-line iR compensation has been demonstrated in aqueous solutions. It was demonstrated that the surface of the electrode plays an important role in fast scan measurements. In $Ru(NH_3)_6^{+3/+2}$ and $Fe(CN)_6^{-3/-4}$ reactions, the surface deteriorated after oxide production. On similar surfaces, adsorption strength of uric acid decreases dramatically.

In addition, a concept of utilizing fast scan voltammetry to characterize redox reactions of a weakly adsorbed molecule was brought to the forefront and was exploited. It has been demonstrated that kinetic information for weakly adsorbed species can be obtained with fast scan voltammetry without interference from diffusing species. This should allow better understanding of redox reactions of weakly adsorbed biological molecules.

The ability of fast scan methods with on-line iR compensation to provide kinetic information of fast reactions in aqueous solutions may be further exploited to investigate fast redox reactions of large biological molecules (such as cytochrome C). Another interesting extension of this work will be in the area of characterization of the polymerization mechanisms of conducting polymers (such as polypyrrole) in aqueous solutions. The life time and the standard potential of pyrrole dimers formed after initial polymerization has been characterized in acetonitrile solvents.[148] However, the properties and mechanism of formation of polypyrrole in organic solvents is significantly different from the properties of polypyrrole formed in aqueous solutions. It will be interesting to compare the polymerization mechanisms in organic and aqueous solvents.

UMEs modified with ultrathin polymer films exhibit excellent permselectivity in spite of the ca. monolayer thickness of the film. The ultrathin film modified UMEs should be suitable for in-vivo detection and should provide better selectivity. Selective and sensitive sensors with fast response time may be obtained for in-vivo measurements by combining the ultrathin film modified UMEs with fast scan voltammetry. Future work should focus on enzyme immobilization on the ultrathin films to provide a better response of enzyme electrodes. Another possible application which could allow the development of more selective sensors is to use the films to trap specific biomolecules and produce templates.

In developing fast scan voltammetry as an analytical tool we are investigating the method for improvement of selectivity and detection limits in analysis. The new strategies already developed and described in this work were proved to be useful. We have found that differences in electrochemical kinetics between probes contribute to the enhancement of selectivity at high scan rates. The sensitivity and detection limit improvement results from the large peak currents of weakly adsorbed analytes and the ability of signal averaging with fast scan methods.

However, to achieve lower detection limits at higher scan rates, the interference of the charging current needs to be eliminated. The high charging current at high scan rates depletes the available resolution of the digital oscilloscope for faradaic currents measurements, which limits the detection of faradaic currents. To extract the signal out of the charging current, an on-line background subtraction circuit is being built in our laboratory. Two working electrodes are needed in the circuit. The first working electrode will be placed in a buffer solution containing an analyte and the second working electrode will be placed in the buffer only. The current from the first electrode will be subtracted from the current from the second electrode using a differential amplifier. Thus, the net output will be the faradic current only. Preliminary results are very promising.

Another interesting application which may be performed in the future will be to apply the strategies developed in this work to HPLC and CZE detection. In addition to providing higher temporal resolution, fast scan voltammetry with UMEs can detect coeluting analytes simultaneously as long as their redox potentials are different. Therefore the selectivity of HPLC and CZE detection can be enhanced. Furthermore, based on our results, the selectivity may be further enhanced by increasing scan rates if the coeluting analytes have different redox kinetics.

APPENDIX A
DATA ACQUISITION, DISPLAY AND PROCESSING PROGRAM SOURCE CODE

The main purpose of this program is to acquire data from LeCroy Digital oscilloscope through the RS232 communication port. The data (voltammograms) are then displayed on the computer screen, saved in a file or further processed to fit the experimental needs.

```
******************************************************************************
**
DECLARE SUB SMOOTH (WFX!(), WFY!())
DEFINT A-T
DECLARE SUB SHOWFILES ()
DECLARE SUB CSCOPE (ORDER$)
DECLARE SUB CLEANS ()
DECLARE SUB FMINMAX (X!(), y!(), NDP, WMAXX!, WMINX!, WMAXY!,
WMINY!, XMAXC, XMINC)
DECLARE SUB GRAPH (WFX!(), WFY!())
DECLARE SUB FILEIO (FLAG%, WFX!(), WFY!())
DECLARE SUB QSCOPE (ORDER$, RESPONSE$)
DECLARE SUB CSTR2NUM (data$, WF!(), CHANEL$)
DECLARE SUB SCOPE (CMD$, RESPONSE$)

DIM WFX(5010), WFY(5010)
COMMON SHARED PATH$, FILENAME$, NDP, XMAXC, XMINC
DECLARE FUNCTION GPullDown (a%, B%, C%)
      DIM MENU$(25)
      SCREEN 9                'swithch to a graphic screen
      LOCATE 2, 1
'      filename$ = "TEMP.DAT"
'Show the meun on screen
MENU:
      FOR i = 0 TO 24: READ MENU$(i): NEXT
REM  first main heading
      DATA "File"
      DATA "Save"
      DATA "Read"
      DATA "File name"
```

```
        DATA "Display"
        DATA "Exit"
REM  NUL string separates main headings
        DATA ""
REM 2nd main heading
        DATA "Setting"
        DATA "Path"
        DATA "Data spacing"
        DATA "P"
        DATA "U"
        DATA ""
        DATA "Getdata"
        DATA "Channel 1"
        DATA "Trace C"
        DATA "Trace A"
        DATA ""
        DATA "Caculation"
        DATA "K"

        DATA ""
        DATA "Smoothing"
        DATA "Smooth"
REM  double NUL strings mark end
        DATA "",""
        CALL menuoption(0, 23)       ' text color
        CALL menuoption(1, 40)       ' menu choice color
        CALL menuoption(2, 31)       ' menu box color
        CALL menuoption(4, 256 + 68)  ' optional exit key
        CALL menuoption(5, -1)       ' exit menu when hotkey pressed
        main = 0: subm = -1
        a = VARPTR(MENU$(0))
        a = GPullDown(a, main, subm)
        SELECT CASE a
            CASE 13
            KEY$ = "Enter"
            CASE 27
            KEY$ = "Escape"
            GOTO again
            CASE ELSE
        END SELECT
        SELECT CASE main
            CASE 0
                IF subm = 1 OR subm = 0 THEN CALL FILEIO(subm, WFX(), WFY())
```

```
          IF subm = 1 THEN CALL GRAPH(WFX(), WFY())
          IF subm = 2 THEN
          CALL CLEANS: INPUT "FILE NAME?  ", FILENAME$
          END IF
          IF subm = 3 THEN CALL SHOWFILES
          IF subm = 4 THEN END

     CASE 1
          IF subm = 0 THEN CALL CLEANS: INPUT "PATH: ", PATH$
          IF subm = 1 THEN
               CALL CLEANS: INPUT "DATA SPARE #:", CMD$
               LOCATE 13, 68: PRINT CMD$
               CMD$ = "WFSU SP," + CMD$
               FOR i = 1 TO 3
               CALL CSCOPE(CMD$): i = i + 1
               NEXT
               'CMD$ = "WFSU?"
               'CALL QSCOPE(CMD$, R$)
          END IF
     CASE 2

          IF subm = 0 THEN
               'CMD$ = "C1:WF? DAT1"
               CMD$ = "TA:INSP? 'WAVEDESC';WF?"
               C$ = "C1"
          END IF
          IF subm = 1 THEN
               'CMD$ = "TC:WF? DAT1"
               CMD$ = "TC:INSP? 'SIMPLE'"
               C$ = "TC"
          END IF
          IF subm = 2 THEN
               'CMD$ = "TA:WF? DAT1"
               CMD$ = "TA:INSP? 'SIMPLE'"
               C$ = "TA"
          END IF

          CALL QSCOPE(CMD$, R$)
          CALL CSTR2NUM(R$, WFY(), C$)

          IF subm = 0 THEN
               CALL QSCOPE("C2:INSP? 'SIMPLE'", R$)
               CALL CSTR2NUM(R$, WFX(), "C2")
```

```
            END IF

            IF subm = 1 OR subm = 2 THEN
                ' CMD$ = "WFSU SP,10"
                ' FOR i = 1 TO 3
                ' CALL CSCOPE(CMD$): i = i + 1
                ' NEXT

                CALL QSCOPE("TB:INSP? 'SIMPLE'", R$)
                CALL CSTR2NUM(R$, WFX(), "TB")
            END IF
            CALL GRAPH(WFX(), WFY())
            main$ = "Getdata"
        CASE 3
            main$ = "Vegetation"
        CASE 4
        CALL SMOOTH(WFX(), WFY())
        CALL GRAPH(WFX(), WFY())
    END SELECT
    ' PRINT KEY$, main$, SUBM
again:
RESTORE
LOCATE 2, 68: PRINT "FILE NAME:"
LOCATE 3, 68: PRINT FILENAME$
LOCATE 4, 68: PRINT "PATH:"
LOCATE 5, 68: PRINT PATH$
LOCATE 6, 68: PRINT "Epa:"
LOCATE 7, 68: PRINT WFX(XMAXC)
LOCATE 8, 68: PRINT "Epc"
LOCATE 9, 68: PRINT WFX(XMINC)
LOCATE 10, 68: PRINT "Ipa"
LOCATE 11, 68: PRINT WFY(XMAXC)
LOCATE 12, 68: PRINT "Data Sparing"
GOTO MENU
CLOSE
'*************************************************************
'End of the main program

'*************************************************************
SUB CLEANS
LOCATE 1, 1
PRINT "                                              "
LOCATE 1, 1
```

```
END SUB
'A subrounitine to send Command to the scope throughr commuication port 2
DEFSNG A-T
SUB CSCOPE (ORDER$)
OPEN "COM2:9600,N,8,1" FOR RANDOM AS #2 LEN = 4096
CMD$ = CHR$(27) + "[" + CHR$(13)
PRINT #2, CMD$
CMD$ = CHR$(27) + "C" + CHR$(13)
PRINT #2, CMD$
FOR i = 1 TO 10000
NEXT
PRINT #2, ORDER$ + CHR$(13)
CLOSE #2
END SUB
'Get data from scope
DEFINT A-T
SUB CSTR2NUM (data$, WF(), CHANEL$)
' Read in data values and store them in the array X.
    data$ = MID$(data$, 12, LEN(data$) - 12)
    LENTH = LEN(data$)
d$ = ""
i = 1
'PRINT data$
ragain:
spc$ = MID$(data$, i, 1)
IF spc$ = " " OR spc$ = CHR$(13) OR spc$ = CHR$(10) THEN
  i = i + 1
  ELSE
  d$ = MID$(data$, i, 12)
  k = k + 1
  WF(k) = VAL(d$)
'  PRINT WF(k)
  i = i + 12
  END IF
IF LEN(data$) > i GOTO ragain
NDP = k - 2
PRINT NDP
END SUB

SUB FILEIO (FLAG, WFX(), WFY())
i = 1
IO$ = PATH$ + FILENAME$
IF FLAG = 0 THEN
```

```
CALL Exist(IO$, oops)
IF oops = -1 THEN PRINT "WARING! FILE EXIST!"
OPEN IO$ FOR OUTPUT AS #5
FOR i = 1 TO NDP
PRINT #5, WFX(i); WFY(i)
NEXT
ELSEIF FLAG = 1 THEN
CALL SHOWFILES
IO$ = PATH$ + FILENAME$
OPEN IO$ FOR INPUT AS #5
WHILE NOT EOF(5)
INPUT #5, WFX(i), WFY(i)
i = i + 1
NDP = i
WEND
END IF
CLOSE #5
END SUB

SUB FMINMAX (X(), y(), NDP, WMAXX, WMINX, WMAXY, WMINY, XMAXC,
XMINC)
'==================================================================
' This subroutine is designed to determin the max and min of an x,y
' data array, and to determine the counter value associated with
' the max an min x values
'==================================================================
'initialize values
WMAXX = X(1)
WMINX = X(1)
WMAXY = y(1)
WMINY = y(1)
XMAXC = 1
XMINC = 1
'determine values
PRINT NDP
FOR i = 2 TO NDP
 IF X(i) > WMAXX THEN WMAXX = X(i)
 IF X(i) < WMINX THEN WMINX = X(i)
 IF y(i) > WMAXY THEN WMAXY = y(i): XMAXC = i
 IF y(i) < WMINY THEN WMINY = y(i): XMINC = i
NEXT i
'==================================================================
END SUB

SUB GRAPH (WFX(), WFY())
CLS
CALL FMINMAX(WFX(), WFY(), NDP, WMAXX, WMINX, WMAXY, WMINY,
XMAXC, XMINC)
WINDOW (WMINX, WMINY)-(WMAXX, WMAXY)
PRINT NDP
PRINT WMINX, WMINY, WMAXX, WMAXY
PSET (WFX(1), WFY(1))
FOR i = 2 TO NDP
LINE -(WFX(i), WFY(i))
NEXT
END SUB



DEFSNG A-T
SUB QSCOPE (ORDER$, RESPONSE$)
CALL CSCOPE("*CLS")
RESPONSE$ = ""
'PRINT CMD$
'DEFINT A-Z
TRYAGAIN:
FALSE = 0
TRUE = NOT FALSE
XOFF$ = CHR$(19)
XON$ = CHR$(17)
PAUSE = FALSE
OPEN "COM2:9600,N,8,1" FOR RANDOM AS #1 LEN = 4096
CMD$ = CHR$(27) + "[" + CHR$(13)
PRINT #1, CMD$
CMD$ = CHR$(27) + "C" + CHR$(13)
PRINT #1, CMD$
'PRINT #1, "CHDR OFF" + CHR$(13)
PRINT #1, CHR$(27) + "R; BWL ON" + CHR$(13)
FOR i = 1 TO 1000
NEXT
PRINT #1, "CORS EO," + "'\r\n\END\r\n'" + CHR$(13)
PRINT ORDER$
PRINT #1, ORDER$ + CHR$(13)
 WHILE EOF(1)
i = i + 1
```

```
IF i > 10000 THEN
CLOSE #1
GOTO TRYAGAIN
END IF
WEND
'I = 0: OPEN "D:\CHARLIE\TEMP.DAT" FOR OUTPUT AS #2
1820 WHILE NOT EOF(1)
1830 IF LOC(1) > 128 THEN PAUSE = TRUE: PRINT #1, XOFF$;
E$ = INPUT$(LOC(1), #1)
d$ = d$ + E$: IF LOC(1) > 0 THEN 1830
IF PAUSE THEN PAUSE = FALSE: PRINT #1, XON$;
WEND
i = i + 1
END$ = RIGHT$(d$, 5)
END$ = LEFT$(END$, 3)
PRINT END$
IF END$ <> "END" THEN 1820
RESPONSE$ = d$
'PRINT D$
CLOSE #1
END SUB

DEFINT A-T
SUB SHOWFILES
      DIM FILE$(100)
      NAMES$ = SPACE$(12)           ' filename$ must be initialized
                              ' as a 12-byte (or longer) string
                              ' or the namelen% will be returned
                              ' as -1
      FileSpec$ = PATH$ + "*.DAT" + CHR$(0)' FileSpec$ must end in CHR$(0)
      fAttr% = 0                    ' search only for normal files
      CALL FindFirstMatch(FileSpec$, fAttr%, oops%)
      'IF oops% = -1 THEN PRINT "FileSpec$ is a nul string"
      IF oops% THEN LOCATE 1, 1: PRINT "No matching files"
      i = 1
      FILE$(0) = "DIRTORY1"
      WHILE oops% = 0
         CALL FindFileName(NAMES$, namelen%)
         IF namelen% = -1 THEN PRINT "filename$ shorter than 12 bytes"
         FILE$(i) = LEFT$(NAMES$, namelen%)
         CALL FindNextMatch(oops%)
         i = i + 1
         IF i = 23 THEN
```

```
       FILE$(i) = ""
       FILE$(24) = "DIRTORY2": i = 25
       END IF
     WEND
     FILE$(i + 1) = "": FILE$(i + 2) = ""
    CALL menuoption(0, 23)       ' text color
    CALL menuoption(1, 30)       ' menu choice color
    CALL menuoption(2, 31)       ' menu box color
    CALL menuoption(4, 256 + 68)  ' optional exit key
    CALL menuoption(5, -1)       ' exit menu when hotkey pressed
    main = 0: subm = -1
    a = VARPTR(FILE$(0))
    a = GPullDown(a, main, subm)
    SELECT CASE a
        CASE 13
        KEY$ = "Enter"
        CASE 27
        KEY$ = "Escape"
        CASE ELSE
    END SELECT
    SELECT CASE main
        CASE 0
        FILENAME$ = FILE$(subm + 1)
        CASE 1
        FILENAME$ = FILE$(subm + 25)

    END SELECT

END SUB

SUB SMOOTH (WFX(), WFY())
FOR i = 1 TO NDP
WFY(i + 2) = (WFY(i) + WFY(i + 1) + WFY(i + 2) + WFY(i + 3) + WFY(i + 4)) / 5
WFX(i + 2) = (WFX(i) + WFX(i + 1) + WFX(i + 2) + WFX(i + 3) + WFX(i + 4)) / 5
NEXT
END SUB
```

APPENDIX B

SEMI-INTEGRAL ANALYSIS PROGRAM SOURCE CODE

```
'=============================================================
' This subroutine is designed to semi-integrate data
'=============================================================
SUB semi (dummy%)
KEY OFF
'call gmama function subroutine if gamma function has not been calculated
IF gma!(1) = 0 THEN CALL gamma
'if number of data points is odd, make it even.
odd = (ndps) MOD (2)
IF odd = 1 THEN ndps = ndps - 1
n = ndps
qq = 0
'begin to integrate the forward part of a cyclic voltammogram
FOR k = 1 TO n / 2
summf! = 0
     FOR j = 1 TO k
     summf! = summf! + gma!(k - j) * SQR(dt) * curr!(j)
     NEXT
sem!(k) = summf!
qq = qq + 1
'tell user to wait
LOCATE 23, 20
IF qq = 1 THEN PRINT "|";
IF qq = 2 THEN PRINT "/";
IF qq = 3 THEN PRINT "-";
IF qq = 4 THEN PRINT "\"; : qq = 0
NEXT
qq = 0
'Begin to integrate the backward part of a cyclic voltammogram
FOR k = n / 2 + 1 TO n
summb! = 0
     FOR j = 1 + n / 2 TO k
     summb! = summb! + gma!(k - j) * SQR(dt) * curr!(j)
     NEXT
sem!(k) = summb! + sem!(n / 2)
qq = qq + 1
 LOCATE 23, 20
```

```
IF qq = 1 THEN PRINT "|";
IF qq = 2 THEN PRINT "\";
IF qq = 3 THEN PRINT "-";
IF qq = 4 THEN PRINT "/"; : qq = 0
NEXT
Plot:
'plot the semi-integrated current on screen
CALL graph(pot!(), sem!(), ndps, try$, try$)
LOCATE 23, 17: PRINT SPACE$(40): LOCATE 24, 17: PRINT SPACE$(40);
KEY ON
'=========================================================================
END SUB


'=========================================================================
' This subroutine calculates values of Gamma Function and places them into
' an array to be used during semi-integration
'=========================================================================
SUB gamma
 gma!(0) = 1
 FOR i = 1 TO 1000 'ndps / 2
  Factorial = (2 * i - 1) / (2 * i)
  gma!(i) = Factorial * gma!(i - 1)
 NEXT
'=========================================================================
END SUB

'=========================================================================
```

REFERENCE LIST

1. P. Bindra, A. P. Brown, M. Fleischmann, D. Pletcher *J. Electroanal. Chem.* **1975**, 58, 31

2. J. L. Ponchon, R. Cespuglio, F. Gonon, M. Jouvet, J. F. Pujol *Anal. Chem.* **1979**, 51, 1483

3. R. N. Adams *Anal. Chem.* **1976**, 48, 1125A

4. K. R. Wehmeyer, M. R. Deakin, R. M. Wightman Anal. Chem. 1985, 57, 1913

5. T. V. Shea, A. J. Bard *Anal. Chem.* **1987**, 59, 2101

6. M. Fleischmann, S. Bandyopadhyay, S. Pons *J. Phys. Chem.* **1985**, 89, 5537

7. R. B. Morris, D. J. Franta, H. S. White *J. Phys. Chem.* **1987**, 91, 3559

8. O. Niwa; H. Tabei Anal. Chem. 1994 66, 285

9. A. M. Bond, T. L. E. Henderson, W. Thormann *J. Phys. Chem.* **1986**, 90, 2911

10. F. Belal, J. L. Anderson *Analyst* **1985**, 110, 1493

11. S. Pons, M. Fleischmann *Anal. Chem.* **1987**, 59, 1391A

12. R. M. Wightman *Science* **1988**, 240, 415

13. J. Heinze *Angew. Chem. Int. Ed. Engl.* **1993**, 32, 1268-1288

14. M. Fleischmann, S. Pons, D. R. Rolison in *Ultramicroelectrodes* (Ed.: P. P. Schmidt), Datatech Systems. Inc. **1987**

15. R. T. Kennedy, L. Huang, M. A. Atkinson, P. Dush *Anal. Chem.* **1993,** 65, 1882-1887

16. J. P. Ng, G. W. Hubert, J. B. Justice, Jr. *J. Neurochem.* **1991**, 56, 1485

17. N. T. Maidment, C. A. Marsden *Neuropharmacology* **1987**, 26, 187

18. D. J. Wiedemann, P. A. Garris, J. A. Near, R. M. Wightman *J. Pharmacol. Exp. Ther.,* **1992,** 261, 574

19. T. K. Chen, Y. Y. Lau, D. K. Y. Wong, A. G. Ewing *Anal. Chem.* **1992**, 64, 1264

20. F. Bailey, T. Malinski, F. Kiechle *Anal. Chem.* **1991**, 63, 395

21. Y. Y. Lau, T. Abe, A. G. Ewing *Anal. Chem.* **1992**, 64, 1702

22. K. T. Kawagoe, J. A. Jankowski, R. M. Wightman *Anal. Chem.* **1991**, 63, 1589

23. L. A. Colon, R. Dadoo, R. N. Zare *Anal. Chem.* **1993**, 65, 476-481

24. S. Sloss, A. G. Ewing *Anal. Chem.* **1993**, 65, 577-581

25. W. Z. Lu, R. M. Cassidy *Anal. Chem.* **1993**, 65, 1649-1653

26. C. P. Andrieux, D. Garreau, P. Hapiot, J. M. Saveant J. Electroanal. Chem. 1988, 248, 447

27. A. M. Bond, T. F. Man *Electrochim Acta* **1987**, 32, 863

28. A. M. Bond, T. L. E. Henderson, W. Thormann *J. Phys. Chem.* **1986**, 90, 2911

29. R. Brina, S. Pons, M. Fleischmann, *J. Electroanal. Chem.* **1988**, 244, 81

30. R. Brina, S. Pons *J. Electroanal. Chem.* **1989**, 264,121

31. J. Ghoroghchian, S. Pons, M. Fleischmann *J. Electroanal. Chem.* **1991**, 317, 101

32. R. Lines, V. D. Park *Acta Chem. Scand. Ser.* **1977** ,B31,369

33. A.M. Bond, P. A. Lay *J. Electroanal. Chem.* **1986**, 199,285

34. J. B. Cooper, A. M. Bond *J. Electroanal. Chem.* **1991**, 315, 143

35. J. B. Cooper, A. M. Bond, K. B. Oldham *J. Electroanal. Chem.* **1992**, 331, 877

36. A. M. Bond, M. Fleischmann, J. Robinson *J. Electroanal. Chem.* **1984**, 172,11

37. C. A. Amatore, B. Fosset, J. Bartelt, M. R. Deakin, R. M. Wightman *J. Electroanal. Chem.* **1988**, 256, 255

38. S. M. Drew, R. M. Wightman, C. A. Amatore *J. Electroanal. Chem.* **1991**, 317,117

39. C. A. Amatore, M. R. Deakin, R. M. Wightman *J. Electroanal. Chem.* **1987**, 220, 49

40. J. Cassidy, S. B. Khoo, S. Pons, M. Fleischmann *J. Phys. Chem.* **1985**, 89, 3933

41. C. Jehoulet, A. J. Bard *Angew. Chem.* **1991**, 103, 882

42. C. P. Andrieux, P. Hapiot, J. M. Saveant *J. Phys. Chem.* **1988**, 92, 5992

43. C. P. Andrieux, D. Garreau, P. Hapiot, J.M. Saveant *J. Electroanal. Chem.* **1988**, 248, 447

44. D. Garreau, P. Hapiot, J.M. Saveant *J. Electroanal. Chem. Interfacial Electrochem.* **1989**, 272,1

45. J. O. Howell, R. M. Wightman *Anal. Chem.* **1984**, 56, 524

46. M. I. Montenegro, D. Pletcher *J. Electroanal. Chem. Interfacial Electrochem.* **1986**, 200, 371

47. C. P. Andrieux, D. Garreau, P. Hapiot, J. Pinson, J.M. Saveant *J. Electroanal. Chem. Interfacial Electrochem.* **1988**, 248, 447

48. A. Fitch, D. H. Evans *J. Electroanal. Chem.* **1986**, 202, 83

49. C. P. Andrieux, P. Hapiot, J. M. Saveant *J. Phys. Chem.* **1988**, 92, 5987

50. P. Hapiot, J. Moiroux, J. M. Saveant *J. Am. Chem. Soc.* **1990**, 112, 1337

51. C. C. Hsueh; A. Brajter-Toth *Anal. Chem.*, **1993**, 65, p. 1570-5

52. J. E. Baur; E. W. Kristensen; L. J. May; D. J. Wiedemann; R. M. Wightman *Anal. Chem.* **1988**, 60, 1268-1272

53. J. Millar; M. Armstrong-James; Z. L. Kruk *Brain Res.* **1981**, 205, 419

54. W. G. Kuhr; R. M. Wightman *Brain Res.* **1986**, 381, 168-171

55. W. G. Kuhr, V. L. Barrett, M. R. Gagnon, P. Hopper, P. Pantano *Anal. Chem.* **1993**, 65, 619

56. D. J. Wiedemann, K. T. Kawagoe, R.T. Kennedy, E. L. Ciolkowski, R. M. Wightman *Anal. Chem.* **1991**, 63, 2965

57. J. C. Imbeaux, J. M. Saveant *J. Electroanal. Chem.* **1970**, 28, 325

58. D. O. Wipf, R. M. Wightman *Anal. Chem.* **1988**, 60,2460

59. D. O. Wipf, E. W. Kristensen, M. R. Deakin and R. M. Wightman *Anal. Chem.* **1988**, 60, 306

60. C. P. Andrieux, D. Garreau, P. Hapiot, J. M. Saveant *J. Electroanal. Chem.* **1988**, 248, 447

61. C. Amatore, C. Lefrou, F. Pfluger *J. Electroanal. Chem.* **1989**, 270, 43

62. D. Britz *Electrochim. Acta* **1980**, 25, 1449

63. D. Garreau, P. Hapiot, J.M. Saveant *J. Electroanal. Chem. Interfacial Electrochem.* **1990**, 289, 73

64. A. Fitch; D. H. Evans *J. Electroanal. Chem. Interfacial Electrochem.* **1986**, 200, 371-374

65. A. M. Bond; M. Fleischmann; J. Robinson *J. Electroanal. Chem. Interfacial Electrochem.* **1984**, 168, 299

66. R. W. Murray, A. G. Ewing, R. A. Durst *Anal. Chem.* **1987**, 59, 379A-390A

67. Edited by R. W. Murray. *Molecular Design of Electrode Surfaces*, 1992, A Wiley-Interscience publication

68. A. R. Guadalupe, H. D. Abruña *Anal. Chem.* **1985**, 57, 142

69. L. D. Whiteley, C. R. Martin *Mol. Cryst. Liq. Cryst.* **1988**, 160, 359

70. J. Wang, P. Tuzhi *Anal. Chem.* **1986**, 58, 3257

71. M. Freund, L. Bodalbhai, A. Brajter-Toth *Talanta* **1991**, 38, 95-99

72. A. Witkowski, M. S. Freund, A. Brajter-Toth *Anal. Chem.* **1991**, 63, 622-626

73. A. Witkowski, A. Brajter-Toth *Anal. Chem.* **1992**, 64, 635-641

74. F. Beck, P. Braun, M. Oberst *Ber. Bunsenges. Phys. Chem.* **1987**, 91, 967

75. I. Rubinstein, J. Rishpon, E. Sabatani, A. Redondo, S. Gottesfeld *J. Am. Chem. Soc.* **1990**, 112, 6135

76. M. Nishizawa, M. Shibuya, T. Sawaguchi, T. Matsue, I. Uchida *J. Phys. Chem.* **1991**, 95, 9042-9044

77. S. Ye, D. Bélanger *J. Electroanal. Chem.* **1993**, 344, 395-400

78. Author R. L. McCreery, Editor A. J. Bard *Electroanalytical Chemistry*; Dekker: New York, **1991**; Vol. 17, p. 221-375

79. P. Kovach, M. Deakin, R. M. Wightman *J. Phys. Chem.* **1986**, 90, 1386

80. D. T. Sawyer; J. L. Roberts *Experimental Electrochemistry for Chemists*; Wiley: New York, **1974**

81. J. Wang, P. Tuzhi, V. Villa *J. Electroanal. Chem.* **1987**, *234*, 119-131

82. D. Garreau, P. Hapiot, J. M. Saveant *J. Electroanal. Chem.* **1990**, *281*, 73-83

83. D. Garreau, J. M. Saveant *J. Electroanal. Chem.* **1972**, 35, 309

84. D. Garreau, J. M. Saveant *J. Electroanal. Chem.* **1978**, 86, 63

85. H. J. Huang, P. He, L. R. Faulkner *Anal. Chem.* **1986**, 58, 2889-2891

86. J. O. Howell; W. G. Kurh; R. E. Ensman; R. M. Wightman *J. Electroanal. Chem. Interfacial Electrochem.* **1986**, 209, 77-90

87. D. O. Wipf; E. W. Kristensen; M. R. Deakin; R. M. Wightman *Anal. Chem.* **1988**, 60 , 306-310

88. A. J. Bard, L. R. Faulkner *Electrochemical Methods*; Wiley: New York, **1980**, p. 215 - 231

89. R. S. Nicholson *Anal. Chem.* **1965**, *37*, 1351

90. E. Laviron *J. Electroanal. Chem.* **1979**, *101*, 19-28

91. R. Bowling, R. L. McCreery *Anal. Chem.* **1988**, *60*, 605-608

92. M. S. Freund, A. Brajter-Toth *J. Phys. Chem.* **1992**, 96 9400.

93. A. J. Bard, L. R. Faulkner *Electrochemical Methods*; Wiley: New York, **1980**, p. 238-239

94. D. A. Gough, J. K. Leypoldt *Anal. Chem.* **1979**, 51, 439

95. D. A. Gough, J. K. Leypoldt *Anal. Chem.* **1980**, 52, 1126

96. J. Leddy, A. Bard, J. T. Maloy, J. M. Saveant *J. Electroanal. Chem.* **1985**, 187, 205

97. A. J. Bard, L. R. Faulkner *Electrochemical Methods*; Wiley: New York, **1980**, p. 200

98. D. J. Wiedemann; K. T. Kawagoe; R. T. Kennedy; E. L. Ciolkowski; R. M. Wightman *Anal. Chem.*, **1991**, V. 63, 2965

99. J. L. Owens, H. A. Marsh, G. Dryhurst *J. Electroanal. Chem.* **1978**, *91*, 231

100. D. Garreau, P. Hapiot, J. M. Saveant *J. Electroanal. Chem.* **1990**, *281*, 73

101. M. S. Freund, A. Brajter-Toth *J. Phys. Chem.*

102. R. Bowling, R. L. McCreery *Anal. Chem.* **1988**, *60*, 605

103. Author R. L. McCreery, Editor A. J. Bard *Electroanalytical Chemistry*; Dekker: New York, 1991; Vol. 17, p. 221

104. E. Sabatani, I. Rubinstein *J. Phys. Chem.* **1987**, *91* , 6663

105. R. A. Marcus *J. Phys. Chem.* **1965**, *43*, 679

106. T. J. Meyer, H. Taube, *Inorg. Chem.* **1968**, *7*, 2369

107. J. E. Baur, R. M. Wightman *J. Electroanal. Chem.* **1991**, *305*, 73

108. M. R. Deakin, K. J. Stutts, R. M. Wightman *J. Electroanal. Chem.* **1985**, *182*, 113

109. I. F. Hu, D. H. Karweik, T. Kuwana *J. Electroanal. Chem.* **1985**, *188*, 59

110. G. N. Kamau, W. S. Willis, J. F. Rusling *Anal. Chem.* **1985**, *57*, 545

111. R. J. Rice, N. M. Pontikos, R. L. McCreery *J. Am. Chem. Soc.* **1990**, *112*, 4617

112. J. L. Owens, H. A. Marsh, G. Dryhurst *J. Electroanal. Chem.* **1978**, *91*, 231

113. J. Y. Gui, D. A. Stern, F. Lu, A. T. Hubbard *J. Electroanal. Chem.* **1991**, 305, 37

114. R. M. Wightman, L. J. May, A. C. Michael *Anal. Chem.* **1988**, 60, 769A

115. *Beilstein*, Fourth Edition, Fifth Supplementary Series, Springer-Verlag Berlin.Heidelberg 1990, Vol. 22 part 1, p 380

116. Edited by R. W. Murray *Molecular Design of Electrode Surfaces*, **1992**, A Wiley-Interscience publication

117. R. John, G. G. Wallace *J. Electroanal. Chem.* **1991**, 306, 157

118. S. Asavapiriyanont, G. K. Chandler, G. A. Gunawardena, D. Pletcher *J. Electroanal. Chem.* **1984**, 177, 229

119. A. Witkowski, M. S. Freund, A. Brajter-Toth *Anal. Chem.* **1991**, 63, 622

120. M. D. Hawley, S. V. Tatawadi, S. Piekarski, R. N. Adams *J. Am. Chem. Soc.* **1967**, 89, 447

121. *CRC Handbook of Chemistry and Physics*, 67th ed.; CRC Press, Inc.: Boca Raton, 1986, p D-161

122. P. M. Kovach, A. G. Ewing, R. L. Wilson, R. M. Wightman *J. Neurosci. Methods* **1984**, 10, 215

123. R. M. Wightman, L. J. May, A. C. Michael *Anal. Chem.* **1988**, 60, 769A

124. J. Y. Gui, D. A. Stern, F. Lu, A. T. Hubbard *J. Electroanal. Chem.* **1991**, 305, 37

125. J. Y. Gui, D. A. Stern, F. Lu, A. T. Hubbard *J. Electroanal. Chem.* **1991**, 305, 37

126. *Beilstein*, Fourth Edition, Fifth Supplementary Series, Springer-Verlag Berlin.Heidelberg **1990**, Vol. 22 part 1, p 380

127. M. G. Cross, D. Walton, N. J. Morse, R. J. Mortimer, D. R. Rosseinsky, D. J. Simmonds *J. Electroanal. Chem.* **1985**, 189, 389

128. D. A. Sten, L. Laguren-Davidson, D. G. Frank, J. Y. Gui, C. H. Lin, F. Lu, G. N. Salaita, N. Walton, D. C. Zapien, A. T. Hubbard *J. Am. Chem. Soc.* **1989**, 111, 877

129. C. Quan, A. Brajter-Toth *Anal. Chem.* **1992**, 64, 1998

130. F. Malem, D. Mandler *Anal. Chem.* **1993**, 65, 37

131. L. Sun, B. Johnson, T. Wade, R. M. Crooks *J. Phys. Chem.* **1990**, 94, 8869

132. R. M. Wightman; L. J. May; A. C. Michael *Anal. Chem.*, **1988**, 60, 769A

133. P. M. Kovach; A. G. Ewing; R. L. Wilson; R. M. Wightman *J. Neurosci. Methods* **1984**, 10, 215

134. G. A. Gerhardt; A. F. Oke; G. Nagy; B. Moghaddam; R. N. Adams *Brain Res.*, **1984**, 290, 390

135. G. Nagy; G. A. Gerhardt; A. F. Oke; M. E. Rice; R. N. Adams; R. B. Moore; M. N. Szentirmay; C. R. Martin *J. Electroanal. Chem.*, **1985**, 188, 85

136. J. Millar; M. Armstrong-James; Z. L. Kruk *Brain Res.* **1981**, 205, 419

137. W. G. Kuhr; R. M. Wightman *Brain Res.* **1986**, 381, 168

138. J. E. Baur; E. W. Kristensen; L. J. May; D. J. Wiedemann; R. M. Wightman *Anal. Chem.* **1988**, 60, 1268

139. A. Marino; A. Brajter-Toth *Anal. Chem.*, **1993**, 65, 370

140. D. T. Fagan; I. F. Hu; T. Kuwana *Anal. Chem.*, **1985**, 57, 2759

141. I. F. Hu; D. T. Karweik; T. Kuwana *J. Electroanal. Chem.*, **1985**, 188, 59

142. A. C. Michael; J. B. Justice *Anal. Chem.* **1987**, 59, 405

143. J. X. Feng; M. Brazell; K. Renner; R. Kasser; R. N. Adams *Anal. Chem.* **1987**, 59, 1863

144. P. M. Kovach; M. R. Deakin; R. M. Wightman *J. Phys. Chem.* **1986**, 90, 4612

145. C. C. Hsueh; A. Brajter-Toth *Anal. Chem.*, **1993**, 65, 1570

146. D. J. Wiedemann; K. T. Kawagoe; R. T. Kennedy; E. L. Ciolkowski; R. M. Wightman *Anal. Chem.*, **1991**, 63, 2965

147. L. J. Kepley; A. J. Bard *Anal. Chem.* , **1988**, V. 60, 1459

148. C. P. Andrieux, P. Audebert, P. Hapiot, J. M. Saveant *J. Am. Chem. Soc.* **1990**, 112, 2440

BIOGRAPHICAL SKETCH

ChenChan Hsueh was born in Taiwan in 1963. After passing the national college entrance exam in 1981, he attended National Tsing Hua University and received a B.S. in chemistry four years later. After graduation, he enlisted in the army for two years. He then worked as a research assistant in the Institute of Atomic and Molecular Science, Taipei, Taiwan.

In 1990, he began his graduate studies at the University of Florida. He went back to Taiwan and married YarJing Yang in 1990. In 1994, he received the Summer Fellowship of the Electrochemical Society. In 1995, Mr. Hsueh completed his Ph.D. in analytical chemistry under the guidance of Professor Anna Brajter-Toth. His current research interests include analytical applications of fast-scan voltammetry, instrumentation design for microelectrode applications, and development of electrochemical biosensors.

I certify that I have read this study and that in my opinion it conforms to acceptable standards of scholarly presentation and is fully adequate, in scope and quality, as a dissertation for the degree of Doctor of Philosophy.

Anna Brajter-Toth, Chair
Associate Professor of Chemistry

I certify that I have read this study and that in my opinion it conforms to acceptable standards of scholarly presentation and is fully adequate, in scope and quality, as a dissertation for the degree of Doctor of Philosophy.

James D Winefordner
James D. Winefordner
Graduate Research Professor of Chemistry

I certify that I have read this study and that in my opinion it conforms to acceptable standards of scholarly presentation and is fully adequate, in scope and quality, as a dissertation for the degree of Doctor of Philosophy.

Martin Vala
Martin Vala
Professor of Chemistry

I certify that I have read this study and that in my opinion it conforms to acceptable standards of scholarly presentation and is fully adequate, in scope and quality, as a dissertation for the degree of Doctor of Philosophy.

Kirk Schanze
Associate Professor of Chemistry

I certify that I have read this study and that in my opinion it conforms to acceptable standards of scholarly presentation and is fully adequate, in scope and quality, as a dissertation for the degree of Doctor of Philosophy.

Paul Holloway
Professor of Materials Science and Engineering

LD
1780
1995
.H873

UNIVERSITY OF FLORIDA
3 1262 08554 5589